

New aspects of deglaciation in southern Norway

**Climate variability derived from surface exposure ages of Late Quaternary
and Holocene landforms**

Dissertation

zur Erlangung des Doktorgrades Dr. rer. nat.

der Mathematisch-Naturwissenschaftlichen Fakultät

der Rheinischen Friedrich-Wilhelms-Universität Bonn

Bonn, September 2019

Vorgelegt von

Philipp Marr

aus Kronach

Angefertigt mit Genehmigung der Mathematisch-Naturwissenschaftlichen Fakultät der
Rheinischen Friedrich-Wilhelms-Universität Bonn

1. Gutachter: Prof. Dr. Jörg Löffler

Geographisches Institut, Rheinische Friedrich-Wilhelms-Universität Bonn

2. Gutachter: Prof. Dr. Lothar Schrott

Geographisches Institut, Rheinische Friedrich-Wilhelms-Universität Bonn

Tag der mündlichen Prüfung: 29. Januar 2020

Erscheinungsjahr: 2020

Abstract

The investigation of periglacial and related landforms in South Norway is of high interest for exploring timings of deglaciation and to assess their geomorphological connectivity to palaeoclimatic changes during the Late Quaternary and the Holocene. The ice margins of the Scandinavian Ice Sheet during the Last Glacial Maximum (LGM) are fairly well known, the palaeo-ice thickness, however, which can only be estimated by modelling, remains unclear over large parts of Norway owing to rare field based evidences. Due to the significant influence of the former horizontal and vertical ice-sheet extent on sea-level rise, atmospheric and oceanic circulation patterns, erosive properties of glaciers and ice sheets, englacial thermal boundaries and deglaciation dynamics, it is crucial to better understand the topographic features of the LGM ice sheet. Despite recent advances, there is a lack of terrestrial evidences from numerical data in South Norway. In this thesis two high-mountain regions and their surroundings in west (Dalsnibba, 1476 m a.s.l.) and east (Blåhø, 1617 m a.s.l.) South Norway were used to reconstruct palaeoclimatic conditions and deglaciation patterns. Terrestrial cosmogenic nuclides (^{10}Be) and Schmidt-hammer exposure-age dating (SHD) have been utilized to determine the surface exposure of glacially transported boulders as well as of boulder-dominated glacial, periglacial and paraglacial landforms and bedrock outcrops. By developing calibration curves at both study sites for the first time, through young and old control points of known age, it was possible to obtain landform age estimates from Schmidt hammer R-(rebound) values. Beside age estimates, the formation and stabilization of those landforms and the involved processes have provided indications about the Late Quaternary and Holocene climate variability and its connectivity to landform development. The first deglaciation chronology for the western study area could be constructed based on ^{10}Be surface exposure ages. Final local deglaciation on the summit of Dalsnibba probably started between 13.3 ± 0.6 and 12.7 ± 0.5 ka and progressed down to the valley bottom of Opplendskedalen (~ 1050 m a.s.l.) with an SHD age estimate of 7.47 ± 0.73 ka. Deglaciation during the Bølling–Allerød Interstadial ($\sim 14.7 - 12.9$ ka) indicates that the summit was not ice-covered during the Younger Dryas ($12.9 - 11.7$ cal. ka BP). A glacially transported boulder in the summit area and summit bedrock ages without cosmogenic nuclide inheritance further imply a minimum vertical ice extent of 1476 m and the presence of erosive warm-based ice. The SHD Dalsnibba results show that most landforms stabilized during the Holocene Thermal Maximum ($\sim 8.0 - 5.0$ ka) and that their R-value characteristics with negative skewness were indicative for the reworking of boulders or continuous debris supply. The SHD ages from Dalsnibba imply that periglacial landforms in the western maritime setting sensitively reacted to Holocene climate variability. Rock-slope failures investigated at both study sites demonstrate that they do not necessarily occur shortly after local deglaciation as often inferred. Furthermore, most of the recorded rock-slope failures appear to have occurred during warm climatic conditions. Most likely, prevailing warm conditions led to permafrost degradation, enhanced snow melt and increasing cleftwater pressure contributed to slope instabilities probably resulting in rock-slope failures.

The Blåhø SHD ages also suggest landform response on climate variations, though, in a different temporal context. Landforms above 1450 m a.s.l. largely shared overlapping ages and therefore appear to have stabilized during the Karmøy/Bremanger readvance ($\sim 18.5 - 16.5$ ka). This, however, seems to have been the last major geomorphic activity of these landforms as they were not reactivated by several, partly severe cold climate events such as the Younger Dryas. The SHD ages from landforms above 1450 m a.s.l. are in contrast to the previous deglaciation chronology which suggested cold-based ice coverage and slow thinning down to ~ 1450 m a.s.l. at 15.0 ± 1.0 ^{10}Be ka. Based on the results from this thesis, a severe periglacial climate without ice coverage since about 18 ka is proposed for the summit area of Blåhø. The ^{10}Be ages from Blåhø with 20.9 ± 0.8 ka for the erratic boulder and 46.4 ± 1.7 ka for the bedrock, which extend the previous deglaciation chronology, are discussed within the framework of the two most popular scenarios. Within the first scenario the boulder age represented the timing of deglaciation and the bedrock age showed inherited cosmogenic nuclides, suggesting the presence of low erosive cold-based ice at Blåhø during the LGM. In the second scenario, the boulder age was affected by post-depositional disturbance, frost heave processes or shielding, potentially indicating ice-free conditions on Blåhø since at least 46.4 ± 1.7 ka. Analyzing the different onset of deglaciation in the study areas within a rather short west-east distance, together with the timing of deglaciation in neighboring regions, demonstrates complex deglaciation dynamics in southern Norway. Not only the timing of deglaciation was highly variable, the results also imply diverse basal ice temperatures within this relatively small area. In general, this thesis positively contributes new evidences pointing to a more complex and dynamic Scandinavian Ice Sheet throughout the last glacial cycle than previously assumed.

Neue Aspekte zur Deglaziation in Südnorwegen

Klimavariabilität abgeleitet von Oberflächenexpositionsaltern von spät-Quartären und Holozänen Landformen

Zusammenfassung

Die Untersuchung periglazialer und verwandter Landformen in Südnorwegen ist von großem Interesse, um den Zeitpunkt der Deglaziation zu bestimmen und ihre geomorphologische Konnektivität mit paläoklimatischen Veränderungen während des spät-Quartärs und des Holozäns zu bewerten. Die Lokationen der Eistränder des Skandinavischen Eisschildes während des letzten glazialen Maximums (Last Glacial Maximum, LGM) sind vergleichsweise gut bekannt, die Mächtigkeit des Paläoeises hingegen, welches lediglich modelliert werden kann, bleibt über weite Teile Norwegens aufgrund sehr weniger Geländebefunde, unklar. Aufgrund des signifikanten Einflusses der früheren horizontalen und vertikalen Ausdehnung des Eisschildes auf den Meeresspiegelanstieg, die atmosphärischen und ozeanischen Zirkulationsmuster, die erosiven Eigenschaften von Gletschern und Eisschilden, die englazialen thermischen Grenzen sowie die Dynamik der Vereisung, ist es entscheidend die topographischen Strukturen und Eigenschaften des LGM-Eisschildes besser zu verstehen. Trotz der jüngsten Forschungsfortschritte mangelt es in Südnorwegen an terrestrischen Geländebefunden basierend auf numerischen Daten. Für diese Arbeit wurden zwei Hochgebirgsregionen und ihre Umgebungen im Westen (Dalsnibba, 1476 m ü.d.M., über dem Meeresspiegel) und Osten (Blåhø, 1617 m ü.d.M.) Südnorwegens zur Rekonstruktion paläoklimatischer Bedingungen und Vergletscherung ausgewählt. Sowohl terrestrische kosmogene Nuklide (^{10}Be) als auch Schmidt-hammer exposure-age dating (SHD) wurden angewendet, um die Dauer der Oberflächenexposition von glazial-transportierten Felsblöcken sowie von blockdominierten glazialen, periglazialen und paraglazialen Landformen und anstehendem Festgestein zu bestimmen. Durch die erstmalige Erstellung von Kalibrierungskurven an beiden Untersuchungsstandorten, durch junge und alte Kontrollpunkte bekannten Alters, konnten aus Schmidt Hammer R-(Rückprall-) Werten, Landform-Altersschätzungen vorgenommen werden. Neben Altersschätzungen konnten die Bildung und Stabilisierung dieser Landformen und die damit verbundenen Prozesse nun neue Hinweise auf die spätquartäre und holozäne Klimavariabilität und ihre Konnektivität zur Landformentwicklung liefern.

Die erste Deglaziationschronologie für das westliche Untersuchungsgebiet konnte auf Grundlage von ^{10}Be Oberflächenexpositionsaltern erstellt werden. Die endgültige lokale Deglaziation auf dem Gipfel des Dalsnibba begann wahrscheinlich zwischen 13.3 ± 0.6 und 12.7 ± 0.5 ka und endete am Talboden des Opplendskedalen (~ 1050 m ü.d.M.) um 7.47 ± 0.73 ka, basierend auf einer SHD-Altersschätzung. Die Deglaziation während des Bølling–Allerød Interstadials ($\sim 14.7 - 12.9$ ka) zeigt, dass der Gipfel während der Jüngeren Dryas ($12.9 - 11.7$ cal. ka BP) nicht von Eis bedeckt war. Ein glazial-transportierter Felsblock im Gipfelbereich und untersuchtes Grundgestein auf dem Gipfel ohne kosmogene Nuklid-Vererbung implizieren weiterhin eine vertikale Mindesteisausdehnung von 1476 m und das Vorhandensein von erosivem, warm-basalem Eis. Die SHD-Ergebnisse von Dalsnibba zeigen, dass sich die meisten Landformen während des holozänen thermischen Maximums stabilisierten ($\sim 8.0 - 5.0$ ka) und dass ihre R-Wert-Eigenschaften,

mit negativer Schiefe, auf eine Re-Aktivierung von Felsblöcken oder auf kontinuierliche Zufuhr von Schuttmaterial hinweisen. Die SHD-Alter von Dalsnibba deuten zudem darauf hin, dass periglaziale Landformen im westlichen maritimen Umfeld empfindlich auf die Klimavariabilität des Holozäns reagierten. Die an beiden Untersuchungsorten untersuchten Felsstürze (rock-slope failures) implizieren, dass Felsstürze nicht unweigerlich gehäuft kurz nach der lokalen Enteisung auftraten. Darüber hinaus scheinen die meisten der aufgezeichneten Felsstürze unter warmen klimatischen Bedingungen aufgetreten zu sein. Es ist anzunehmen, dass die vorherrschenden warmen klimatischen Bedingungen zu Permafrostdegradation, verstärkter Schneeschmelze und steigendem Wasserdruck in Klüften zu Hanginstabilitäten führten, die wahrscheinlich Massenbewegungen von Felshängen auslösten.

Die Blåhø-SHD-Alter deuten ebenfalls auf eine Reaktion der Landformen auf Klimaschwankungen hin, jedoch in einem anderen temporalen Kontext. Bei den Landformen über 1450 m ü.d.M. überschneiden sich die Alter weitgehend, diese Landformen stabilisierten sich wahrscheinlich während des Karmøy/Bremanger Vorstoßes (~18.5 – 16.5 ka). Dies scheint jedoch die letzte größere geomorphe Aktivität dieser Landformen gewesen zu sein, da sie nicht durch mehrere, teilweise starke Kälteereignisse wie der Jüngeren Dryas reaktiviert wurden. Die SHD-Alter der Landformen oberhalb von 1450 m ü.d.M. stehen im Gegensatz zu einer vorherigen Deglaziationschronologie, die eine kalt-basale Eisbedeckung und eine langsame Ausdünnung auf 1450 m ü.d.M. bei 15.0 ± 1.0 ^{10}Be ka nahe legte. Basierend auf den Ergebnissen dieser Arbeit wird für das Gipfelgebiet von Blåhø ein strenges Periglazialklima ohne Eisbedeckung seit etwa 18 ka postuliert. Die ^{10}Be -Alter von Blåhø mit 20.9 ± 0.8 ka für den erratischen Block und 46.4 ± 1.7 ka für das Grundgestein, die die bisherige Deglaziationschronologie erweitern, werden im Rahmen der beiden verbreitetsten Szenarien diskutiert. Im ersten Szenario stellt das Expositionsalter des Blockes den Zeitpunkt der Deglaciation dar und das Grundgesteinszeitalter weist vererbte kosmogene Nuklide auf, was auf das Vorhandensein von schwach erosivem, kalt-basalem Eis auf Blåhø während des LGMs hinweist. Im zweiten Szenario wurde das Expositionsalter des Blockes durch nachträgliche Störung nach der Ablagerung, Frosthebungsprozessen oder der Abschirmung von kosmogenen Nukliden, beeinflusst, was möglicherweise auf eisfreie Bedingungen auf dem Blåhø seit mindestens 46.4 ± 1.7 ka hindeutet. Die Analyse der unterschiedlichen Zeiten des Beginns der Deglaciation in den Untersuchungsgebieten innerhalb einer relativ kurzen Entfernung von West nach Ost sowie des Zeitpunkts der Enteisung in benachbarten Regionen zeigen die komplexe Enteisungsdynamik in Südnorwegen. Die Enteisungszeitpunkte waren nicht nur sehr unterschiedlich, die Ergebnisse implizieren auch differierende basale Eistemperaturen in diesem relativ kleinen Areal. Zusammenfassend legt diese Arbeit neue Beweise vor, die auf ein komplexeres und dynamischeres Skandinavisches Eisschild während des letzten glazialen Zyklus hinweisen als bisher angenommen.

Acknowledgements

I express my gratitude to Prof. Dr. Jörg Löffler and Prof. Dr. Lothar Schrott for supervising me and for the great opportunity to work on this doctoral thesis. Thank you very much for your guidance, patience and support during the last years. Furthermore, thank you for being members of my thesis committee.

At this point I also thank PD Dr. Gösta Hoffmann and Prof. Dr. Wulf Amelung for being members of my oral examination committee.

I want to thank my colleagues and friends Stefan Winkler, Simone Ackermann, Nils Hein, Niklas Beckers, Camilla Kurth, Steve Binnie, Tibor Dunai, Jenny Müller, Claire Pfalzner-Gibbon, Sven-Oliver Franz who participated actively in this study, either in field, lab, at the summer schools, in Svalbard and at office. Thank you for all your contributions, help and advices, and the good times in the Norwegian mountains.

I thank the Svare family for their hospitality and support during long field-work periods in Vågå and the DAAD for financial support.

I deeply acknowledge my family and friends who accompanied and supported me during my studies. I am especially grateful to my parents Edith and Hans-Jürgen, my sister Julia and my brother Oliver, my niece Lotti and my nephew Karl, and my partner Tabitha who always supported me. Thank you for all your encouragement, patience and moral support that helped me to finish this thesis.

This doctoral study was only possible with the financial support of the Friedrich-Ebert-Stiftung for which I am very grateful.

Table of Contents

Abstract.....	I
Zusammenfassung.....	III
Acknowledgements.....	V
Table of Contents.....	VI
1 Introduction.....	1
2 Study Areas.....	4
3 Research Design and Methodology.....	7
3.1 Schmidt-Hammer Exposure-Age Dating (SHD).....	7
3.1.1 Sampling Strategy and Analyses.....	8
3.1.2 Age Calibration.....	9
3.2 Terrestrial Cosmogenic Nuclides (TCN).....	9
3.2.1 Research Design and Age Calculation.....	10
4 Results and Discussion.....	11
4.1 Dalsnibba.....	11
4.2 Blåhø.....	13
4.3 Methodological Implications.....	16
4.4 Implications for the Deglaciation History of Southern Norway.....	18
5 General Conclusions.....	21
6 References.....	24
7 Investigations on Blockfields and Related Landforms at Blåhø (Southern Norway) Using Schmidt-Hammer Exposure-Age Dating (SHD): Palaeoclimatic and Morphodynamic Implications.....	33
8 Schmidt-Hammer Exposure-Age Dating (SHD) Performed on Periglacial and Related Landforms in Oplendskedalen, Geirangerfjellet, Norway: Implications for Mid- and Late-Holocene Climate Variability.....	61
9 ¹⁰ Be-Based Exploration of the Timing of Deglaciation in Two Selected Areas of Southern Norway.....	75

1 Introduction

Climate change and the ongoing debates about its consequences are gaining political and public momentum worldwide (OWEN et al. 2009; IPCC 2014). Mountain areas, particularly glaciers and ice sheets, react sensitively to changing climatic conditions. They are currently facing rapid and comprehensive changes with wide-ranging ramifications which are expected to accelerate in the future (ZEMP et al. 2008; BARRY and GAN 2011; GOBIET et al. 2014; ZEMP et al. 2015; BENISTON et al. 2018). Glaciers store large amounts of freshwater and their run-off is crucial for irrigation systems as well as hydropower production (ANDREASSEN and WINSVOLD 2012; HUSS et al. 2017). Additionally, they are an integrated part of the global climate system with important effects on global, regional and local environments, e.g. sea-level rise, geomorphological hazards and ecological changes in glacier forelands (MATTHEWS 1992; KASER et al. 2006; BALLANTYNE 2018). In this context, diminishing mountain glaciers and ice sheets can be recognized as key components for current and future societal and environmental systems (ZEMP et al. 2008; BARRY and GAN 2011; IPCC 2014). For the purpose of improving the predictions for future glacier and ice-sheet development together with assessing the consequences of their retreat or disappearance, it is essential to better constrain their (de)glaciation history, past glacier dynamics as well as their influence on landscape evolution (OWEN et al. 2009; SOLOMINA et al. 2015; HUGHES et al. 2016).

Glacier and ice sheet fluctuations throughout the Quaternary (~ 2.6 Ma) and the Holocene (< 11.7 ka) have had major impacts on environmental conditions and the shape of landscapes worldwide (BÖSE et al. 2012; EHLERS et al. 2018). During the Last Glacial Maximum (LGM, 26.5 – 20 ka, CLARK et al. 2009) the Eurasian ice-sheet complex represented the third largest ice mass worldwide (PATTON et al. 2016), from which the Scandinavian Ice Sheet (SIS) comprised the largest component (HUGHES et al. 2016). This qualifies Scandinavian landscapes as potential palaeoclimatic archives for information about (de-)glaciation dynamics together with exploring magnitude and frequency of glacier fluctuations during the LGM towards the Holocene (see STROEVEN et al. 2016). Investigating the late Quaternary glaciation history in Scandinavia, especially in Norway, has raised the attention of scientists since more than a century (BLYTT 1876; SOLLID and SØRBEL 1994; MANGERUD 2004; ANDERSEN et al. 2018a). Knowledge about the former horizontal and vertical extent of glaciers can be valuable in order to better understand palaeo-environmental components, such as sea-level changes, atmospheric and oceanic circulation patterns, landform evolution, (de)glaciation dynamics, erosive capacities of ice, glacial thermal boundaries and is crucial for palaeoclimatic, isostatic and numerical-glaciological modelling (KUTZBACH et al. 1998; LINGE et al. 2006; RINTERKNECHT et al. 2006; HUGHES et al. 2016; STROEVEN et al. 2016). Comprehensive review studies drew a rather clear picture of the SIS margins in Norway throughout different stages within and following the last glaciation (HUGHES et al. 2016; PATTON et al. 2016, 2017; STROEVEN et al. 2016). By contrast, the exact vertical ice extent during this time remains uncertain in large areas, also because reconstructions were mostly based on isostatic rebound models and not on direct field evidences (BROOK et al. 1996; MANGERUD 2004; PELTIER 2004; LINGE et al. 2006; PAUS et al. 2006; GOEHRING et al. 2008).

The diverse landscape in Norway, high mountain areas with isolated summits in south-central and fjord landscapes in southwestern Norway, offers the possibility to explore palaeo-ice thickness conditions (GOEHRING et al. 2008). Differently weathered landscapes in high mountain areas are considered as important components of Pleistocene ice-sheet dynamics and as indicators for ice thickness since decades (DAHL 1955; BALLANTYNE 1998; BRINER et al. 2006; MCCARROLL 2016). The contrast is often reflected in highly weathered uplands, comprising blockfields or tors, and relatively unweathered or freshly exposed glaciated bedrock in lower locations, separated by a trimline (REA et al. 1996; GOODFELLOW 2007; BALLANTYNE 2010). This sometimes well-defined boundary is discussed as a potential indicator of former ice-sheet thickness (NESJE et al. 1988; LINGE et al. 2006). Palaeo-ice thickness estimates in Norway are ranging from minimum models with large ice-free areas within a multi-domed ice-sheet configuration (NESJE et al. 1988; DAHL et al. 1997; FOLLESTAD 2003), to maximum models suggesting ice cover for most or all summits, alongside with a thick SIS (MANGERUD 2004; PELTIER 2004). In the interest of more accurate reconstructions, several concepts are discussed in explaining the appearance of differently weathered mountain landscapes, from which the following two are the most frequently used (e.g. STROEVEN et al. 2002). The first scenario implies that highly weathered uplands were ice-free (nunataks) during recent glaciation(s), where the trimline reflected the upper vertical erosional limit of the former ice sheet (e.g. NESJE and DAHL 1990; RAE et al. 2004). Secondly, low-erosive cold-based ice is considered to cover and protect landscape features, where the trimline mirrored an englacial boundary between warm- and cold-based ice (e.g. KLEMAN 1994; STROEVEN et al. 2002). Alongside with a recent paradigm shift towards the latter scenario and increasing evidence for a more complex ice sheet during the LGM (RINTERKNECHT et al. 2006; MANGERUD et al. 2010), this requires a critical re-assessment of the role of blockfields and related periglacial landforms as palaeoclimatic proxies and previous deglaciation chronologies (e.g. MCCARROLL 2016).

The wide application of terrestrial cosmogenic nuclides (TCN) in glacial and periglacial geomorphology revolutionized deglaciation chronologies (DUNAI 2010). It largely improved the understanding of the timing of deglaciation and rates of ice thickness degradation (BRINER et al. 2006; LINGE et al. 2007, NESJE et al. 2007). The importance of periglacial and related landforms as palaeoclimatic proxies is often overseen despite their potential to provide information on deglaciation and past climate variabilities (BAUMHAUER and WINKLER 2014; WINKLER et al. 2016; DENN et al. 2018; MATTHEWS et al. 2018). These landforms appear to be valuable proxies for past cold periods, as they are considered to have formed during cold climatic conditions and are widespread worldwide (cf. WILSON et al. 2017). However, the formation history and the underlying processes shaping these landforms largely remain ambiguous. Beside the utilisation of TCN in identifying the exposure or burial age of landforms (FABEL et al. 2002; BRINER et al. 2006; NESJE et al. 2007), Schmidt-hammer exposure-age dating (SHD) has proved to be appropriate for investigating surface exposure ages by constructing a calibration curve from control points of known age, together with exploring geomorphic processes of boulder-dominated landforms in the periglacial zone (MATTHEWS and OWEN 2010; SHAKESBY et al. 2011; WILSON and MATTHEWS 2016).

Despite the advances in reconstructing former ice configurations and its implications on landscape evolution as well as the long research tradition (e.g. NESJE et al. 1994b; GOEHRING et al. 2008; LONGVA et al. 2009), there is little knowledge about palaeo-ice thickness as well as timing and rates of local deglaciation in South Norway owing to few terrestrial exposure ages (HUGHES et al. 2016; PATTON et al. 2016). Along with this, Holocene climate variability and its impacts on geomorphological activity often remain elusive (MCCARROLL and NESJE 1993; DAHL et al. 1997; GOEHRING et al. 2008; MATTHEWS and WINKLER 2011). Deglaciation reconstructions, particularly in the western part of South Norway mostly rely on interpolations of numerical ages from neighbouring areas which require more ground truth data by numerical data at specific locations. Recent studies on the deglaciation history in Scandinavia (e.g. HUGHES et al. 2016; STROEVEN et al. 2016) did not provide details of complex local deglaciation histories and mechanisms in South Norway.

In the light of the abovementioned research gaps, this thesis aims to contribute to a better understanding of the timing and rates of local deglaciation and the connectivity between Late Quaternary as well as Holocene climate variability and landform evolution, based on TCN and SHD investigations in two selected mountain areas in southern Norway. By applying different surface exposure dating methods, it is possible to explore the involved geomorphic processes, together with surface exposure ages which would be not feasible by applying a single method. Opplendskedalen in the Geirangerfjord together with the prominent peak of Dalsnibba is one of the study areas as it is largely unexplored in terms of past climate variability and timing of deglaciation, despite few studies carried out in Geiranger (FARETH 1987) and its neighbouring fjords (e.g. RYE et al. 1997; BLIKRA et al. 2006). A beneficial effect of this site is the rather small extent of current glaciers. Their faster response to climatic variability in this maritime setting allows to detect smaller changes at higher resolution which would be not possible at larger glaciers (DAHL et al. 2003). At the second study site in eastern South Norway, on the summit of Blåhø, several studies have been carried out dealing with palaeo-ice thickness estimations and deglaciation chronologies (NESJE et al. 1994b; GOEHRING et al. 2008). This enables to validate numerical ages from this study with the previously published chronology and to farther develop the existing chronology with new numerical data. The previously published numerical ages from GOEHRING et al. (2008) allowed to construct a high-precision calibration curve for SHD, ensuring robust surface exposure ages. In order to provide new insights into the mentioned issues, this thesis anticipates to tackle the following four questions:

- 1) What were the timing and dynamics of local deglaciation in two selected areas of South Norway during and following the Last Glacial Maximum?
- 2) How did periglacial and related landforms react to climate variability following the Last Glacial Maximum and during the Holocene?
- 3) Are periglacial and related landforms potential palaeoclimatic archives which can be explored by the application of Schmidt-hammer exposure-age dating in these areas?
- 4) Which implications do the findings have on the regional deglaciation history?

2 Study Areas

The research work presented in this thesis focusses on periglacial and related landforms in two high mountain areas in South Norway (Figure 1). Both research areas are stretched along the 62° latitude north, from the west Norwegian coast eastwards to the Swedish border. The western study area is located around Dalsnibba (1476 m a.s.l.) in Opplendskedalen, next to the town of Geiranger in Møre og Romsdal county (62°04'43 N, 7°17'35 E), Breheimen is located south and Reinheimen west of Dalsnibba (see Figure 1). The topography of the area is characterized by strong elevation gradients within short distances. Dominant landscape features comprise the changes between well-developed glacial valleys and deeply incised fjords as results of repeated glaciations during the Quaternary (HOLTEDAHL 1967; KLEMSDAL and SJULSEN 1988; BÖHME et al. 2015). The smooth landscape between the valleys at higher altitudes (~1800 – 1500 m a.s.l.) are largely characterized by flat or gently undulated surfaces of pre-glacial origin, also called paleic surfaces (GJESSING 1967; NESJE and WHILLANS 1994). Moderately weathered, glacially eroded bedrock is widespread at the summit area of Dalsnibba, where a blockfield is absent.

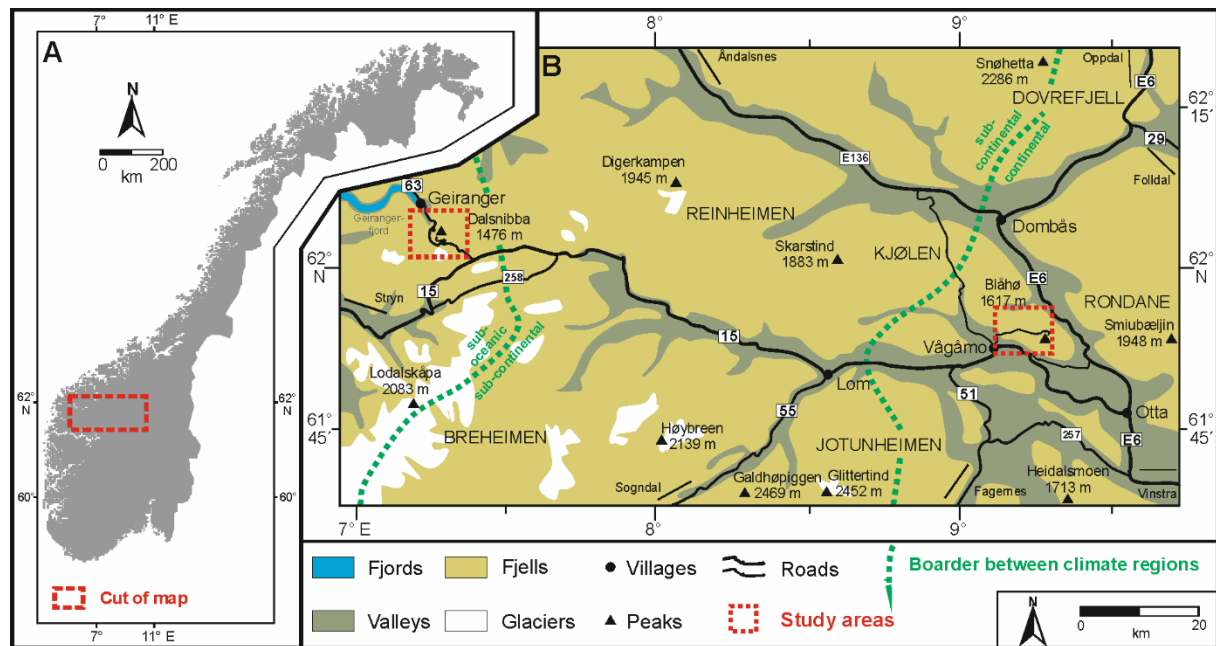


Figure 1: Study areas in southern Norway with the location of Dalsnibba in the west and Blåhø in the east, marked with red squares (B) and their location in Norway (A) (modified after LÖFFLER and PAPE 2004).

The climate in the western study area is characterized by sub-oceanic conditions, implying a mild periglacial climate with a mean annual air temperature between 0°C and 2°C (1971 – 2000) and a mean annual precipitation between 2000 and 3000 mm yr⁻¹ (<http://senorge.no>, last access: 24. July 2019). Snow depths of more than 5 cm were recorded on 200 – 350 days from 1971 to 2000 (<http://senorge.no>, last access: 24. July 2019). No permafrost was detected at Dalsnibba. Geologically, the Geiranger region is part of the Norwegian basement which consists of Proterozoic rocks (SIGMOND et al. 1984). It is part of the so-called Western Gneiss Region spanning large areas of South Norway and the bedrock consists mainly of quartz dioritic to granitic and is partly migmatitic (TIVETEN et al. 1998).

There is no detailed deglaciation chronology or palaeo-ice thickness estimation for the western study site, but deglaciation most likely reached the Geirangerfjord during the Bølling–Allerød Interstadial (~14.7 – 12.9 ka, PATTON et al. 2017). During this period glacier dynamics were characterized by several short-term standstills in the fjord (LONGVA et al. 2009). Glaciers readvanced in the area during the Younger Dryas (YD, ~12.9 – 11.7 cal. ka BP, LOHNE et al. 2013), reflected in the terminal moraines located at the fjord mouth (LONGVA et al. 2009). According to FARETH (1987) the maximum glacier extent was reached 10.5 ± 0.2 ^{14}C ka BP which subsequently melted rapidly and is expected to have disappeared 500 years later (LONGVA et al. 2009). Following the YD, the final deglaciation in the fjords in western South Norway is expected to have taken place within 11.2 ± 0.4 and 10.9 ± 0.2 cal. ka BP (cf. NESJE and DAHL 1993, calibrated by HUGHES et al. 2016). One of the few palaeo-ice thickness estimations suggested 1200 – 800 m vertical ice extent in the fjords which turned ice-free during Bølling–Allerød Interstadial (ANDERSEN et al. 1995). However, most of the reconstructions are based on rather old ^{14}C ages which can be problematic and have been questioned in the past (see DONNER et al. 1996; MANGERUD 2004).

The second study site is located in east South Norway at the summit and surroundings of Blåhø (1617 m a.s.l.) in Ottadalen, close to the town of Vågåmo in Oppland county (61°53'51 N, 9°16'58 E). Blåhø is situated between Rondane in the west, Reinheimen in the north-east and Jotunheimen in the south-east. Gently undulating surfaces dominate the summit area which has a steep slope towards the east and gentler slope angles to the north and south (MARR et al. 2018). West of the summit three lower lying peaks namely Rundhø (1556 m a.s.l.), Veslrundhø (1514 m a.s.l.) and Storhøi (1455 m a.s.l.) are located. An autochthonous blockfield at the summit of Blåhø extends downslope to a trimline at ~1500 m a.s.l. (NESJE et al. 1994b).

The climate is dominated by strong continental conditions. This is reflected in the mean annual air temperature of -2° to -1°C and the mean annual precipitation between 750 and 1000 mm yr^{-1} at the summit (<http://senorge.no>, last access: 24. July 2019) and <500 mm yr^{-1} in valleys which represents one of the driest locations in Norway. A snow depth of >25 cm was recorded at 100 – 200 days (mean) between 1971 and 2000 at most of the investigated landforms. The sites around Rundhø experienced slightly longer snow accumulation of 200 – 350 days (<http://senorge.no>, last access: 24. July 2019). At the summit more than 5 cm of snow were measured on 200 – 350 days, in contrast only 100 – 200 days in areas lower than 1000 m a.s.l. (1971 – 2000) (<http://senorge.no>, last access: 24. July 2019). It is assumed that high wind velocities limit the snow coverage in the summit area. Permafrost measurements by FARBROT et al. (2011) show mean ground temperatures at 5 cm depth of 0.9°C (2008 – 2009) and 1.0°C (2009 – 2010) and 0.7°C (September 2008 to August 2010) at 10 cm depth. In the latter period, an active layer thickness of 6 to 7 meters was recorded by FARBROT et al. (2011). The area around Blåhø is geologically part of the Kvitola Nappe, comprised of late Precambrian sedimentary rocks (cf. FARBROT et al. 2011). The quartz-rich Precambrian bedrock is present as meta-conglomerate at higher slopes and as meta-sandstone at lower slopes (TVETEN et al. 1998).

Blåhø's deglaciation history is part of an ongoing discussion which focusses on whether the summit was covered by cold-based ice (GOEHRING et al. 2008) or escaped glaciation as a nunatak (NESJE et al. 1994b).

The ^{10}Be based deglaciation chronology of Blåhø was presented along a vertical transect by GOEHRING et al. (2008) with an erratic boulder from the summit dated to 25.1 ± 1.8 ka (recalculated to 21.8 ± 1.6 ka by MARR et al. (2019b)) which was interpreted as the start of deglaciation. They successively sampled six lower lying glacially transported boulders between 1481 – 1086 m a.s.l. from which the lowermost sample dates to 11.7 ± 1.0 ka. Although the cold-based ice concept is largely accepted by the scientific community (e.g. FABEL et al. 2002), there are indications that this concept does not apply to all blockfields (MCCARROLL 2016) and that the glaciation was more dynamic and complex than previously assumed (e.g. RINTERKNECHT et al. 2006). There is evidence of mountain summits (e.g. Skåla) have escaped glaciation in vicinity to Blåhø (BROOK et al. 1996) which agrees with the assumption that the LGM ice sheet was multi-domed and rather thin (FOLLESTAD 2003; WINGUTH et al. 2005).

3 Research Design and Methodology

In order to get chronological control of the different periglacial and related landforms, Schmidt-hammer exposure-age dating (SHD) and terrestrial cosmogenic nuclides (TCN) were applied in this thesis. The research design of this thesis is described in Figure 2.

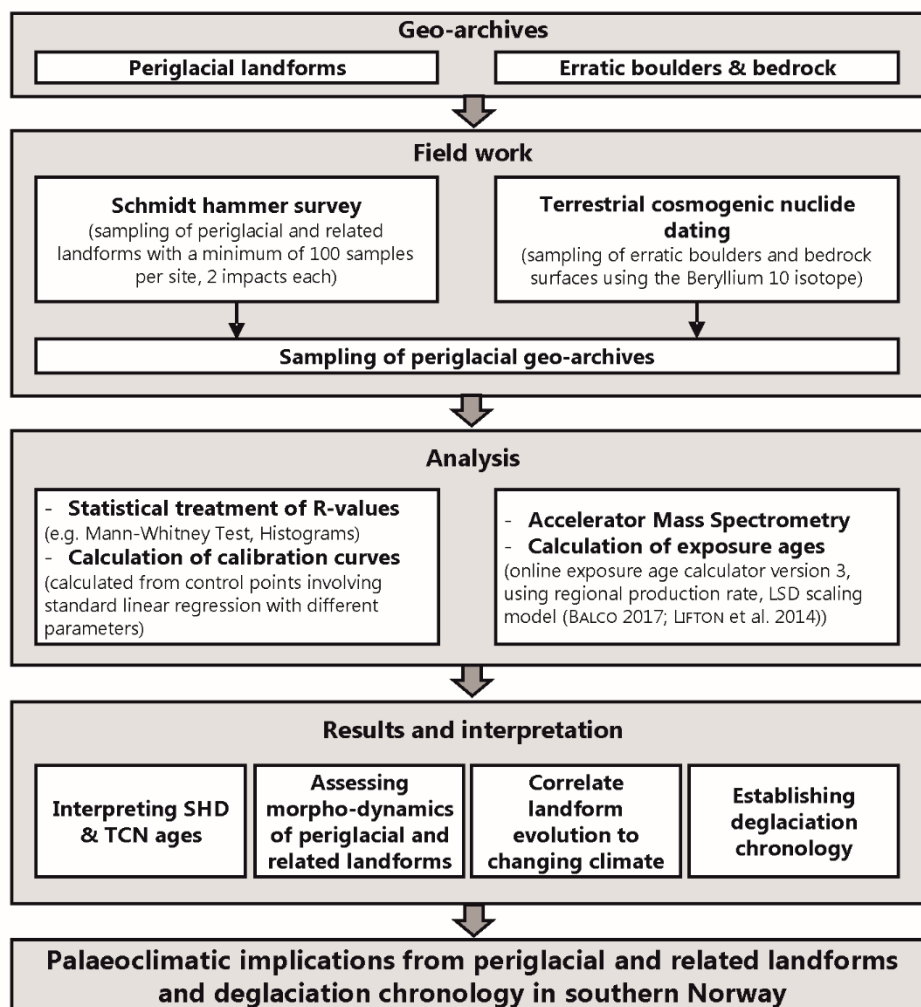


Figure 2: Research design of this thesis (modified after BARTZ 2018).

3.1 Schmidt-Hammer Exposure-Age Dating (SHD)

The Schmidt hammer was originally designed to test concrete hardness in situ (SCHMIDT 1950) but has been used in geomorphological research since the 1960s (see GOUDIE 2006). It was mostly utilized to relatively date boulder-dominated landforms such as moraines (WINKLER 2005), rock glaciers (HUMLUM 1998) and rock avalanches (CLARK and WILSON 2004) and was recently developed towards surface exposure dating (e.g. SHAKESBY et al. 2006; MATTHEWS and OWEN 2010). Schmidt hammer measurements reflect the compressive strength of a rock surface which is assumed to decrease with the degree of rock exposure to subaerial weathering. This allows comparisons between relative surface weathering of boulders, provided that the factor lithology is uniform (ČERNÁ and ENGEL 2011; MATTHEWS et al. 2013). The rebound (R-) values generated by the Schmidt hammer mirror the rebound velocity of the plunger which was released on

the rock surface (WINKLER and MATTHEWS 2014). Higher R-values are anticipated from freshly exposed rock surfaces. In turn, low R-values are expected from rock surfaces which experienced long subaerial exposure (MATTHEWS et al. 2013). SHD can estimate surface exposure ages of boulder-related periglacial landforms and permits to explore the dynamics and processes in their formation and stabilization utilizing control points of known age to construct a calibration curve (SHAKESBY et al. 2011; MATTHEWS et al. 2014; WILSON and MATTHEWS 2016). This technique was successfully applied in numerous studies on various boulder-dominated landforms in Norway (MATTHEWS et al. 2013; WILSON et al. 2017), United Kingdom (TOMKINS et al. 2016; WILSON and MATTHEWS 2016) and New Zealand (WINKLER 2014). The ages obtained from Schmidt hammer surveys are largely in accordance with findings by radiocarbon dating (e.g. NESJE et al. 1994a), lichenometry (e.g. MATTHEWS and SHAKESBY 1984), optically stimulated luminescence (e.g. STAHL et al. 2013) and TCN (e.g. TOMKINS et al. 2018; WILSON et al. 2019).

3.1.1 Sampling Strategy and Analyses

Schmidt hammer measurements were obtained from boulder or bedrock surfaces from different boulder-dominated periglacial and related landforms such as blockfields, rock-slope failures and sorted polygons. From each control point and landform at least 100 and up to 450 boulders and/or bedrock surfaces were measured, each with two impacts per sampled surface. Sampling near rock cracks or edges, structural weaknesses, at lithological unstable areas or on mosses or lichens were avoided (e.g. SHAKESBY et al. 2011). The rock surfaces were not prepared prior the measurements. Throughout the SHD studies only stable, near-horizontal boulders with a larger diameter than 30 cm were measured to insure that measurements from one landform can be treated as a homogenous sample. The influence of potential sources of error on the results other than surface exposure to weathering processes, including microclimatic variability, lithological heterogeneities and post-depositional disturbance have been limited by the relatively large sample sizes (see WINKLER 2005, 2009). A similar sampling design was used by WILSON and MATTHEWS (2016) which assures the reliability of the approach and adequate samples sizes (SHAKESBY et al. 2006; NIEDZIELSKI et al. 2009). In sum, in both studies (MARR et al. 2018, 2019a) 3700 boulders with 7400 impacts of 13 periglacial and related landforms were measured.

The results ran through standard statistical treatment such as the calculation of the standard mean, standard error of the mean (SEM), 95% confidence interval, kurtosis, skewness and the Shapiro-Wilk test for normality. In order to determine the statistical significance between pair of sites the Mann-Whitney test was applied (MARR et al. 2018, 2019a). Landforms with overlapping 95% confidence intervals ($\alpha = 0.05$) were treated as the same population and therefore of the same age (SHAKESBY et al. 2006). Histograms were created to visualize R-value distributions which can be associated with depositional boulder disturbances, incorporation of anomalously old boulders or complex formation histories (MCCARROLL and NESJE 1993; WILSON and MATTHEWS 2016). As the studied landforms did not show signs of post-depositional disturbance, the SHD ages were interpreted as maximum ages for boulder stabilization and the landform becoming inactive. Beneath all studied landforms older boulders were present, consequently, the SHD ages were treated as minimum ages of landform initiation (WILSON and MATTHEWS 2016).

3.1.2 Age Calibration

Age estimations by SHD require a calibration curve, constructed by independently numerically dated control points (SHAKESBY et al. 2006; MATTHEWS et al. 2013). Subsequently, it was possible to relate R-values of previously undated surfaces to surface exposure ages (STAHL et al. 2013). Based on young and old control points, separate calibration equations for the eastern and western part of South Norway have been calculated (for details see MARR et al. 2018, 2019a), from which calibration curves with a standard linear regression have been derived (MATTHEWS and OWEN 2010). The accuracy of the age estimates derived by the calibration curves are largely dependent on the reliability of the control sites (MATTHEWS and OWEN 2010; WINKLER 2014). The estimation of the uncertainties for the SHD ages of the sampling and the control sites were determined by the calculation of the 95% confidence interval (WINKLER 2009). The young control point for the high-precision calibration equation at Blåhø was established from a construction site where boulders were ‘freshly’ exposed to the surface. The old control points were derived from previously ^{10}Be dated bedrock outcrops at Blåhø by GOEHRING et al. (2008). In order to test the assumption of linear weathering relationship beyond the Holocene towards the Late Glacial (MATTHEWS and WILSON 2015; WINKLER and LAMBIEL 2018) two old control sites have been investigated with ages of 11.4 ± 1.0 ka and 15.0 ± 1.1 ka dated by GOEHRING et al. (2008). In the western study area it was not possible to derive a high-precision calibration equation due to the lack of previously numerically dated rock surfaces suitable for an old control point. Therefore, already existing data from a locality about 50 km north-east of the western study site were utilized (MATTHEWS et al. 2016) due to its lithological similarity to the migmatitic gneiss at Dalsnibba. Following WINKLER and MATTHEWS (2014), these R-values were converted as the mechanical Schmidt hammer was used in the study by MATTHEWS et al. (2016). Two young control points were derived from a location next to a construction site at Dalsnibba where ‘fresh’ boulders were exposed to the surface. The consequences of the application of a local high-precision in the east and a regional calibration curve in the west are discussed in chapter 4.3.

Following previously published SHD calibration curves, a linear relationship between R-values and age among the young and old control points have been assumed (WINKLER et al. 2016; WILSON et al. 2017). The linear relationship was mostly stressed within the Holocene, sometimes even beyond (SÁNCHEZ et al. 2009; MATTHEWS and WINKLER 2011; TOMKINS et al. 2016). This is sustained by the notion that resistant bedrock (e.g. hard crystalline) types in periglacial environments tend to have slow and practically linear weathering rates throughout the Holocene (COLMAN 1981; NICHOLSON 2008).

3.2 Terrestrial Cosmogenic Nuclides (TCN)

The build-up of cosmogenic nuclides, such as ^{10}Be or ^{26}Al by secondary cosmic rays, has been applied for surface exposure age dating in order to assess the duration of surface exposure near or at the earth’s surface (BALCO et al. 2008). The application of TCN in glacial environments to constrain the timing and dynamics of deglaciation relies on multiple assumptions. It is necessary that the samples were uniformly exposed to the surface throughout a single period only. Therefore, any inherited cosmogenic nuclide concentration accumulated prior the last deglaciation is assumed to have been removed by erosional processes (FABEL et

al. 2002; BRINER et al. 2006). Consequently, the amount of cosmogenic nuclides in a sample exemplifies the past erosive capacity of ice sheets. As the erosive capability of ice sheets is strongly related to the basal ice temperature, it is possible to distinguish between cold- and warm-based ice (low- and high-erosive) reflecting englacial boundaries, or can help to evaluate past ice-thickness of warm-based glaciers (KLEMAN 1994; HARBOR et al. 2006). Furthermore, the sample should not have been influenced by burial, erosion or snow shielding (STROEVEN et al. 2002; BRINER et al. 2006). In this thesis exposure ages were obtained from a single nuclide (^{10}Be) which were interpreted as minimum ages (DUNAI 2010). Details on laboratory procedures and protocols used are given in MARR et al. (2019b).

3.2.1 Research Design and Age Calculation

The aim at the western study site was to establish the first local deglaciation chronology and to gain information on the erosional and thermal properties of the palaeo-ice sheet. By sampling both bedrock and a glacially transported boulder lying on top of glacially modified bedrock, it is potentially possible to obtain these information (FABEL et al. 2002; HEYMANN et al. 2011). Therefore, four bedrock sites and one glacially transported boulder have been sampled. The bedrock samples were obtained from glacially eroded bedrock surfaces from four different elevations between 1476 m a.s.l. to 1334 m a.s.l. (for details see MARR et al. 2019b). The original plan to sample a vertical transect from the summit to the valley bottom of the proximal Opplendskedalen down to ~ 1050 m a.s.l. had to be omitted due to limited accessibility or unsuitable site conditions. The glacially transported boulder showed similar lithological properties present on Dalsnibba, seated on a glacially eroded bedrock surface in the summit area. The samples from Blåhø add two new exposure ages to the existing deglaciation chronology from GOEHRING et al. (2008). One sample was obtained from a bedrock outcrop from the summit of Blåhø, in proximity one erratic boulder sitting on the blockfield was sampled. Generally, with this limited dataset conclusive statements about the deglaciation history at Blåhø and identifying potential outliers as well as geological bias were not feasible (STROEVEN et al. 2016). However, the ages provide valuable new insights into the erosive capacity of the ice sheet and help to validate numerical ages from the previous deglaciation chronology (GOEHRING et al. 2008).

Age calculations were carried out with the online exposure age calculator version 3, formerly known as the CRONUS-Earth online exposure age calculator (BALCO et al. 2008; BALCO 2017, <http://hess.ess.washington.edu/>). The ages further discussed below were calculated with an assumed erosion of 1 mm ka^{-1} and without shielding by snow, vegetation or sediment. Post-glacial glacio-isostatic rebound was considered in the calculation with an uplift of 30 m for Dalsnibba and 100 m for Blåhø (for details see MARR et al. 2019b).

4 Results and Discussion

The main results of this thesis are presented together with the research context of the publications. Linking the findings from MARR et al. (2018, 2019a, 2019b) allows to reconstruct the (de)glaciation history on Dalsnibba and Blåhø following the LGM as well as to establish deglaciation scenarios on the basis of exposure ages and morphodynamic implications of periglacial and related landforms. Applying consistent methodology in both study areas ensures comparable results and opens the possibility to integrate them in a wider context.

4.1 Dalsnibba

The surfaces exposure ages offer the opportunity to construct the first deglaciation chronology of Opplendskedalen and the summit of Dalsnibba. The anomalously old boulder age (16.5 ± 0.6 ka) in relation to previous estimates of the timing deglaciation (NESJE and DAHL 1993) and the bedrock ages from comparable altitudinal setting (13.3 ± 0.6 to 12.7 ± 0.5 ka) have led to the assumption that the boulder shows cosmogenic nuclide inheritance. Consequently, the boulder age did not reflect the timing of deglaciation. The bedrock samples did not show inheritance, implying that glacial erosion was sufficient to remove previously accumulated nuclides. High-erosive warm-based ice was most likely responsible for the removal of previously accumulated cosmogenic nuclides in bedrock, which agrees with earlier findings (e.g. AARSETH et al. 1997). The presence of warm-based ice and a palaeo-ice thickness of at least 1476 m a.s.l. at Dalsnibba during the LGM is supported by the deposition of the sampled boulder in the summit area. Accumulation of the inherited cosmogenic nuclides in the boulder could have occurred during transport or by accumulation of deep ^{10}Be production by muons (BRINER et al. 2016). However, this is most likely not applicable for these samples as higher elevations sites were not prone to this as neutron produced ^{10}Be production rapidly increases with altitude (BRINER et al. 2016). By increasingly slower retreat rates of the SIS (14 – 12 ka, HUGHES et al. 2016) parts of the boulder might already have been exposed to cosmic radiation, whereas the deposition together with the subsequent ice disappearance at the summit took until 13.3 ± 0.6 to 12.7 ± 0.5 ka. These results represent the first minimum palaeo-ice thickness estimation based on terrestrial numerical evidence in this area. They oppose the concept that the ice cover in coastal areas was relatively thin, with possible ice-free high coastal areas (NESJE et al. 1987; MANGERUD 2004; WINGUTH et al. 2005).

Furthermore, it is possible to narrow down the potential time window of the timing of deglaciation. According to the uppermost bedrock ages the deglaciation started between 13.3 ± 0.6 to 12.7 ± 0.5 ka. Dalsnibba became ice-free during the end of Bølling–Allerød Interstadial (14.7 – 12.9 ka) which corresponds with the estimated deglaciation timing at Storfjord (LONGVA et al. 2009) and the modelled deglaciation by HUGHES et al. (2016). On the basis of the overlap between the bedrock ages and the Greenland Interstadial 1a (13.3 – 12.9 ka, RASMUSSEN et al. 2014), it is suggested that the timing of deglaciation most likely occurred during the latter. Moraines in Sweden suggested a comparable timing of deglaciation (STROEVEN et al. 2016) and the timing of glacier retreat at Dalsnibba is also overlapping with the latest of the three ice margin fluctuations between 25 and 12 ^{10}Be ka (RINTERKNECHT et al. 2004, 2005, 2006). In the light of this, a rather late ice-free situation on Dalsnibba is suggested within the range of the bedrock ages. Another implication

derived by the surface exposure ages is that the summit was most likely ice-free during the YD which is supported by ice-free conditions in nearby mountain plateaus of Dovrefjell (cf. MANGERUD 2004).

The bedrock results towards the valley bottom inferred that ice persisted at about 1330 m a.s.l. until 10.3 ± 0.5 ka. It was during this time when final local deglaciation was suggested for the region 11.2 ± 0.4 and 10.9 ± 0.2 cal. ka BP (cf. NESJE and DAHL 1993, calibration from HUGHES et al. 2016). Consequently, it is likely that the ice cover at Dalsnibba persisted longer than previously assumed and also longer than in the neighbouring Reinheimen region (11 ± 0.2 ka, ANDERSEN et al. 2018a), except for the possibility that the final deglaciation stage included a sudden ice collapse (MARR et al. 2019b). A longer ice cover might be explained by the persistence of a local ice-cap or a glacier readvance during the YD. In order to comprehensively assess the rate of deglaciation, the evaluation of the surface exposure ages by SHD can be helpful in places where TCN samples could not be obtained. The SHD age from the valley bottom sheds light into the largely unknown timing of final deglaciation in the Scandinavian mountains (cf. HUGHES et al. 2016). The final deglaciation is thought to have been completed by ~ 9 ka (LUNDQVIST and MEJDAHL 1995; NESJE et al. 2004; HARBOR et al. 2006) or slightly earlier (FABEL et al. 2006), the SHD age of 7.47 ± 0.73 ka indicates a longer residual ice body at the valley bottom. This suggests a thinning rate of ~ 7.3 cm yr⁻¹, LINGE et al. (2007) calculated comparable a rate for an inland location. The origin of the ice body persisting in the valley bottom remains elusive, possibly remnants of the YD readvance survived the following climate amelioration and covered the area through the short climate deterioration known as the ‘Finse Event’ ($\sim 8.4 - 8.0$ cal. ka BP, NESJE and DAHL 2001). As the ‘Finse Event’ overlaps with the valley bottom surface exposure age, it is proposed that Opplendskedalen became ice-free following the ‘Finse Event’. This timing seems plausible compared to largely retreating glaciers in Norway and Scandinavia (NESJE 2009; SOLOMINA et al. 2015).

Furthermore, SHD ages and R-value characteristics have the capability to explore the climate variations and periglacial processes during the mid-/late-Holocene at the valley bottom and its surroundings. Most of the studied boulder-related periglacial and related landforms have been stabilized within the Holocene Thermal Maximum (HTM, $\sim 8.0 - 5.0$ ka, CLARK et al. 2009), shortly after the deglaciation of Opplendskedalen. The investigated rock-slope failures mostly stabilized during the HTM which is supported by BÖHME et al. (2015) and HERMANNNS et al. (2017). Climatically induced factors, such as increased cleftwater pressure, permafrost degradation and enhanced freeze-thaw activity, caused by increasing temperatures and precipitation pattern changes, are considered amongst others, as important triggering mechanisms (e.g. BLIKRA et al. 2006; MCCOLL 2012; BALLANTYNE et al. 2013). Most likely, RSFs were related to the interplay of long-term stress release and triggering factors linked to warming climate or subsequent, slow permafrost degradation (MARR et al. 2019a). RSFs occurrences during warm periods were supported by findings from MATTHEWS et al. (2018) from nearby Jotunheimen. This opposes the concept that RSFs occur shortly after local deglaciation (BALLANTYNE et al. 2014). The interpretation that causes of RSFs were climatically controlled has been strengthened by the conceptual rock-slope failure model developed by MATTHEWS et al. (2018). However, one RSF was recorded which most likely did not occur during a warm phase, implying delayed response to prolonged paraglacial stress release throughout the Holocene by climate variability (MARR et al.

2019a). However, single factors triggering RSFs cannot be identified because they can act in various combinations along different time scales where cause and effect can hardly be distinguished (cf. MARR et al. 2018).

The geomorphological dynamics of the different landforms can be explored by the characterization and distribution of R-values. The non-uniform boulder populations observed at some of the investigated landforms suggest that those share complex diachronous formation histories (MARR et al. 2018, 2019a). This was reflected in the broad confidence intervals and platykurtic distribution of the R-values indicating reactivation or reworking of already existing landforms or the continuing supply of debris after the initial event, e.g. at RSFs (see MARR et al. 2019a). Boulder-dominated periglacial landforms are expected to increase in dynamism during cooler climatic conditions (e.g. BALLANTYNE and HARRIS 1994; WILSON et al. 2017) and landforms can be reactivated as old, pre-weathered boulders were transported to the surface by frost heave or other processes, leading to negative skewness. Therefore, the mixed age of the pronival rampart can be interpreted as a continuous build-up of the landform most likely since the beginning of the Holocene (MARR et al. 2019a). In contrast to this, a rather uniform boulder population, e.g. RSF-II second fan, suggested that they formed during a single event. Due to the high amount of high R-values within the population of RSF-II first fan, it is inferred that fan was still fed by rockwall above and that landform formation is still active even though the landform appears inactive (MARR et al. 2019a).

4.2 Blåhø

According to the TCN results from MARR et al. (2019b) and the previously published deglaciation chronology from GOEHRING et al. (2008), generally two scenarios for the (de)glaciation history for Blåhø are conceivable:

1) The boulder age of 20.9 ± 0.8 ka represents the timing of deglaciation and is broadly in agreement with the recalculated boulder age sampled by GOEHRING et al. (2008) of 21.8 ± 1.6 ka (MARR et al. 2019b). This appears plausible as ice retreat was suggested after the peak of global ice volume during the LGM between 23 – 21 ka (CLARK et al. 2009). Glacier retreat on Blåhø could be a response to the observed warming at GISP 2 between ~ 24 – 21 ka (cf. GOEHRING et al. 2008). In this scenario, the bedrock age of 46.4 ± 1.7 ka indicates that the summit experienced negligible erosion during the last glaciation. A possible explanation is the coverage by low-erosive cold-based ice protecting the bedrock from glacial erosion which can also explain the inherited cosmogenic nuclide inventory. This scenario is the most favoured option for Blåhø and surroundings for some authors (KLEMAN and HÄTTESTRAND 1999; BOULTON et al. 2001; GOEHRING et al. 2008). Taking into account the ~ 21 ka of exposure since deglaciation, the bedrock sample is supposed to have been exposed for a cumulative time of ~ 25 ka prior deglaciation. Depending on the glaciation history model, it seems possible that the blockfield was exposed since the early Weichselian or the Eem Interglacial according to the time scale from MANGERUD (2004).

However, there are indications that this scenario might have to be partly reconsidered. The melting of cold-based ice covering the blockfield would have left geomorphological traces, e.g. meltwater channels cutting

through the blockfield (SOLLID and SØRBEL 1994) which cannot be observed at Blåhø. Additionally, interpreting the trimline as an englacial boundary is not unproblematic as thermal boundaries might be unstable and change frequently, unable to produce a well-defined trimline (NESJE et al. 1987). NESJE and DAHL (1990) point out that the boundary between warm- and cold-based ice are commonly not parallel to the ice surface. Also TCN ages from glacially transported boulders are not unproblematic, age estimations might be erroneous because of post-depositional disturbance or shielding by sediment, following upward migration and surface exposure by upheave (BRINER et al. 2006; HEYMANN et al. 2011). Interestingly, the timing of blockfield stabilization underneath the sampled boulder is determined at ~ 18 ka, close the inferred time of boulder deposition. This could be either explained by rapid thinning of the ice-sheet on Blåhø with both features becoming exposed to the surface at $\sim 4 - 2$ ka apart from each other or the prevailing periglacial (and ice-free) environment with permafrost conditions together with frost-heave processes which have led to the upheave and subsequent boulder deposition. Shortly after this, the blockfield formation has ceased as climate conditions became warmer and the blockfield surface stabilized. In this case the boulder would not reflect the timing of deglaciation but the timing of exhumation. Additionally, it can be ruled out that initial blockfield formation occurred following the deglaciation in scenario 1 because the timing of formation with $4 - 2$ ka is not sufficient (e.g. BALLANTYNE 2010). Due to the blockfield's old appearance, subsurface structure (MARR and LÖFFLER 2017), the negative skewness of R-values as well as indications that blockfields probably can date back to the Tertiary (REA et al. 1996), it is suggested that the initial formation began prior the LGM.

2) Assuming that the bedrock nuclide concentration did not involve inherited cosmogenic nuclides, the summit of Blåhø was probably a nunatak during the LGM. The bedrock age corresponds with the Greenland Interstadial 12 (RASMUSSEN et al. 2014) supporting the possibility that the summit became ice-free during this time and escaped ice-cover since then. Additionally, WOHLFAHRT (2010) suggest that the SIS had completely melted away during the early part of MIS 3 (60 – 45 ka) which alternates with the Bø/Austnes Interstadial (MANGERUD et al. 2010) during which parts of Sweden were ice-free (WOHLFAHRT 2010). Prolonged ice-free conditions on Blåhø appear to have been possible in the light of the suggested ice-free conditions at nearby Skåla (BROOK et al. 1996), model results indicating ice-free locations during the LGM (WINGUTH et al. 2005) and the unclear Early/Middle Weichselian glaciation history of Norway (MANGERUD 2004). Recent findings from STEER et al. (2012) and ANDERSEN et al. (2018b) have inferred that high-elevation low-relief areas in south-central Norway significantly contributed to erosion and were consequently not covered by cold-based low-erosive ice. A nunatak situation is also feasible when considering ice-flow dynamics. Within the first stage the rather thick ice sheet, covered the Norwegian Channel, and transported erratics to Denmark. Subsequently, ice streams developed from the shelf edge upstream, causing major ice thinning further inland (MANGERUD 2004). However, due to the limited sample size on Blåhø no conclusive statement about its glaciation history can be made.

SHD ages and R-value characteristics of the different landforms reveal information about climate variations following the LGM. In general, the investigated landforms appear have been inactive with platykurtic R-

value distributions and broad confidence intervals indicating complex, long-term formation histories. In the wake of a cold climate event, it has been suggested that boulder-related landforms were (re)activated as they are largely associated with permafrost, often occurring following the local deglaciation (BALLANTYNE and HARRIS 1994; LILLEØREN et al. 2012). The stabilization periglacial landforms located above 1450 m a.s.l. could be correlated for the first time with the Karmøy/Bremanger readvance (~18.5 – 16.5 ka) which has been observed in both western and southern Norway (WINGUTH et al. 2005; OLSEN and BERGSTRØM 2007) and has also been detected in an ice advance into the North Sea from the British Ice Sheet (cf. HUGHES et al. 2016). Additionally, this cold stage overlaps with Heinrich event I at ~16.8 cal. ka BP (HEMMING 2004). Hence, it is striking that the periglacial landforms above 1450 m a.s.l. appear to not have been reactivated by several cold climatic events during the Late Glacial and Holocene. These cold climate events comprise the YD, the ‘Erdalen Event’ (10.1 – 9.7 cal. ka BP), the ‘Finse Event’, the Neoglacial (starting at ~6 ka) and the ‘Little Ice Age’ just to mention a few (SEJRUP et al. 2000; MATTHEWS and DRESSER 2008; Nesje 2009). Possibly, the non-reactivation was linked to the structural strength of the landforms, insufficient moisture supply, changes in freeze-thaw conditions and decreasing frost susceptibility of deformable sediment in the inner part of sorted polygons, resulting in the cessation of frost sorting (WINKLER et al. 2016; MARR et al. 2018). Important indications for the magnitude of the YD in the area can be derived from the obtained exposure ages. With the deglaciation ages from GOEHRING et al. (2008) and the landform dynamics by MARR et al. (2018, 2019b) it becomes evident that the summit area has escaped the YD readvance which is supported by MANGERUD (2004). Despite the formation of YD moraines close to Blåhø at Lesjakog (FOLLESTAD 2007), the summit area escaped re-glaciation. Concerning the palaeo-ice thickness, a rather thin SIS is expected, either due to cold-based ice coverage or the ice-free location on Blåhø and the topographical dependent glaciers in the surrounding valleys.

The Rundhø blockfield, along with the blockstream, stabilized earlier, during the Tampen readvance ~22 – 19 ka (SEJRUP et al. 2009). The stabilization of the sorted polygons at the foot of Rundhø occurred most likely at the beginning of the Karmøy/Bremanger readvance. Both landform stabilizations have been associated with decreasing temperatures and declining moisture supply leading to the termination of frost sorting and heaving processes (cf. MARR et al. 2018). These findings are in contrast to the deglaciation chronology by GOEHRING et al. (2008) as they have suggested cold-based ice coverage and slow thinning down to ~1450 m a.s.l. at 15.0 ± 1.0 ^{10}Be ka. Based on the results from MARR et al. (2018) a severe periglacial climate without ice coverage since about 19 ka at Rundhø was indicated. Age and characteristics of the RSFs studied around Blåhø have implied that they occurred during warm phases during the Late Glacial and the Holocene (MCCOLL 2012, see chapter 4.4) and not shortly after deglaciation (CRUDEN and HU 1993). For instance, RSF II appeared to have occurred towards the end of the Bølling–Allerød Interstadial, which is accordance with the Greenland Interstadial 1a (13.3 – 12.9 ka) (RASMUSSEN et al. 2014) and overlaps with the deglaciation of Dalsnibba.

4.3 Methodological Implications

Connecting the findings from several articles with similar research design offers the possibility to reflect methodological aspects related to the application of different surface exposure dating techniques. The comparison of the results from SHD applied in this thesis with similar studies shows that the obtained numerical ages are plausible and reliable (e.g. MATTHEWS and OWEN 2010; SHAKESBY et al. 2011; WINKLER et al. 2016). Due to similar SHD sampling strategy (e.g. two impacts per boulder) it is possible to compare calibration curves (Table 1, Figure 3) and results. The most important difference lies between the local high-precision calibration-curve in the eastern and a rather regional calibration curve in the western study area. Problematic about the latter approach was that the old control point had to be derived from a non-local source and can therefore not account for lithological differences present at the initial study site (cf. MARR et al. 2019a). Therefore, it is expected that the age accuracy of the landforms in the western study area was weakened. However, exploring the uncertainties involved in the SHD studies shows that the landforms in the west have a mean total uncertainty of 0.64 ka, the eastern landforms of 0.92 ka. This difference can most likely be explained by the landform ages itself. The landforms from the west were of mid-/late-Holocene age and generally exhibited lower R-value uncertainties, because lithological inhomogeneities usually become more pronounced with time, as evident in the landforms from the east (see MATTHEWS et al. 2013). There, the landforms have higher standard deviations and confidence intervals. Significant difference of the estimated landform ages based on the different calibration curve calculations cannot be observed. The age error seems to be negligible in comparison with statistical and other inaccuracies involving SHD as also shown by MATTHEWS et al. (2014). Further, it was shown in a previous study that the application of a non-local old control point can be successful (MATTHEWS et al. 2014) and the control point measurements from WILSON et al. (2017) from the similar lithology show comparable results.

Table 1: Schmidt hammer R-values and statistics for the control sites from the western (MARR et al. 2019a) and eastern (MARR et al. 2018) study area. Mean R-values are obtained from the means of two impacts on each boulder, 95% confidence intervals were calculated from the number (n) of sampled boulders.

Control point	Age (in yr) ^a	R-value	σ	95% CI ^b	Kurtosis	Skewness	Boulders (n)
Young (west)	3	70.3	5.22	0.51	-0.37	-0.38	200
Young (east)	1	68.3	4.62	0.45	-0.45	0.52	200
Old (west)	11500	40.3	-	2.4			
Old (east) ^c	11400	49.7	9.84	0.97	-0.81	-0.15	200

^a Age and R-value from MATTHEWS et al. (2016), the used R-value for the calibration curve was 50.3.

^b Mean of R-values with 95% confidence intervals ($\alpha = 0.05$).

^c This is the old control point used in calculating the landform ages at (MARR et al. 2018).

For the purpose of improving accuracy, two young control points instead of one were used which were later amalgamated to one control point (MARR et al. 2019a). However, this does not necessarily improve the

reliability of the control point compared to the results of MARR et al. (2018). It seems that the amount of boulders measured for the control points are the key for an accurate determination of a young control point and not the amount of control points. In general, there are only minor differences between the young control points of both studies (Table 1). This shows that both approaches are adequate to produce statistically profound data. Unfortunately, due to the inaccessibility of the raw data from the old control point from MATTHEWS et al. (2016), it was not possible to compare the uncertainties between the old control points. To increase the number of old control points, with each point representing different age, could be a possible improvement for generating exposure ages with lower uncertainties. Especially, as the application of SHD beyond the Holocene requires reliable old control points as the linearity of calibration curves can decrease with time (SHAKESBY et al. 2011; MARR et al. 2018).

Both calibration curves are shown in Figure 3. The young and old control points from both study areas show comparable values with only minor differences (Table 1, Figure 3). This implies that both lithologies have comparable rock strength properties when being ‘freshly’ exposed and also when being aerially exposed for about 11 ka. The similarities between the young and old control points opens the possibility for testing whether a single control point for both, weathered and unweathered surfaces, could be used as ‘regional’ control points in a larger areas of similar lithological properties. It is interesting that despite the distance and the lithological variability between the two locations, only minor differences can be observed.

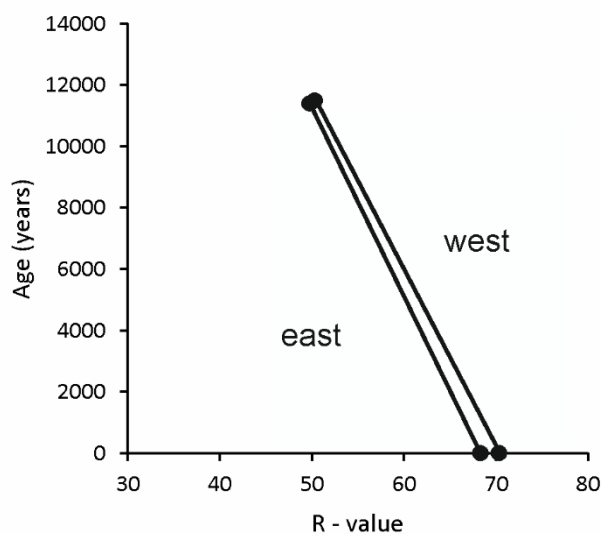


Figure 3: Calibration curves with old and young control points from the western and eastern study area.

Despite the successful application of the Schmidt hammer in this research its usage is not without obstacles. The SHD age from a moraine in the western study area showed that ages need to be assessed together with geomorphological evidences (MARR et al. 2019a). Ensuring this, problematic SHD ages can be identified and reconsidered. By integrating these aspects into the interpretation it became clear that the obtained moraine age did not reflect the true landform age, but was an overestimation. This was related to the reworking and reactivation of the landform leading to the exposure of older boulders to the surface. This shows the

importance of geomorphological analysis in order to avoid potential misinterpretations by simply relying on numerical surface exposure ages from e.g. TCN (WINKLER 2018).

Cosmogenic nuclides have shown to be a valuable tool to explore the deglaciation dynamics, even though a larger sample size would have been desirable. However, as mentioned above, a straightforward interpretation of the numerical ages without taking into account geomorphological factors can result in misinterpretations (WINKLER 2018). The ^{10}Be boulder age from Dalsnibba might be interpreted as the timing of deglaciation, but when considering the sampling location and the ages of the bedrock samples in proximity, it became clear that the boulder showed cosmogenic nuclide inheritance. Therefore, the bedrock ages from the summit were used to estimate the timing of deglaciation. Constructing the deglaciation chronology with the available samples was challenging as not all parts of the mountain could be sampled to generate a valuable vertical transect with TCN. Hence, SHD ages were partly able to fill this gap which made it possible to construct the deglaciation chronology.

4.4 Implications for the Deglaciation History of Southern Norway

This thesis contributes new aspects to the ongoing discussion about the deglaciation in South Norway. Exploring the obtained deglaciation chronologies in a regional context, especially in the light of recent deglaciation ages from Reinheimen (ANDERSEN et al. 2018a), located between the study areas, might reveal new insights into regional deglaciation dynamics. Based on the timing of deglaciation from Dalsnibba with $13.3 \pm 0.6 - 12.7 \pm 0.5$ ka, it appears that the deglaciation in the western part in South Norway has started earlier compared to the assumed timing of deglaciation in Reinheimen at 11 ± 0.2 ka (ANDERSEN et al. 2018a). Accepting that the boulder age from Blåhø represents the timing of deglaciation (20.9 ± 0.8 ka), the comparison with Reinheimen reveals a divergence of the timing of deglaciation of about 10 ka, even though both areas are at comparable altitudes and only ~ 30 km apart. The deglaciation at Dalsnibba and Reinheimen have occurred rather late. HUGHES et al. (2016) pointed out that the LGM SIS lost half of its size already at the beginning of the Bølling–Allerød Interstadial. This underpins the asynchronous timing of deglaciation in Norway (e.g. STROEVEN et al. 2016). The differences in ^{10}Be ages further point to variable basal ice temperatures over a short distance in South Norway. Whereas the ice in the western study area was erosive and warm-based, it appears that the basal temperature properties changed to partly cold-based towards the east as suggested by the results from ANDERSEN et al. (2018a) in Reinheimen. However, they detected only a few bedrock ages showing inheritance.

Because of the proximity to areas investigated by ice-thickness models, it seems valuable to assess the applicability of existing ice-thickness models for Dalsnibba. The ice-thickness model (11 – 10 km resolution) brought forward by WINGUTH et al. (2005) for the area of Skåla (~ 25 km from Dalsnibba) shows an ice thickness of 1100 m a.s.l. at 12.7 ka. Around this time the summit of Dalsnibba was probably already recently ice-free and the vertical ice extent was ~ 350 m bigger than on Skåla during this time. Accepting the second Blåhø scenario (chapter 4.2) with ice-free conditions since about 46 ka, most of the models would overestimate ice-thickness in the south-central Norway during the LGM (e.g. PELTIER 2004). Blåhø would stand in line with Skåla, being one of the few nunataks in this area of Norway which could have wide-ranging

ramifications for the glaciation history of Scandinavia. However, this scenario has to be tested in more detail in the future.

With the TCN and SHD ages from Dalsnibba, it is now possible to draw a clearer picture of palaeoclimatic conditions from deglaciation into the mid-Holocene (Figure 4). Summarizing the above-mentioned results and implications, the deglaciation of Dalsnibba took about 5500 years. It started between 13.3 ± 0.6 and 12.7 ± 0.5 ka at the summit and terminated with the valley bottom, becoming ice-free shortly after the 'Finse event' around 7.47 ± 0.73 ka. Figure 4 shows both the aspects which could be answered in this thesis and which aspects remain elusive. The major problem of integrating the findings of this thesis to the regional context towards the west are the lack of numerical ages. The deglaciation ages were obtained from the few numerical age constraints from older studies which were based on radiocarbon dating, implying ice-free conditions at 13.5 ± 0.1 ka (REITE 1968, Figure 4, green star 2, calibrated by HUGHES et al. 2016) and deglaciation at 13.8 ± 0.2 ka (HENNINGSEN and HOVDEN 1984, Figure 4, green star 3, calibrated by HUGHES et al. 2016). Therefore, the deglaciation history of large parts of the area from Dalsnibba towards the sea still remain unclear.

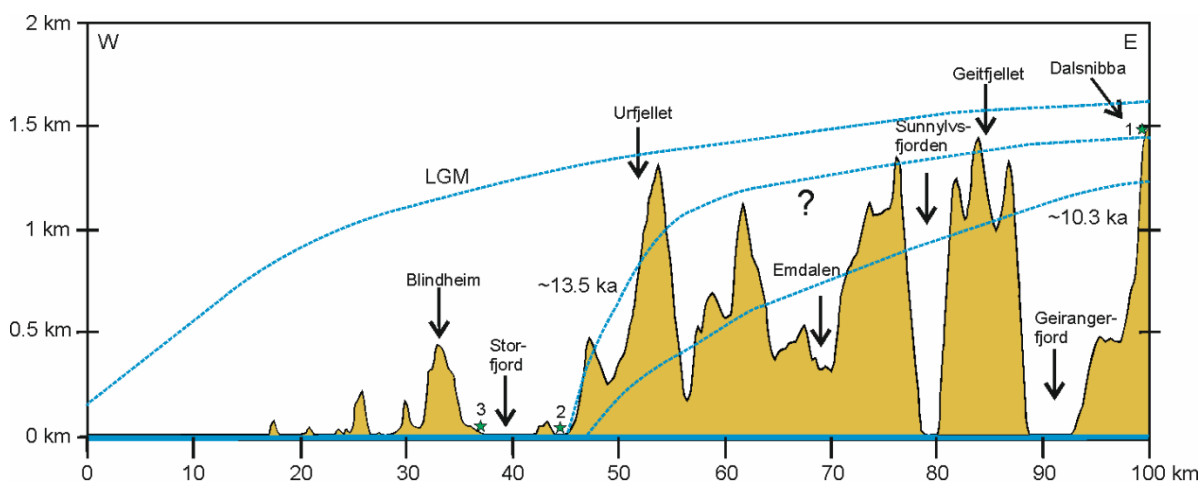


Figure 4: Topographic model with an west-east profile in western South Norway showing generalized the mountain summits and landform assemblages and the palaeo-ice thickness from the LGM to the early Holocene. The palaeo-ice thickness profile is indicated by the dashed blue line for time slices related to the ^{10}Be ages obtained from Dalsnibba. The location of numerical ages in the area are displayed by green stars, explanations in the text (modified after Gump et al. (2017)).

Maritime glaciers have been characterized by a higher mass-turnover than continental glaciers and are therefore anticipated to react faster to climatic changes (WINKLER et al. 2010; PAUL et al. 2011; STROEVEN et al. 2016). This behaviour is also expected for past glaciations. This could be tentatively be demonstrated with the age of the different periglacial and related landforms, as the western landforms reacted more sensitively to climate variability, especially within the Holocene, than those in the eastern study area (Figure 5). However, it has to be noted that the altitude where the landforms were investigated differed about 500 m and that in both cases boulder-related periglacial landforms were studied, but not exactly the same landform types. It cannot be ruled out that either younger landforms in the east or older landforms in the west could be found. Nevertheless, the results of the SHD appear to sustain the notion that western landforms reacted

more sensitively to climatic variability. RSFs from both areas occurred during the Bølling–Allerød Interstadial which were probably related to similar climatically induced processes leading to their occurrence (Figure 5). During warm climatic conditions precipitation changes and increased temperatures led to enhanced snow melt, permafrost degradation causing increased cleftwater pressure, and enhanced freeze-thaw activity which are expected as potential triggers of RSFs (MCCOLL 2012; BALLANTYNE et al. 2013; WILSON and MATTHEWS 2016; MARR et al. 2019a).

In sum, this demonstrates that rather small scale interstadials (within the last 130 ka, see RASMUSSEN et al. 2014) did have a measureable impact on landform evolution. At the same time as the deglaciation started on Dalsnibba, the RSF II on the foot of Blåhø occurred. This shows that climate variability has differently affected landscape evolution.

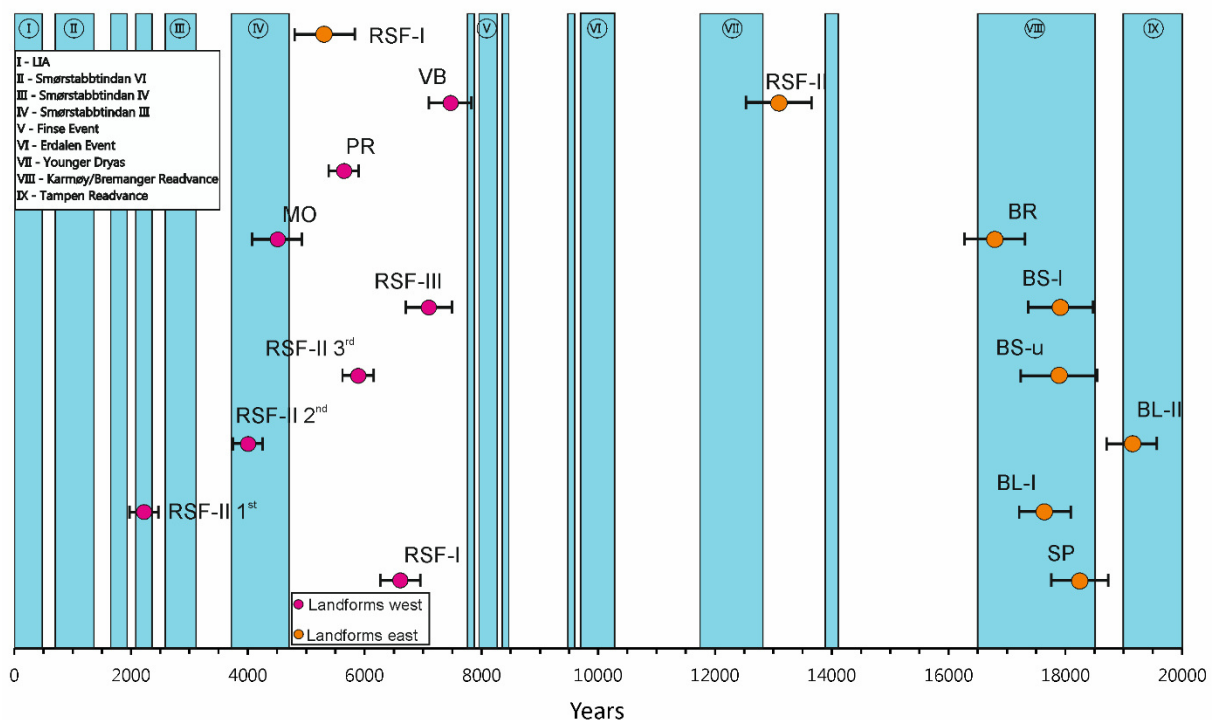


Figure 5: Plot showing all obtained Schmidt-hammer exposure-age dating results of periglacial and related landforms (Data from MARR et al. (2018, 2019a)). For abbreviations see MARR et al. (2018, 2019a). The exposure ages are plotted with their total error. Major cold climate events from 20 ka towards the present are drawn in blue (data from NYGÅRD et al. 2004; WINGUTH et al. 2005; OLSEN and BERGSTRØM 2007; MATTHEWS and DRESSER 2008; SEJRUP et al. 2009; LOHNE et al. 2013).

5 General Conclusions

This geomorphological and geochronological study provides new information on the timing of deglaciation and the response of periglacial and related landforms to climate variability since the Late Quaternary. In general, this thesis adds to evidences that point to a more complex and dynamic Scandinavian Ice Sheet throughout the last glacial cycle than previously assumed (RINTERKNECHT et al. 2006; MANGERUD et al. 2010). The research was conducted along the abovementioned four research questions and are answered as follows:

What were the timing and dynamics of local deglaciation in two selected areas of South Norway during and following the Last Glacial Maximum?

The first deglaciation chronology at Dalsnibba and surroundings in western South Norway shows that the local deglaciation started between 13.3 ± 0.6 to 12.7 ± 0.5 ka. Warm-based ice covered the summit of Dalsnibba during the Last Glacial Maximum up to at least 1476 m a.s.l. The ice subsequently lowered down to the valley bottom of Opplendskedalen with an average thinning rate of ~ 7.3 cm yr⁻¹ which became ice-free shortly after the 'Finse event' around ~ 7.5 ka. In sum, the deglaciation took about 5500 years from summit to valley bottom. Glacier readvances during the Younger Dryas have not reached the summit but most likely reached lower parts of the mountain, resulting in a longer ice persistence that previously assumed.

The timing of local deglaciation at Blåhø could not be finally resolved. Boulders at the summit were exposed to the surface at 20.9 ± 0.8 ka and 21.8 ± 1.6 ka (GOEHRING et al. 2008, recalculated by MARR et al. 2019b) the process resulting in this exposure ages can be explained by two models. The boulder age either reflects the timing of local deglaciation and the bedrock sample with 46.4 ± 1.7 ka showed inheritance of cosmogenic nuclides. Or the boulder age represents the timing of exhumation, as it is close the timing of stabilization of the blockfield which was characterized by active geomorphic processes such as frost-heave before its stabilization. Here, the age of the bedrock represents the timing of deglaciation. In this case, the summit was not ice-covered during the Last Glacial Maximum and the boulder age is erroneous due to shielding or reworking. The documented timing of blockfield stabilization on Blåhø requires ice-free conditions which colludes with inferred ice-coverage at this altitude at that time as suggested by GOEHRING et al. (2008). Based on this, it is assumed that the previous deglaciation chronology on Blåhø needs to be reconsidered. Together with growing evidence that parts of Greenland and Svalbard were ice-free during large parts of the Pleistocene (LANDVIK et al. 2003; SCHAEFER et al. 2016), geomorphic evidence and the inconsistencies of numerical ages, it appears possible that Blåhø has escaped the last glaciation.

It became clear that there is a strong need for more terrestrial numerical chronological data, especially in western South Norway, to better constrain the timing of deglaciation and ice-sheet characteristics during the Last Glacial Maximum. Therefore, an increase in surface exposure age data could be a vital point in interesting spatial situations, e.g. vertical transects from summit to fjord bottom. Due to the problems involving cosmogenic nuclides, e.g. post-depositional disturbance of boulders or inheritance (HEYMANN et

al. 2011), other numerical dating techniques such as optically stimulated luminescence from sediment underlying the blockfield should be considered. The application of paired cosmogenic nuclides (e.g. $^{10}\text{Be}/^{26}\text{Al}$, $^{10}\text{Be}/^{21}\text{Ne}$) seems to be a possible approach to explore the complex burial history of blockfield surfaces which was not undertaken yet to the knowledge of the author. In order to improve the understanding of the involved processes operating on present blockfields, the application of InSAR might be helpful to constrain vertical and horizontal displacement rates (FUHRMANN and GARTHWAITE 2019) and frequencies as shown on permafrost in Svalbard (ROUYET et al. 2019).

How did periglacial and related landforms react to climate variability following the Last Glacial Maximum and during the Holocene?

In general, periglacial and related landforms reacted on climate variability, especially to climate deteriorations. Schmidt-hammer exposure-age dating provided information on the landform dynamics through changing climatic conditions. R-value distributions provided insights into the timing of formation and stabilization of landforms, together with minimum and maximum age estimates from boulder configurations and exposure ages. Most landforms on Blåhø stabilized during the cold climate periods during the Karmøy/Bremanger and Tampen readvances in the Late Glacial. Landform responses to subsequent climate variability could not be reported despite severe cold events following their stabilization in the Holocene, the landforms were not reactivated. Within the western study area, the oldest landform was estimated to have been exposed to the surface since ~ 7.5 ka. This is significantly later than the exposure ages from the east which implies that western landforms reacted more sensitively to climatic changes, despite the differences of investigated landforms in both areas. It appears that boulder-dominated landforms located in maritime climatic conditions, as in the western study area, reacted more sensitively to Holocene climate variations than the continental influenced eastern landforms. However, landform responses were not limited to cold climate periods. Rocks-slope failures from the western study area indicated that they mostly stabilized during the mid-Holocene coinciding with the Holocene Thermal Maximum. This is generally associated with climate-driven factors, such as permafrost degradation and increasing cleftwater pressure resulting in slope instability. Rock-slope failures in both study areas did not support the concept of higher rock-slope failure frequencies shortly following deglaciation, but they tend to occur during warm periods, several millennia after the local deglaciation. The simultaneous occurrence of deglaciation at Dalsnibba and a rock-slope failure on Blåhø shows that climate variability is differently affecting the landscape. It could be demonstrated that rather small scale interstadials had a measureable impact on landform evolution.

Are periglacial and related landforms potential palaeoclimatic archives which can be explored by the application of Schmidt-hammer exposure-age dating in these area?

The successful application of Schmidt-hammer exposure-age dating in this thesis demonstrated that boulder-dominated landforms are an often overseen, but valuable source of palaeoclimatic information. After taking the necessary precautions for accurate sampling locations and strategy, the Schmidt hammer is a strong tool in Late Quaternary dating studies (WILSON et al. 2019). It could be shown that interstadials (e.g.

Bølling–Allerød) together with colder climate phases were manifested in distinct landforms in South Norway. For instance, due to Schmidt-hammer exposure-age dating cold climate periods such as the Karmøy/Bremanger readvance could be identified at periglacial landforms located above 1450 m a.s.l. for the first time in the Blåhø area. After the tentative previous reconstructions of the deglaciation reaching the Geirangerfjord, the timing of deglaciation can now be linked to the Bølling–Allerød Interstadial for the first time.

The application of Schmidt-hammer exposure-age dating over larger areas in Norway would be desirable. The Schmidt hammer is a cost and time efficient, user-friendly instrument and with conscious utilization it is possible to obtain a large dataset within a short time. The similarity of both calibration curves, despite their spatial and lithological differences showed that the possibility of regional calibration curves should be considered in the future. Already published calibration curves could be utilized in areas with similar lithological properties, therefore, the construction of single calibration curves for each study site would become obsolete. A potential future research prospect is to construct and test the application of a regional calibration curve for larger areas in southern Norway with similar or comparable lithology. However, the regional lithological variations might become obvious when sampling older surfaces causing significant differences between Younger Dryas and Preboreal surfaces (SHAKESBY et al. 2006). It is necessary to be aware of the detailed lithological differences and to explore their impact on the precision and accuracy of age estimates.

Which implications do the findings on the regional deglaciation history?

Reconstructing the timing and rates of deglaciation and processes involved on a local scale are crucial in the wake of a more dynamic Scandinavian Ice Sheet throughout the last glacial cycle. It was demonstrated that deglaciation started earlier in western South Norway in comparison to a nearby location towards the east. The divergence of the timing of deglaciation between the neighbouring Reinheimen area and Blåhø by ~10 ka point to an asynchronous timing of deglaciation, differing basal temperatures and variable ice thickness in South Norway. Considering the glaciation history of Blåhø involved parts of ice-free conditions during the Last Glacial Maximum, this would have consequences on the deglaciation history of the Eurasian Ice Sheet and the palaeo-ice thickness reconstructions from Scandinavia. A relatively thin ice sheet raises questions about the sea-level history during the transition from glacial to interglacial due to imbalances between global ice volume estimates and the sum of suggested ice volumes by glacial rebound histories (cf. WINGUTH et al. 2005).

In conclusion, this study presents new insights into the timing of deglaciation, the involved dynamics as well as the role of periglacial and related Late Quaternary and Holocene landforms as palaeoclimatic and morphodynamic proxies for two areas in South Norway. Additionally, the results contribute to a wider database of terrestrial numerical deglaciation estimates in the inner mountainous areas of western South Norway. Implementing these findings based on terrestrial sources might help to improve models reconstructing deglaciation history in South Norway.

6 References

- AARSETH, I., AUSTBO, P. K. and RISNES, H. (1997): Seismic stratigraphy of Younger Dryas ice-marginal deposits in western Norwegian fjords. In: *Norsk Geologisk Tidsskrift* 77, 65–85.
- ANDERSEN, B. G., MANGERUD, J., SØRENSEN, R., REITE, A., SVEIAN, H., THORESEN, M. and BERGSTRÖM, B. (1995): Younger Dryas ice-marginal deposits in Norway. In: *Quaternary International* 28, 147–169. [https://doi.org/10.1016/1040-6182\(95\)00037-J](https://doi.org/10.1016/1040-6182(95)00037-J)
- ANDERSEN, J. L., EGHOLM, D. L., KNUDSEN, M. F., LINGE, H., JANSEN, J. D., GOODFELLOW, B. W., PEDERSEN, V. K., TIKHOMIROV, D., OLSEN, J. and FREDIN, O. (2018a): Pleistocene Evolution of a Scandinavian Plateau Landscape. In: *Journal of Geophysical Research: Earth Surface* 123, 3370–3387. <https://doi.org/10.1029/2018JF004670>
- ANDERSEN, J. L., EGHOLM, D. L., KNUDSEN, M. F., LINGE, H., JANSEN, J. D., PEDERSEN, V. K., NIELSEN, S. B., TIKHOMIROV, D., OLSEN, J., FABEL, D. and XU, S. (2018b): Widespread erosion on high plateaus during recent glaciations in Scandinavia. In: *Nature Communications* 9, 830. <https://doi.org/10.1038/s41467-018-03280-2>
- ANDREASSEN, L. M. and WINSVOLD, S. H. (2012): Inventory of Norwegian Glaciers. Norwegian Water Resources and Energy Directorate (NVE), Oslo, Rapport 38-2012.
- BALCO, G. (2017): Production rate calculations for cosmic-ray-muon-produced ^{10}Be and ^{26}Al benchmarked against geological calibration data. In: *Quaternary Geochronology* 39, 150–173. <https://doi.org/10.1016/j.quageo.2017.02.001>
- BALCO, G., STONE, J. O., LIFTON, N. A. and DUNAI, T. J. (2008): A complete and easily accessible means of calculating surface exposure ages or erosion rates from ^{10}Be and ^{26}Al measurements. In: *Quaternary Geochronology* 3, 174–195. <http://dx.doi.org/10.1016/j.quageo.2007.12.001>
- BALLANTYNE, C. K. (1998): Age and Significance of Mountain-Top Detritus. In: *Permafrost and Periglacial Processes* 9, 327–345. [https://doi.org/10.1002/\(SICI\)1099-1530\(199810/12\)9:4<327::AID-PPP298>3.0.CO;2-9](https://doi.org/10.1002/(SICI)1099-1530(199810/12)9:4<327::AID-PPP298>3.0.CO;2-9)
- BALLANTYNE, C. K. (2010): A general model of autochthonous blockfield evolution. In: *Permafrost and Periglacial Processes* 21, 289–300. <https://doi.org/10.1002/ppp.700>
- BALLANTYNE, C. K. (2018): *Periglacial Geomorphology*. Oxford.
- BALLANTYNE, C. K. and HARRIS, C. (1994): *The Periglaciation of Great Britain*. Cambridge.
- BALLANTYNE, C. K., WILSON, P., SCHNABEL, C. and Xu, S. (2013): Lateglacial rock slope failures in north-west Ireland: Age, causes and implications. In: *Journal of Quaternary Science* 28, 789–802. <https://doi.org/10.1002/jqs.2675>
- BALLANTYNE, C. K., SANDEMAN, G. F., STONE, J. O. and WILSON, P. (2014): Rock-slope failure following Late Pleistocene deglaciation on tectonically stable mountainous terrain. In: *Quaternary Science Reviews* 86, 900–913. <https://doi.org/10.1016/j.quascirev.2013.12.021>
- BARRY, R. G. and GAN, T. Y. (2011): *The global cryosphere: past, present, future*. Cambridge.
- BARTZ, M. (2018): Quaternary fluvial environments in NE Morocco inferred from geochronological and sedimentological investigations. Dissertation, Universität zu Köln.
- BAUMHAUER, R. and WINKLER, S. (2014): *Glazialgeomorphologie – Formung der Landoberfläche durch Gletscher*. Stuttgart.
- BENISTON, M., FARINOTTI, D., STOFFEL, M., ANDREASSEN, L. M., COPPOLA, E., ECKERT, N., FANTINI, A., GIACONA, F., HAUCK, C., HUSS, M., HUWALD, H., LEHNING, M., LÓPEZ-MORENO, J. I., MAGNUSSON, J., MARTY, C., MORÁN-TEJEDA, E., MORIN, S., NAAIM, M., PROVENZALE, A., RABATEL, A., SIX, D., STÖTTER, J., STRASSER, U., TERZAGO, S. and VINCENT, C. (2018): The European mountain cryosphere: a review of its current state, trends, and future challenges. In: *Cryosphere* 12, 759–794. <https://doi.org/10.5194/tc-12-759-2018>
- BLIKRA, L. H., LONGVA, O., BRAATHEN, A., Anda, E., Dehls, J. F. and Stalsberg K. (2006): Rock slope failures in Norwegian fjord areas: Examples, spatial distribution and temporal pattern. In: EVANS, S. G., MUGNOZZA, G. S., STROM, A. and HERMANNNS, R. L. (eds.): *Landslides from Massive Rock Slope Failure*. Dordrecht, 475–496. https://doi.org/10.1007/978-1-4020-4037-5_26
- BLYTT, A. (1876): *Immigration of the Norwegian Flora*. Christiania.

- BOULTON, G. S., DONGELMANS, P., PUNKARI, M. and BROADGATE, M. (2001): Palaeoglaciology of an ice sheet through a glacial cycle: the European ice sheet through the Weichselian. In: *Quaternary Science Reviews* 20, 591–625. [https://doi.org/10.1016/S0277-3791\(00\)00160-8](https://doi.org/10.1016/S0277-3791(00)00160-8)
- BÖHME, M., OPPIKOFER, T., LONGVA, O., JABOYEDOFF, M., HERMANN, R. L. and DERRON, M.-H. (2015): Analyses of past and present rock slope instabilities in a fjord valley: Implications for hazard estimations. In: *Geomorphology* 248, 464–474. <https://doi.org/10.1016/j.geomorph.2015.06.045>
- BÖSE, M., LÜTHGENS, C., LEE, J. R. and ROSE, J. (2012): Quaternary glaciations of northern Europe. In: *Quaternary Science Reviews* 44, 1–25. <https://doi.org/10.1016/j.quascirev.2012.04.017>
- BRINER, J. P., MILLER, G. H., THOMPSON DAVIS, P. and FINKEL, R. C. (2006): Cosmogenic radionuclides from fiord landscapes support differential erosion by overriding ice sheets. In: *GSA Bulletin* 118, 406–420. <https://doi.org/10.1130/B25716.1>
- BRINER, J. P., GOEHRING, B. M., MANGERUD, J. and SVENDSEN, J. I. (2016): The deep accumulation of ^{10}Be at Utsira, southwestern Norway: Implications for cosmogenic nuclide exposure dating in peripheral ice sheet landscapes. In: *Geophysical Research Letters* 43, 9121–9129. <https://doi.org/10.1002/2016GL070100>
- BROOK, E. J., NESJE, A., LEHMAN, S. J., RAISBECK, R. M. and YIOU, F. (1996): Cosmogenic nuclide exposure ages along a vertical transect in western Norway: Implications for the height of the Fennoscandian ice sheet. In: *Geology* 24, 207–210. [https://doi.org/10.1130/0091-7613\(1996\)024<0207:CNEAAA>2.3.CO;2](https://doi.org/10.1130/0091-7613(1996)024<0207:CNEAAA>2.3.CO;2)
- ČERNÁ, B. and ENGEL, Z. (2011): Surface and sub-surface Schmidt hammer rebound value variation for a granite outcrop. In: *Earth Surface Processes and Landforms* 36, 170–179. <https://doi.org/10.1002/esp.2029>
- CLARK, P. U., DYKE, A. S., SHAKUN, J. D., CARLSON, A. E., CLARK, J., WOHLFARTH, B., MITROVICA, J. X., HOSTETLER, S. W. and MCCABE, A. M. (2009): The last glacial maximum. In: *Science* 325, 710–714. <https://doi.org/10.1126/science.1172873>
- CLARK, R. and WILSON, P. (2004): A rock avalanche deposit in Burtness Comb, Lake District, northwest England. In: *Geological Journal* 39, 419–430. <https://doi.org/10.1002/gj.965>
- COLMAN, S. M. (1981): Rock-weathering rates as functions of time. In: *Quaternary Research* 15, 250–264. [https://doi.org/10.1016/0033-5894\(81\)90029-6](https://doi.org/10.1016/0033-5894(81)90029-6)
- CRUDEN, D. M. and HU, X. Q. (1993): Exhaustion and steady state models for predicting landslide hazards in the Canadian Rocky Mountains. In: *Geomorphology* 8, 279–285. [https://doi.org/10.1016/0169-555X\(93\)90024-V](https://doi.org/10.1016/0169-555X(93)90024-V)
- DAHL, E. (1955): Biogeographic and geological indications of unglaciated areas in Scandinavia during the glacial ages. *Bulletin Geological Society of America* 66, 1499–1520. [https://doi.org/10.1130/0016-7606\(1955\)66\[1499:BAGIOU\]2.0.CO;2](https://doi.org/10.1130/0016-7606(1955)66[1499:BAGIOU]2.0.CO;2)
- DAHL, S. O., NESJE, A. and ØVSTEDAL, J. (1997): Cirque glaciers as morphological evidence for a thin Younger Dryas ice sheet in the east-central southern Norway. In: *Boreas* 26, 161–180. <https://doi.org/10.1111/j.1502-3885.1997.tb00850.x>
- DAHL, S. O., BAKKE, J., LIE, O. and NESJE, A. (2003): Reconstruction of former glacier equilibrium-line altitudes based on proglacial sites: An evaluation of approaches and selection of sites. In: *Quaternary Science Reviews* 22, 275–287. [https://doi.org/10.1016/S0277-3791\(02\)00135-X](https://doi.org/10.1016/S0277-3791(02)00135-X)
- DENN, A. R., BIERMANN, P. R., ZIMMERMANN, S. R. H., CAFFEE, M. W., CORBETT, L. B. and KIRBY, E. (2018): Cosmogenic nuclides indicate that boulder fields are dynamic, ancient, multigenerational features. In: *The Geological Society of America* 28, 4–10. <https://doi.org/10.1130/GSATG340A.1>
- DONNER, J. (1996): The early and middle Weichselian Interstadials in the central area of the Scandinavian glaciations. In: *Quaternary Science Reviews* 15, 471–479. [https://doi.org/10.1016/0277-3791\(96\)00002-9](https://doi.org/10.1016/0277-3791(96)00002-9)
- DUNAI, T. J. (2010): *Cosmogenic Nuclides: Principles, Concepts and Applications in the Earth Surface Sciences*. Cambridge. <https://doi.org/10.1017/CBO9780511804519>
- EHLERS, J., GIBBARD, P. L. and HUGHES, P. D. (2018): Quaternary Glaciations and Chronology. In: MENZIES, J. and VAN DER MEER, J. J. M. (eds.): *Past Glacial Environments*. Amsterdam, 77–101. <https://doi.org/10.1016/B978-0-08-100524-8.00003-8>

- FABEL, D., STROEVEN, A. P., HARBOR, J., KLEMAN, J., ELMORE, D. and FINK, D. (2002): Landscape preservation under Fennoscandian ice sheets determined from in situ produced ^{10}Be and ^{26}Al . In: *Earth and Planetary Science Letters* 201, 397–406. [https://doi.org/10.1016/S0012-821X\(02\)00714-8](https://doi.org/10.1016/S0012-821X(02)00714-8)
- FABEL, D., FINK, D., FREDIN, O., HARBOR, J., LAND, M. and STROEVEN, A. P. (2006): Exposure ages from relict lateral moraines overridden by the Fennoscandian ice sheet. In: *Quaternary Research* 65, 136–146. <https://doi.org/10.1016/j.yqres.2005.06.006>
- FARBROT, H., HIPPE, T. F., ETZELMÜLLER, B., ISAKSEN, K., ØDEGÅRD, R. S., SCHULER, T. V. and HUMMUM, O. (2011): Air and ground temperature variations observed along elevation and continentality gradients in Southern Norway. *Permafrost and Periglacial Processes* 22, 343–360. <https://doi.org/10.1002/ppp.733>
- FARETH, O. W. (1987): Glacial geology of Middle and Inner Nordfjord, western Norway. Geological Survey of Norway, Technical Report 408. Trondheim.
- FOLLESTAD, B. A. (2003): Development of minor late-glacial ice domes east of Oppdal, Central Norway. In: *Norges geologiske undersøkelse Bulletin* 441, 39–49.
- FOLLESTAD, B. A. (2007): Lesjaskog 1419 III. Preliminært kvartargeologisk kart M 1:50.000. Norges geologiske undersøkelse.
- FUHRMANN, T. and GARTHWAITE, M. C. (2019): Resolving Three-Dimensional Surface Motion with InSAR Constraints from Multi-Geometry Data Fusion. In: *Remote Sensing* 11, 241. <https://doi.org/10.3390/rs11030241>
- GJESSING, J. (1967): Norway's paleic surface. In: *Norsk Geologisk Tidsskrift* 21, 69–132.
- GOBIET, A., KOTLARSKI, S., BENISTON, M., HEINRICH, G., RAJCZAK, J. and STOFFEL, M. (2014): 21st century climate change in the European Alps – a review. In: *Science of The Total Environment* 493, 1138–1151. <https://doi.org/10.1016/j.scitotenv.2013.07.050>
- GOEHRING, B. M., BROOK, E. J., LINGE, H., RAISBECK, G. M. and YIOU, F. (2008): Beryllium-10 exposure ages of erratic boulders in southern Norway and implications for the history of the Fennoscandian Ice Sheet. In: *Quaternary Science Reviews* 27, 320–336. <https://doi.org/10.1016/j.quascirev.2007.11.004>
- GOODFELLOW, B. W. (2007): Relict non-glacial surfaces in formerly glaciated landscapes. In: *Earth-Science Reviews* 80, 47–73. <https://doi.org/10.1016/j.earscirev.2006.08.002>
- GOUDIE, A. S. (2006): The Schmidt Hammer in geomorphological research. In: *Progress in Physical Geography* 30, 703–718. <https://doi.org/10.1177/0309133306071954>
- GUMP, D. J., BRINER, J. P., MANGERUD, J. and SVENDSEN, J. I. (2017): Deglaciation of Boknafjorden, south-western Norway. In: *Journal of Quaternary Science* 32, 80–90. <https://doi.org/10.1002/jqs.2925>
- HARBOR, J., STROEVEN, A. P., FABEL, D., CLARHÄLL, A., KLEMAN, J., LI, Y., ELMORE, D. and FINK, D. (2006): Cosmogenic nuclide evidence for minimal erosion across two subglacial sliding boundaries of the late glacial Fennoscandian ice sheet. In: *Geomorphology* 75, 90–99. <https://doi.org/10.1016/j.geomorph.2004.09.036>
- HEMMING, S. R. (2004): Heinrich events: massive late Pleistocene detritus layers of the north Atlantic and their global climate imprint. In: *Reviews of Geophysics* 42, 1–43. <https://doi.org/10.1029/2003RG000128>
- HENNINGSEN, T. and HOVDEN, Ø. (1984): Weichsel stratigrafi, deglasiasjon, lokalglasiasjon og strandforskryvning i Alesundområdet. Masters Thesis, University of Bergen, Norway.
- HERMANN, R. L., SCHLEIER, M., BÖHME, M., BLIKRA, L. H., GOSSE, J., IVY-OCHS, S. and HILGER, P. (2017): Rock-Avalanche activity in W and S Norway peaks after the retreat of the Scandinavian ice sheet. In: MIKOŠ, M., VILIMEK, V., YIN, Y. and SASSA, K. (eds.): *Advancing Culture of Living with Landslides (WLF 2017)*. Cham, 331–338.
- HEYMANN, J., STROEVEN, A. P., HARBOR, J. M. and CAFFEE, M. W. (2011): Too young or too old: Evaluating cosmogenic exposure dating based on an analysis of compiled boulder exposure ages. In: *Earth and Planetary Science Letters* 302, 71–80. <https://doi.org/10.1016/j.epsl.2010.11.040>
- HOLTEDAHL, H. (1967): Notes on the formation of fjord and fjord-valleys. In: *Geografiska Annaler: Series A, Physical Geography* 49, 188–203. <https://doi.org/10.1080/04353676.1967.11879749>

- HUGHES, A. L. C., GYLLENCREUTZ, R., LOHNE, Ø. S., MANGERUD, J. and SVENDSEN, J. I. (2016): The last Eurasian ice sheets – a chronological database and time-slice reconstruction, DATED-1. In: *Boreas* 45, 1–45. <https://doi.org/10.1111/bor.12142>
- HUMLUM, O. (1998): Rock glaciers on the Faeroe Islands, the north Atlantic. In: *Journal of Quaternary Science* 13, 293–307. [https://doi.org/10.1002/\(SICI\)1099-1417\(199807/08\)13:4<293::AID-JQS370>3.0.CO;2-S](https://doi.org/10.1002/(SICI)1099-1417(199807/08)13:4<293::AID-JQS370>3.0.CO;2-S)
- HUSS, M., BOOKHAGEN, B., HUGGEL, C., JACOBSEN, D., BRADLEY, R. S., CLAGUE, J. J., VUILLE, M., BUYTAERT, W., CAYAN, D. R., GREENWOOD, G., MARK, B. G., MILNER, A. M., WEINGARTNER, R. and WINDER, M. (2017): Toward mountains without permanent snow and ice. In: *Earths Future* 5, 418–435. <https://doi.org/10.1002/2016EF000514>
- IPCC (2014): *Climate change 2013: The physical science basis. Contribution of working group I to the 5th Assessment report of the Intergovernmental Panel on Climate Change.* Cambridge.
- KASER, G., COGLEY, J. G., DYURGEROV, M. B., MEIER, M. F. and OHMURA, A. (2006): Mass balance of glaciers and ice caps: Consensus estimates for 1961–2004. In: *Geophysical Research Letters* 33 (L19501). doi:10.1029/2006GL027511
- KLEMAN, J. (1994): Preservation of landforms under ice sheets and ice caps. In: *Geomorphology* 9, 19–32. [http://dx.doi.org/10.1016/0169-555X\(94\)90028-0](http://dx.doi.org/10.1016/0169-555X(94)90028-0)
- KLEMAN, J. and HÄTTESTRAND, C. (1999): Frozen-bed Fennoscandian and Laurentide ice sheets during the Last Glacial Maximum. In: *Nature* 402, 63–66. <http://dx.doi.org/10.1038/47005>
- KLEMSDAL, T. and SJULSEN, E. (1988): The Norwegian macrolandforms: Definition, distribution and system of evolution. In: *Norsk Geologisk Tidsskrift* 42, 133–147. <https://doi.org/10.1080/00291958808552192>
- KUTZBACH, J., GALLIMORE, R., HARRISON, S., BEHLING, P., SELIN, R. and LAARIF, F. (1998): Climate and biome simulations for the past 21,000 years. In: *Quaternary Science Reviews* 17, 473–506. [https://doi.org/10.1016/S0277-3791\(98\)00009-2](https://doi.org/10.1016/S0277-3791(98)00009-2)
- LANDVIK, J. Y., BROOK, E. J., GUALTIERI, L., RAISBECK, G., SALVIGSEN, O. and YIOU, F. (2003): Northwest Svalbard during the last glaciation: Ice-free areas existed. In: *Geology* 31, 905–908. <https://doi.org/10.1130/G19703.1>
- LIFTON, N., SATO, T. and DUNAI, T. J. (2014): Scaling in situ cosmogenic nuclide production rates using analytical approximations to atmospheric cosmic-ray fluxes. In: *Earth and Planetary Science Letters* 386, 149–160. <https://doi.org/10.1016/j.epsl.2013.10.052>
- LILLEØREN, K. S., ETZELMÜLLER, B., SCHULER, T. V., GISNÅS, K. and HUMLUM, O. (2012): The relative age of permafrost – estimation of Holocene permafrost limits in Norway. In: *Global and Planetary Change* 92–93, 209–223. <https://doi.org/10.1016/j.gloplacha.2012.05.016>
- LINGE, H., BROOK, E. J., NESJE, A., RAISBECK, G., YIOU, F. and CLARK, H. (2006): In situ ¹⁰Be exposure ages from southeastern Norway: implications for the geometry of the Weichselian Scandinavian ice sheet. In: *Quaternary Science Reviews* 25, 1097–1109. <https://doi.org/10.1016/j.quascirev.2005.10.007>
- LINGE, H., OLSEN, L., BROOK, E. J., DARTER, J. R., MICKELSON, D. M., RAISBECK, G. M. and YIOU, F. (2007): Cosmogenic nuclide surface exposure ages from Nordland, northern Norway: implications for deglaciation in a coast to inland transect. In: *Norsk Geologisk Tidsskrift* 87, 269–280.
- LÖFFLER, J. and PAPE, R. (2004): Across scale temperature modelling using a simple approach for the characterization of high mountain ecosystem complexity. In: *Erdkunde* 58, 331–348. <https://doi.org/10.3112/erdkunde.2004.04.04>
- LOHNE, Ø. S., MANGERUD, J. and BIRKS, H. H. (2013): Precise ¹⁴C ages of the Vedde and Saksunarvatn ashes and the Younger Dryas boundaries from western Norway and their comparison with the Greenland Ice Core (GICC05) chronology. In: *Journal of Quaternary Science* 28, 490–500. <https://doi.org/10.1002/jqs.2640>
- LONGVA, O., BLIKRA, L. H., and DEHLS, J. F. (2009): Rock avalanches: distribution and frequencies in the inner part of Storfjorden, Møre og Romsdal County, Norway, Technical Report 2009.002, Geological Survey of Norway.
- LUNDQVIST, J. and MEJDAHL, V. (1995): Luminescence dating of the deglaciation in northern Sweden. In: *Quaternary International* 28, 193–197. [https://doi.org/10.1016/1040-6182\(95\)00031-D](https://doi.org/10.1016/1040-6182(95)00031-D)

- MANGERUD, J. (2004): Ice sheets limits in Norway and on the Norwegian continental shelf. In: EHLERS, J. and GIBBARD, P. L. (eds.): *Quaternary Glaciations Extent and Chronology*. Amsterdam, 271–294.
- MANGERUD, J., GULLIKSEN, S. and LARSEN, E. (2010): ¹⁴C-dated fluctuations of the western flank of the Scandinavian Ice Sheet 45–25 kyr BP compared with Bølling–Younger Dryas fluctuations and Dansgaard–Oeschger events in Greenland. In: *Boreas* 39, 328–342. [10.1111/j.1502-3885.2009.00127.x](https://doi.org/10.1111/j.1502-3885.2009.00127.x)
- MARR, P. and LÖFFLER, J. (2017): Establishing a multi-proxy approach to alpine blockfield evolution in south-central Norway. In: *AUC Geographica* 52, 219–236. <https://doi.org/10.14712/23361980.2017.18>
- MARR, P., WINKLER, S. and LÖFFLER, J. (2018): Investigations on blockfields and related landforms at Blåhø (Southern Norway) using Schmidt-hammer exposure-age dating: palaeoclimatic and morphodynamic implications. In: *Geografiska Annaler: Series A, Physical Geography* 100, 285–306. <https://doi.org/10.1080/04353676.2018.1474350>
- MARR, P., WINKLER, S. and LÖFFLER, J. (2019a): Schmidt-hammer exposure-age dating (SHD) performed on periglacial and related landforms in Opplendskedalen, Geirangerfjellet, Norway: Implications for mid- and late-Holocene climate variability. In: *The Holocene* 29, 97–109. <https://doi.org/10.1177/0959683618804634>
- MARR, P., WINKLER, S., BINNIE, S. A. and LÖFFLER, J. (2019b): ¹⁰Be-based exploration of the timing of deglaciation in two selected areas of southern Norway. In: *E&G Quaternary Science Journal* 68, 165–176. <https://doi.org/10.5194/egqsj-68-165-2019>
- MATTHEWS, J. A. (1992): *The Ecology of Recently-deglaciated Terrain: A Geocological Approach to Glacier Forelands*. Cambridge.
- MATTHEWS, J. A. and SHAKESBY, R. A. (1984): The status of ‘Little Ice Age’ in southern Norway: a relative-age dating of Neoglacial moraines with Schmidt hammer and lichenometry. In: *Boreas* 13, 333–346. <https://doi.org/10.1111/j.1502-3885.1984.tb01128.x>
- MATTHEWS, J. A. and DRESSER, P. Q. (2008): Holocene glacier variation chronology of Smørstabbtindan massif, Jotunheimen, Southern Norway, and the recognition of century- to millennial-scale European Neoglacial Events. In: *The Holocene* 18, 181–201. <https://doi.org/10.1177/0959683607085608>
- MATTHEWS, J. A. and OWEN, G. (2010): Schmidt hammer exposure-age dating: developing linear age-calibration curves using Holocene bedrock surfaces from the Jotunheimen–Jostedalbreen regions of southern Norway. In: *Boreas* 39, 105–115. <https://doi.org/10.1111/j.1502-3885.2009.00107.x>
- MATTHEWS, J. A. and WINKLER, S. (2011): Schmidt-hammer exposure-age dating (SHD): application to early Holocene moraines and a reappraisal of the reliability of terrestrial cosmogenic-nuclide dating (TCND) at Austanbotnbreen, Jotunheimen, Norway. In: *Boreas* 40, 256–270. <https://doi.org/10.1111/j.1502-3885.2010.00178.x>
- MATTHEWS, J. A. and WILSON, P. (2015): Improved Schmidt-hammer exposure ages for active and relict pronival ramparts in southern Norway, and their palaeoenvironmental implications. In: *Geomorphology* 246, 7–21. <https://doi.org/10.1016/j.geomorph.2015.06.002>
- MATTHEWS, J. A., NESJE, A. and LINGE, H. (2013): Relict Talus-Foot Rock Glaciers at Øyberget, Upper Ottadalen, Southern Norway: Schmidt hammer Exposure Ages and Palaeoenvironmental Implications. In: *Permafrost and Periglacial Processes* 24, 336–346. <https://doi.org/10.1002/ppp.1794>
- MATTHEWS, J. A., WINKLER, S. and WILSON, P. (2014): Age and origin of ice-cored moraines in Jotunheimen and Breheimen, southern Norway: Insights from Schmidt-hammer exposure-age dating. In: *Geografiska Annaler: Series A, Physical Geography* 96, 531–548. <https://doi.org/10.1111/geoa.12046>
- MATTHEWS, J. A., OWEN, G., WINKLER, S., VATER, A. E., WILSON, P., MOURNE, R. W. and HILL, J. L. (2016): A rock-surface microweathering index from Schmidt hammer R-values and its preliminary application to some common rock types in southern Norway. In: *Catena* 143, 35–44. <https://doi.org/10.1016/j.catena.2016.03.018>
- MATTHEWS, J. A., WINKLER, S., WILSON, P., TOMKINS M. D., DORTCH, J. M., MOURNE, R. W., HILL, J. L., OWEN, G. and VATER, A. E. (2018): Small rock-slope failures conditioned by Holocene permafrost degradation: A new approach and conceptual model based on Schmidt-hammer exposure-age dating in Jotunheimen, southern Norway. In: *Boreas* 47, 1144–1169. <https://doi.org/10.1111/bor.12336>

- MCCARROLL, D. (2016): Trimline trauma: the wider implications of a paradigm shift in recognising and interpreting glacial limits. In: *Scottish Geographical Journal* 132, 130–139. <https://doi.org/10.1080/14702541.2016.1157203>
- MCCARROLL, D. and NESJE, A. (1993): The vertical extent of ice sheets in Nordfjord, western Norway: measuring degree of rock surface weathering. In: *Boreas* 22, 255–265. <https://doi.org/10.1111/j.1502-3885.1993.tb00185.x>
- MCCOLL, S. T. (2012): Paraglacial rock-slope stability. In: *Geomorphology* 153–154, 1–16. <https://doi.org/10.1016/j.geomorph.2012.02.015>
- NESJE, A. (2009): Latest Pleistocene and Holocene alpine glacier fluctuations in Scandinavia. In: *Quaternary Science Reviews* 28, 2119–2136. <https://doi.org/10.1016/j.quascirev.2008.12.016>
- NESJE, A. and DAHL, S. O. (1990): Autochthonous block fields in southern Norway: Implications for the geometry, thickness, and isostatic loading of the Late Weichselian Scandinavian ice sheet. In: *Journal of Quaternary Science* 5, 225–234. <https://doi.org/10.1002/jqs.3390050305>
- NESJE, A. and DAHL, S. O. (1993): Lateglacial and Holocene glacier fluctuations and climatic variations in western Norway: A review. In: *Quaternary Science Reviews* 12, 255–261. [https://doi.org/10.1016/0277-3791\(93\)90081-V](https://doi.org/10.1016/0277-3791(93)90081-V)
- NESJE, A. and WHILLANS, I. M. (1994): Erosion of Sognefjord, Norway. In: *Geomorphology* 9, 33–45. [https://doi.org/10.1016/0169-555X\(94\)90029-9](https://doi.org/10.1016/0169-555X(94)90029-9)
- NESJE, A. and DAHL, S. O. (2001): The Greenland 8200 cal. yr BP event detected in loss-on-ignition profiles in Norwegian lacustrine sediment sequences. In: *Journal of Quaternary Science* 16, 155–166. <https://doi.org/10.1002/jqs.567>
- NESJE, A., BLIKRA, L. H. and ANDA, E. (1994a): Dating rockfall-avalanche deposits from degree of rock-surface weathering by Schmidt-hammer tests: a study from Norangsdalen, Sunnmøre, Norway. In: *Norsk Geologisk Tidsskrift* 74, 108–113.
- NESJE, A., MCCARROLL, D. and DAHL, S. O. (1994b): Degree of rock surface weathering as an indicator of ice-sheet thickness along an east–west transect across Southern Norway. In: *Journal of Quaternary Science* 9, 337–347. <https://doi.org/10.1002/jqs.3390090404>
- NESJE, A., DAHL, S. O. and BAKKE, J. (2004): Were abrupt Lateglacial and early-Holocene climatic changes in northwest Europe linked to freshwater outbursts to the North Atlantic and Arctic Oceans? In: *The Holocene* 14, 299–310. <https://doi.org/10.1191/0959683604hl708fa>
- NESJE, A., ANDA, E., RYE, N., LIEN, R., HOLE, P. A. and BLIKRA, H. (1987): The vertical extent of the Late Weichselian ice sheet in the Nordfjord-Møre area, western Norway. In: *Norsk Geologisk Tidsskrift* 67, 125–141.
- NESJE, A., DAHL, S. O., RYE, E. A. and RYE, N. (1988): Block fields in southern Norway: Significance for the late Weichselian ice sheet. In: *Norsk Geologisk Tidsskrift* 68, 149–169.
- NESJE, A., DAHL, S. O., LINGE, H., BALLANTYNE, C. K., MCCARROLL, D., BROOK, E. J., RAISBECK, G. M. and YIOU, F. (2007): The surface geometry of the Last Glacial Maximum ice sheet in the Andøya–Skånland region, northern Norway, constrained by surface exposure dating and clay mineralogy. In: *Boreas* 36, 227–239. <https://doi.org/10.1111/j.1502-3885.2007.tb01247.x>
- NICHOLSON, D. T. (2008): Rock control in microweathering of bedrock surfaces in a periglacial environment. In: *Geomorphology* 101, 655–665. <https://doi.org/10.1016/j.geomorph.2008.03.009>
- NIEDZIELSKI, T., MIGON, P. and PLACEK, A. (2009): A minimum sample size required from Schmidt hammer measurements. In: *Earth Surface Processes and Landforms* 34, 1713–1725. <https://doi.org/10.1002/esp.1851>
- NYGÅRD, A., SEJRUP, H. P., HAFLIDASON, H., CECCHIE, M. and OTTESEN, D. (2004): Deglaciation history of the southwestern Fennoscandian ice sheet between 15 and 13 ¹⁴C ka BP. In: *Boreas* 33, 1–17. <https://doi.org/10.1111/j.1502-3885.2004.tb00992.x>
- OLSEN, L. and BERGSTRØM, B. (2007): Glacier variations during the LGM interval in the Karmøy – Jæren district, SW Norway. In: *NGF Abstracts and Proceedings* 1, 73–74.
- OWEN, L. A., THACKRAY, G., ANDERSON, R. S., BRINER, J., KAUFMAN, D., ROE, G., PFEFFER, W. and YI, C. (2009): Integrated research on mountain glaciers: current status, priorities and future prospects. In: *Geomorphology* 20, 158–171. <https://doi.org/10.1016/j.geomorph.2008.04.019>

- PATTON, H., HUBBARD, A., ANDREASSEN, K., WINSBORROW, M. and STROEVEN, A. P. (2016): The build-up, configuration, and dynamical sensitivity of the Eurasian ice-sheet complex to Late Weichselian climatic and oceanic forcing. In: *Quaternary Science Reviews* 154, 97–121. <http://dx.doi.org/10.1016/j.quascirev.2016.10.009>
- PATTON, H., HUBBARD, A., ANDREASSEN, K., AURIAC, A., WHITEHOUSE, P. L., STROEVEN, A. P., SHACKLETON, C., WINSBORROW, M., HEYMAN, J. and HALL, A. M. (2017): Deglaciation of the Eurasian ice sheet complex. In: *Quaternary Science Reviews* 169, 148–172. <https://doi.org/10.1016/j.quascirev.2017.05.019>
- PAUL, F., ANDREASSEN, L. M. and WINSVOLD, S. H. (2011): A new glacial inventory for the Jostedalbreen region, Norway, from Landsat TM scenes of 2006 and changes since 1966. In: *Annals of Glaciology* 52, 153–162. <https://doi.org/10.3189/172756411799096169>
- PAUS, A., VELLE, G., LARSEN, J., NESJE, A. and LIE, Ø. (2006): Lateglacial nunataks in central Scandinavia: Biostratigraphical evidence for ice thickness from Lake Flåfattjønn, Tynset, Norway. In: *Quaternary Science Reviews* 25, 1228–1246. <https://doi.org/10.1016/j.quascirev.2005.10.008>
- PELTIER, W. R. (2004): Global glacial isostasy and the surface of the Ice-Age earth: The ICE-5G (VM2) model and GRACE. In: *Annual Review of Earth and Planetary Sciences* 32, 111–149. <https://doi.org/10.1146/annurev.earth.32.082503.144359>
- RAE, A. C., HARRISON, S., MIGHALL, T. and DAWSON, A. G. (2004): Periglacial trimlines and nunataks of the Last Glacial Maximum: The Gap of Dunloe, southwest Ireland. In: *Journal of Quaternary Science* 19, 87–97. <https://doi.org/10.1002/jqs.807>
- RASMUSSEN, S. O., BIGLER, M., BLOCKLEY, S. P., BLUNIER, T., BUCHARDT, S. L., CLAUSEN, H. B., CVIJANOVIC, I., DAHL-JENSEN, D., JOHNSEN, S. J., FISCHER, H., GKINIS, V., GUILLEVIC, M., HOEK, W. Z., LOWE, J. J., PEDRO, J. B., POPP, T., SEIERSTAD, I. K., STEFFENSEN, J. P., SVENSSON, A. M., VALLELONGA, P., VINTHER, B. M., WALKER, M. J. C., WHEATLEY, J. J. and WINSTRUP, M. (2014): A stratigraphic framework for abrupt climatic changes during the Last Glacial period based on three synchronized Greenland ice-core records: refining and extending the INTIMATE event stratigraphy. In: *Quaternary Science Reviews* 106, 14–28. <https://doi.org/10.1016/j.quascirev.2014.09.007>
- REA, B. R., WHALLEY, W., RAINEY, M. M. and GORDON, J. E. (1996): Blockfields, old or new? Evidence and implications from some plateaus in northern Norway. In: *Geomorphology* 15, 109–121. [https://doi.org/10.1016/0169-555X\(95\)00118-O](https://doi.org/10.1016/0169-555X(95)00118-O)
- REITE, A. (1968): Lokalglaciation på Sunnmøre. In: *Norges Geologiske Undersøkelse* 247, 262–287.
- RINTERKNECHT, V. R., CLARK, P. U., RAISBECK, G. M., YIOU, F., BROOK, E. J., TSCHUDI, S. and LUNKKA, J.-P. (2004): Cosmogenic ^{10}Be dating of the Salpausselkä I Moraine in southwestern Finland. In: *Quaternary Science Reviews* 23, 2283–2289. <https://doi.org/10.1016/j.quascirev.2004.06.012>
- RINTERKNECHT, V. R., MARKS, L., PIOTROWSKI, J. A., RAISBECK, G. M., YIOU, F., BROOK, E. J. and CLARK, P. U. (2005): Cosmogenic ^{10}Be ages on the Pomeranian Moraine, Poland. In: *Boreas* 34, 186–191. <https://doi.org/10.1080/03009480600781982>
- RINTERKNECHT, V. R., CLARK, P. U., RAISBECK, G. M., YIOU, F., BROOK, E. J., MARKS, L., ZELČS, V., LUNKKA, J.-P., PAVLOVSKAYA, I. E., PIOTROWSKI, J. A. and RAUKAS, A. (2006): The last deglaciation of the southeastern sector of the Scandinavian Ice Sheet. In: *Science* 311, 1449–1452. <https://doi.org/10.1126/science.1120702>
- ROUYET, L., LAUKNES, T. R., CHRISTIANSEN, H. H., STRAND, S. M. and LARSEN, Y. (2019): Seasonal dynamics of a permafrost landscape, Adventdalen, Svalbard, investigated by InSAR. In: *Remote Sensing of Environment* 231, 111236. <https://doi.org/10.1016/j.rse.2019.111236>
- RYE, N., NESJE, A., LIEN, R., BLIKRA, L. H., EIKENAES, O., HOLE, P. A. and TORSNES, I. (1997): Glacial geology and deglaciation chronology of the area between inner Nordfjord and Jostedalbreen – Strynefjellet, western Norway. In: *Norsk Geologisk Tidsskrift* 77, 51–63.
- SÁNCHEZ, J. S., MOSQUERA, D. F. and VIDAL ROMANÍ, J. R. V. (2009): Assessing the age-weathering correspondence of cosmogenic ^{21}Ne dated Pleistocene surfaces by the Schmidt Hammer. In: *Earth Surfaces Processes and Landforms* 34, 1121–1125. <https://doi.org/10.1002/esp.1802>
- SCHAEFER, M. J., FINKEL, R. C., BALCO, G., ALLEY, R. B., CAFFEE, M. W., BRINER, J. P., YOUNG, N. E., GOW, A. J. and SCHWARTZ, R. (2016): Greenland was nearly ice-free for extended periods during the Pleistocene. In: *Nature* 540, 252–255. <https://doi.org/10.1038/nature20146>

- SCHMIDT, E. (1950): Der Beton-Prüfhammer. Schweizer Baublatt, Zürich 68(28): 378.
- SEJRUP, H. P., LARSEN, E., LANDVIK, J., KING, E. L., HAFLIDASON, H. and NESJE, A. (2000): Quaternary glaciations in southern Fennoscandia: evidence from southwestern Norway and the northern North Sea region. In: *Quaternary Science Reviews* 19, 667–685. [https://doi.org/10.1016/S0277-3791\(99\)00016-5](https://doi.org/10.1016/S0277-3791(99)00016-5)
- SEJRUP, H. P., NYGÅRD, A., HALL, A. M. and HAFLIDASON, H. (2009): Middle and Late Weichselian (Devensian) glaciation history of south-western Norway, North Sea and eastern UK. In: *Quaternary Science Reviews* 28, 370–380. <https://doi.org/10.1016/j.quascirev.2008.10.019>
- SHAKESBY, R. A., MATTHEWS, J. A. and OWEN, G. (2006): The Schmidt hammer as a relative-age dating tool and its potential for calibrated-age dating in Holocene glaciated environments. In: *Quaternary Science Reviews* 25, 2846–2867. <https://doi.org/10.1016/j.quascirev.2006.07.011>
- SHAKESBY, R. A., MATTHEWS, J. A., KARLÉN, W. and LOS, S. O. (2011): The Schmidt hammer as a Holocene calibrated-age dating technique: Testing the form of the R-value-age relationship and defining the predicted age errors. In: *The Holocene* 21, 615–628. <https://doi.org/10.1177/0959683610391322>
- SIGMOND, E. M. O., GUSTAVSON, M. and ROBERTS, D. (1984): Berggrunnskart over Norge 1:1 milion. Trondheim, Norges Geologiske Undersøkelse.
- SOLLID, J. L. and SØRBEL, L. (1994): Distribution of Glacial Landforms in Southern Norway in Relation to the Thermal Regime of the Last Continental Ice Sheet. In: *Geografiska Annaler: Series A, Physical Geography* 76, 25–35. <https://doi.org/10.2307/521317>
- SOLOMINA, O. N., BRADLEY, R. S., JOMELLI, V., GEIRSDOTTIR, A., KAUFMAN, D. S., KOCH, J., MCKAY, N. P., MASIOKAS, M., MILLER, G., NESJE, A., NICOLUSSI, K., OWEN, L. A., PUTNAM, A. E., WANNER, H., WILES, G. and YANG, B. (2016): Glacier fluctuations during the past 2000 years. In: *Quaternary Science Reviews* 149, 61–90. <https://doi.org/10.1016/j.quascirev.2016.04.008>
- STAHL, T., WINKLER, S., QUIGLEY, M., BEBBINGTON, M., DUFFY, B. and DUKE, D. (2013): Schmidt hammer exposure-age dating (SHD) of late Quaternary fluvial terraces in New Zealand. In: *Earth Surface Processes and Landforms* 38, 1838–1850. <https://doi.org/10.1002/esp.3427>
- STEER, P., HUISMANS, R. S., VALLA, P. G., GAC, S. and HERMAN, F. (2012): Bimodal Plio-Quaternary glacial erosion of fjords and low-relief surfaces in Scandinavia. In: *Nature Geoscience* 5, 635–639. <https://doi.org/10.1038/NGEO1549>
- STROEVEN, A. P., FABEL, D., HÄTTESTRAND, C. and HARBOR, J. (2002): A relict landscape in the centre of Fennoscandian glaciation: cosmogenic radionuclide evidence of tors preserved through multiple glacial cycles. In: *Geomorphology* 44, 145–154. [https://doi.org/10.1016/S0169-555X\(01\)00150-7](https://doi.org/10.1016/S0169-555X(01)00150-7)
- STROEVEN, A. P., HÄTTESTRAND, C., KLEMAN, J., HEYMAN, J., FABEL, D., FREDIN, O., GOODFELLOW, B. W., HARBOR, J. M., JANSEN, J. D., OLSEN, L., CAFFEE, M. W., FINK, D., LUNDQVIST, J., ROSQVIST, G. C., STRÖMBERG, B. and JANSSON, K. N. (2016): Deglaciation of Fennoscandia. In: *Quaternary Science Reviews* 147, 91–121. <https://doi.org/10.1016/j.quascirev.2015.09.016>
- TOMKINS, M. D., DORTCH, J. M. and HUGHES, P. D. (2016): Schmidt hammer exposure dating (SHED): Establishment and implications for the retreat of the last British Ice Sheet. In: *Quaternary Geochronology* 33, 46–60. <https://doi.org/10.1016/j.quageo.2016.02.002>
- TOMKINS, M. D., DORTCH, J. M., HUGHES, P. D., HUCK, J. J., STIMSON, A. G., DELMAS, M., CALVET, M. and PALLÀS, R. (2018): Rapid age assessment of glacial landforms in the Pyrenees using Schmidt hammer exposure dating (SHED). In: *Quaternary Research* 90, 26–37. <https://doi.org/10.1017/qua.2018.12>
- TVETEN, E., LUTRO, O. and THORSNES, T. (1998): Geologisk kart over Norge, 1:250,000. Ålesund: Norges Geologiske Undersøkelse.
- WILSON, P. and MATTHEWS, J. A. (2016): Age assessment and implications of late Quaternary periglacial and paraglacial landforms on Muckish Mountain, northwest Ireland, based on Schmidt-hammer exposure-age dating (SHD). In: *Geomorphology* 270, 134–144. <https://doi.org/10.1016/j.geomorph.2016.07.002>
- WILSON, P., MATTHEWS, J. A. and MOURNE, R. W. (2017): Relict Blockstreams at Insteheia, Valdalen-Talfjorden, Southern Norway: Their Nature and Schmidt Hammer Exposure Age. In: *Permafrost and Periglacial Processes* 28, 286–297. <https://doi.org/10.1002/ppp.1915>

- WILSON, P., LINGE, H., MATTHEWS, J. A., MOURNE, R. W. and OLSEN J. (2019): Comparative numerical surface exposure-age dating (^{10}Be and Schmidt hammer) of an early-Holocene rock avalanche at Alstadfjellet, Valdalen, southern Norway. In: *Geografiska Annaler: Series A, Physical Geography* (online first). <https://doi.org/10.1080/04353676.2019.1644815>
- WINGUTH, C., MICKELSON, D., LARSEN, E., DARTER, J. R., MOELLER, C. A. and STALSBERG, K. (2005): Thickness evolution of the Scandinavian ice sheet during the late Weichselian in Nordfjord, Western Norway: evidence from ice-flow modeling. In: *Boreas* 34, 176–185. <https://doi.org/10.1111/j.1502-3885.2005.tb01013.x>
- WINKLER, S. (2005): The Schmidt Hammer as a relative-age dating technique: potential and limitations of its application on Holocene moraines in Mt Cook National Park, Southern Alps, New Zealand. In: *New Zealand Journal of Geology and Geophysics* 48, 105–116. <https://doi.org/10.1080/00288306.2005.9515102>
- WINKLER, S. (2009): First attempt to combine terrestrial cosmogenic nuclide (^{10}Be) and Schmidt hammer relative-age dating: Strauchon Glacier, Southern Alps, New Zealand. In: *Central European Journal of Geosciences* 1, 274–290. <https://doi.org/10.2478/v10085-009-0026-3>
- WINKLER, S. (2014): Investigation of late-Holocene moraines in the western Southern Alps, New Zealand, applying Schmidt-hammer exposure-age dating. In: *The Holocene* 24, 48–66. <https://doi.org/10.1177/0959683613512169>
- WINKLER, S. (2018): Investigating Holocene mountain glaciations: A plea for the supremacy of glacial geomorphology when reconstructing glacier chronologies (supported by an example from the Southern Alps/New Zealand). In: *Erdkunde* 72, 215–234. <https://doi.org/10.3112/erdkunde.2018.03.04>
- WINKLER, S. and MATTHEWS, J. A. (2014): Comparison of electronic and mechanical Schmidt hammers in the context of exposure-age dating: are Q- and R-values interconvertible? In: *Earth Surface Processes and Landforms* 39, 1128–1136. <https://doi.org/10.1002/esp.3584>
- WINKLER, S. and LAMBIEL, C. (2018): Age constraints of rock glaciers in the Southern Alps/New Zealand – exploring their palaeoclimatic potential. In: *The Holocene* 28, 778–790. <https://doi.org/10.1177/0959683618756802>
- WINKLER, S., CHINN, T., GÄRTNER-ROER, I., NUSSBAUMER, S. U., ZEMP, M. and ZUMBÜHL, H. J. (2010): An introduction to mountain glaciers as climate indicators with spatial and temporal diversity. In: *Erdkunde* 64, 97–118. <https://doi.org/10.3112/erdkunde.2010.02.01>
- WINKLER, S., MATTHEWS, J. A., MOURNE, R. W. and WILSON, P. (2016): Schmidt-hammer exposure ages from periglacial patterned ground (sorted circles) in Jotunheimen, Norway, and their interpretative problems. In: *Geografiska Annaler: Series A, Physical Geography* 98, 265–285. <https://doi.org/10.1111/geoa.12134>
- WOHLFARTH, B. (2010): Ice-free conditions in Sweden during Marine Oxygen Isotope Stage 3? In: *Boreas* 39, 377–398. <https://doi.org/10.1111/j.1502-3885.2009.00137.x>, 2010
- ZEMP, M., ROER, I., KÄÄB, A., HOELZLE, M., PAUL, F. and HAEBERLI, W. (2008): *Global glaciers changes: facts and figures*. WGMS/UNEP. Zürich.
- ZEMP, M., FREY, H., GÄRTNER-ROER, I., NUSSBAUMER, S. U., HOELZLE, M., PAUL, F., HAEBERLI, W., DENZINGER, F., AHLSTRØM, A. P., ANDERSON, B., BAJRACHARYA, S., BARONI, C., BRAUN, L. N., CÁCERES, B. E., CASASSA, G., COBOS, G., DÁVILA, L. R., DELGADO GRANADOS, H., DEMUTH, M. N., ESPIZUA, L., FISCHER, A., FUJITA, K., GADEK, B., GHAZANFAR, A., HAGEN, J. O., HOLMLUND, P., KARIMI, N., LI, Z., PELTO, M., PITTE, P., POPOVNIK, V. V., PORTOCARRERO, C. A., PRINZ, R., SANGEWAR, C. V., SEVERSKIY, I., SIGURÐSSON, O., SORUCO, A., USUBALIEVM, R. and VINCENT, C. (2015): Historically unprecedented global glacier decline in the early 21st century. In: *Journal of Glaciology* 61, 745–762. <https://doi.org/10.3189/2015JG15J017>

7 Investigations on Blockfields and Related Landforms at Blåhø (Southern Norway) Using Schmidt-Hammer Exposure-Age Dating (SHD): Palaeoclimatic and Morphodynamic Implications

This chapter is the authors accepted manuscript of the following publication with permission from Geografiska Annaler: Series A, Physical Geography © 2018 Informa UK Limited, trading as Taylor & Francis Group which can be found at <https://doi.org/10.1080/04353676.2018.1474350>

MARR, P., WINKLER, S. and LÖFFLER, J. (2018): Investigations on blockfields and related landforms at Blåhø (Southern Norway) using Schmidt-hammer exposure-age dating: palaeoclimatic and morphodynamic implications. In: Geografiska Annaler: Series A, Physical Geography 100, 285–306.

Abstract

Schmidt-hammer exposure-age dating (SHD) was performed on blockfields and related landforms on Blåhø, southern Norway. By developing a linear high-precision age-calibration curve through young and old control points of known age from terrestrial cosmogenic nuclide dating (TCND), it was possible to gain landform age estimates based on Schmidt hammer R-values. The aim of this study is to relate formation and subsequent stabilization of the landforms investigated to climate fluctuations since the LGM and to explore the palaeoclimatic implication of such periglacial landforms. The SHD ages range from 19137 ± 908 years for the Rundhø blockfield to 5316 ± 731 years for the lowest elevation rock-slope failure. The R-value frequency distributions obtained on the landforms studied indicate complex, long-term formation histories. Landforms above 1450 m a.s.l. share comparable SHD ages and seem to have stabilized during the Karmøy/Bremanger readvance (~ 18.5 - 16.5 ka). The lower elevation rock-slope failures most likely occurred during the Bølling-Allerød interstadial (~ 14.7 - 12.9 ka) and the Holocene Thermal Maximum (~ 8.0 - 5.0 ka). The results contrast with the established model that rock-slope failures occur within the first millennia following deglaciation. Instead of the inferred ice-coverage above 1450 m a.s.l. until 15.0 ± 1.0 ^{10}Be ka, our results suggest severe periglacial and ice free conditions occurred earlier. Landforms above 1450 m a.s.l. do not show any form of re-activation during cold periods within the Late Glacial and Holocene. Our SHD results suggest that the landforms investigated were (at least partly) generated prior the LGM and survived beneath cold-based ice or were located on nunataks.

Keywords

Schmidt-hammer exposure-age dating (SHD), periglacial landforms, permafrost, LGM, Norway

Introduction

Research on autochthonous blockfields has a long tradition in Northwest-Europe (see e.g. Dahl 1966; Rudberg 1988; Ballantyne and Harris 1994; Rea et al. 1996; Rea 2013). One focus is the development of different models for their formation and identifying individual mechanisms involved, in particular the possible influence of pre-glacial chemical weathering processes or their characterization within the context of an alpine periglacial process system (André 2003; Whalley et al. 2004; Fjellanger et al. 2006; Goodfellow et al. 2008; Ballantyne 2010; Rixhon and Demoulin 2013). In addition, blockfields and related landforms play an important role within the reconstruction of the geometry and vertical extent of the Scandinavian ice sheet during the last (Weichselian) glaciation and subsequent deglaciation. Their location on summit areas, especially when trimlines are visible below, suggest the possibility that they may have developed on nunataks (Ballantyne 2013) and blockfields have accordingly been utilized in the reconstruction of the Weichselian ice-sheet in several regions at particular stages (e.g. Nesje et al. 1988; Nesje and Dahl 1990; McCarroll and Nesje 1993; Nesje et al. 1994a; Nesje et al. 2007). In the wake of the more recent paradigm shift that trimlines as no longer undisputable evidence of a former vertical ice-sheet extent but rather a weathering boundaries of several different explanations (including the vertical limit between warm- and cold-based ice; see Ballantyne 2013; McCarroll 2016), the palaeoclimatic significance of blockfields and any potential age constraints also need critical re-evaluation. The application of modern numerical dating techniques (e.g. terrestrial cosmogenic nuclide dating – TCND) has provided some insights with more accurate surface exposure ages (Fabel et al. 2002; Stroeven et al. 2002; Juliussen and Humlum 2007), but the high costs and complicated laboratory procedures involved create the demand for alternative reliable dating methods that are both inexpensive and more efficient. Blockfields and other landforms within the periglacial zone in Scandinavia have considerable potential to provide chronological control on the last deglaciation and characterise the regional Holocene climate history by exploring the palaeoclimatic significance of climate-driven processes and landforms (Matthews et al. 2013, submitted; Winkler et al. 2016). This is, moreover, not a trivial task as by contrast to quite detailed information on the horizontal ice-sheet margins during the Late Glacial (Hughes et al. 2016), there is still relatively less knowledge about the exact mechanism and local timing of deglaciation within the mountainous parts of central Southern Norway (Dahl et al. 1997; Matthews and Winkler 2011).

The prominent summit of Blåhø in south central Norway is characterised by its coarse rock debris accumulations and a variety of Late Weichselian and Holocene landforms that are typical of the alpine periglacial zone. Blåhø may provide valuable regional palaeoclimatic insights due to its location in a highly continental climate (Moen 1998) and the general lack of knowledge about Late Weichselian and Holocene climate dynamics in the area. Nesje et al. (1994a) conducted Schmidt-hammer measurements on Blåhø to investigate the degree of surface weathering as part of a study aimed at identifying blockfield boundaries between different mountain summits in a west-east transect, but did not present any numerical surface exposure ages. For any conclusions about the detailed Holocene climate development of the Blåhø area and the development of its landforms it was, therefore, necessary to transfer related information from the much better studied Jotunheimen mountains to the west (Matthews and Dresser 2008; Nesje 2009; Matthews 2013). An

advantage of our study site in addition to the diversity of boulder-dominated landforms is, however, the availability of permafrost measurements (Farbrot et al. 2011) and recent TCND numerical ages (Goehring et al. 2008). The latter constitute old control points for high-precision Schmidt-hammer exposure-age dating (SHD). For a young control point we used fresh boulders excavated by construction work in July 2017. This enabled us to determine the exposure ages of boulders in blockfields, bedrock, patterned ground features (sorted polygons, blockstreams) and rock-slope failures. The age and dynamics of the variety of landforms on Blåhø are studied for the first time and they may act as palaeoclimatic proxies indicating landform changes in response to changing climatic conditions.

Although the Schmidt-hammer has previously been applied on blockfields and periglacial landforms to identify weathering-related boundaries, identify altitudinal gradients of surface weathering, and as a relative-age dating technique (e.g. Cook-Talbot 1991; McCarroll and Nesje 1993; Nesje et al. 1994a; Ballantyne et al. 1997, 1998), the more recent development has been in exposure-age dating (SHD). This offers a range of new opportunities by providing numerical age constraints for the timing of formation and stabilization, or analysis of involved processes and dynamics, of various periglacial landforms. The progress includes knowledge on the calculation and shape of regional SHD-calibration curves on the basis of available precise numerical age estimates (e.g. by TCND) for the whole Holocene (Matthews and Owen 2010; Shakesby et al. 2011; Matthews and McEwan 2013; Matthews et al. 2014) and even back to the last Last Glacial Maximum (e.g. Tomkins et al. 2016, 2018). The advantage of inexpensively and efficiently sampling large numbers of boulders for the calculation of surface exposure ages, is particularly important for the investigation of boulders on potentially diachronous periglacial landforms built-up by long-term geomorphic processes and/or subject to post-depositional disturbance. This has recently been further improved by the introduction of an electronic version of the Schmidt-hammer (Winkler and Matthews 2014) that already has been successfully applied on sorted stone circles (Winkler et al. 2016) and rock glaciers (Winkler and Lambiel 2018).

The specific aims of our study in the light of this background are

- (1) to calculate a local SHD-calibration curve for our study area and this particular part of southern Norway,
- (2) to determine precise surface-exposure ages for the landforms investigated,
- (3) to interpret mechanisms of formation of these landforms, the timing of their stabilization, and dynamics and processes involved, and
- (4) to compare our results with those from other regions, in particular in the context of climate history during the late Quaternary.

Study area

The investigated landforms are located on Blåhø (1618 m a.s.l.) in south central Norway (61°53'51N, 9°16'58E). Blåhø is situated in Ottadalen, between Jotunheimen in the south east and Rondane in the west (Figure 1). The mountain has three lower elevation peaks: Rundhø (1556 m a.s.l.), Veslrundhø (1514 m a.s.l.) and Storhøi (1455 m a.s.l.), with smoothly undulating surfaces (Figure 2). The summit plateau of Blåhø is surrounded by gentle slopes to the north, south and a steeper eastern slope. Following a small steep cliff at the western edge of the summit the sridge gently descends to the west and is divided into ridges towards south west and north west.

The climatic conditions are characterized by strong continentality. With a mean annual air temperature (MAAT) of $\sim -4^{\circ}\text{C}$ (Strømsøe and Paasche 2011) and a mean annual precipitation (MAP) between 300-400 mm/yr in valleys, it represents one of the driest localities in Norway (Moen 1998). The mean number of days with a snow depth >25 cm is 100-200 for all sites (1971-2000), except for sites around Rundhø that have 200-350 days (<http://senorge.no>). More than 5cm depth of snow was recorded on 200-350 days at the summit and 100-200 days for low lying areas ($\sim <1000$ m a.s.l.) from 1971-2000 (<http://senorge.no>). However, due to the prevailing wind speeds, summit snow accumulation is limited. Recent data from permafrost boreholes indicate a mean ground temperature (0.05 m depth) of 0.9°C and 1.0°C from 2008-2009, and 2009-2010 respectively. The mean ground temperature at 10 cm depth was 0.7°C from September 2008 to August 2010. In the same period the active layer thickness reached 6 to 7 m (Farbrot et al. 2011).

The summit of Blåhø belongs to the upper parts of the Kvitola Nappe which consists of late Precambrian sedimentary rocks (cf. Farbrot et al. 2011). The Precambrian bedrock is quartz-rich and the summit is dominated by meta-conglomerate and meta-sandstone on higher and lower slopes respectively (Tveten et al. 1998). The area from the summit to about 1500 m a.s.l. is covered by an autochthonous blockfield (Nesje et al. 1994a). The middle-alpine vegetation on the ridges and peaks is dominated by lichens and graminoids (Löffler and Pape 2017)

There has been a considerable debate on the glaciation history of Blåhø (Nesje et al. 1994a; Goehring et al. 2008; Strømsøe and Paasche 2011). During the Last Glacial Maximum (LGM, 26.5-20 ka; Clark et al. 2009) the summit may have been covered by cold-based ice (e.g. Kleman 1994) or may have been ice-free (e.g. Balantyne et al. 1997). Goehring et al. (2008) developed a deglaciation chronology for Blåhø, arguing for cold-based ice coverage during the LGM. In contrast to other parts of south central Norway, they consider an early deglaciation commencing at 25.1 ± 1.8 10Be ka. Therefore, the maximum vertical ice extent must have occurred earlier. Rapid thinning led to ice free conditions at 15.0 ± 1.0 10Be ka at about 1450 m a.s.l. Subsequent slower thinning led to a vertical ice extent of ~ 1100 m a.s.l. at 11.3 ± 1.1 10Be ka (Goehring et al. 2008). The most recent contributions to constrain the deglaciation history of Scandinavia (e.g. Hughes et al. 2016) do not provide any further insights into the complex local (de)glaciation history. The cold-based ice theory seems generally accepted and corresponds to a general paradigm shift in the investigation of

blockfields over the whole of northwest Europe (Ballantyne 2010; McCarroll 2016), although some aspects remain ambiguous. It is possible that the ice sheet was thinner than previously assumed and multi-domed, without reaching all mountain peaks in western Norway (Follestad 2003; Winguth et al. 2005). For instance, Mt. Skåla (1848 m a.s.l.) appears to have escaped burial by ice during the last glaciation (Brook et al. 1996). Parts of Greenland and Svalbard have recently been shown to have remained ice-free during extended periods of the Pleistocene, including the LGM (Landvik et al. 2003; Schaefer et al. 2016), meaning that ice-free conditions on Blåhø cannot be entirely excluded prior to more detailed studies.

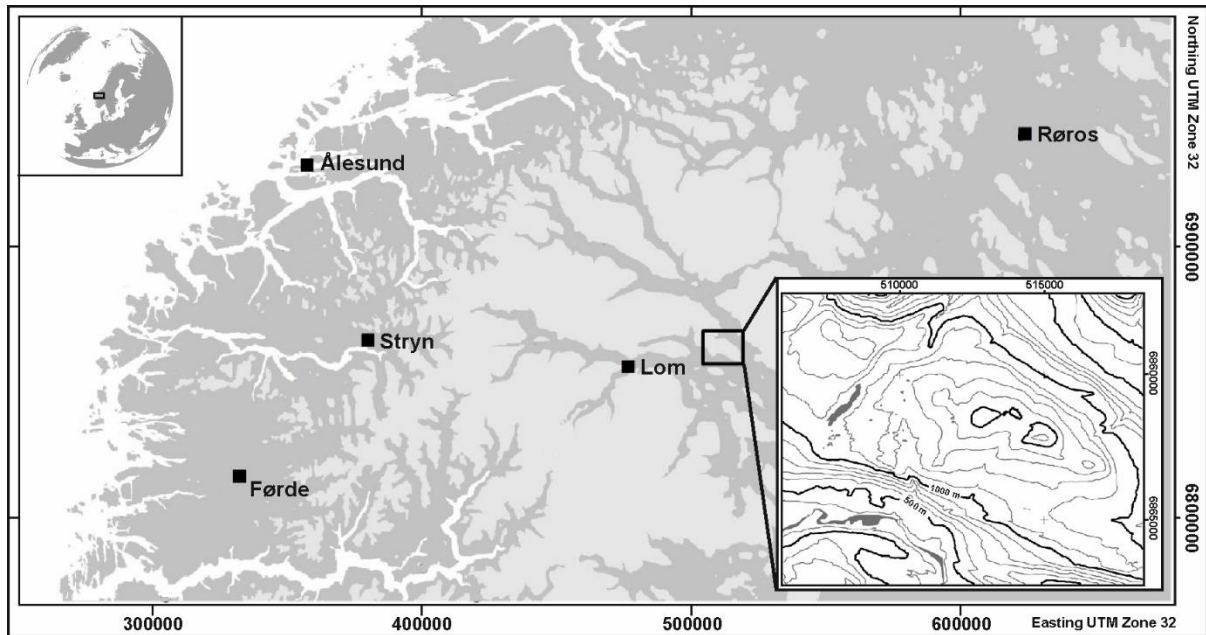


Figure 1. Research location in south central Norway with Blåhø as the study area (modified after Pape et al. 2009).

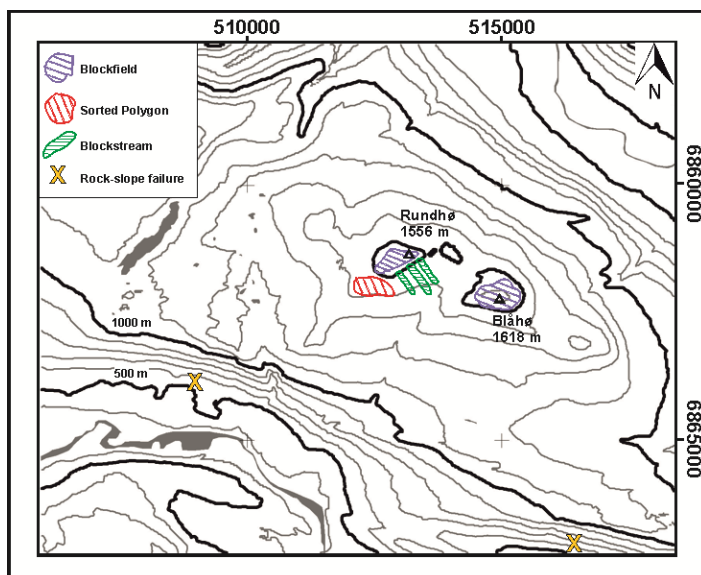


Figure 2. Blockfields and related periglacial landforms investigated above 1450 m a.s.l. (modified after Pape et al. 2009).

Investigated landforms

Different periglacial landforms were investigated with the Schmidt hammer on Blåhø (Figures 2 and 3). These landform types are common features of mountain regions, which experience permafrost at present or experienced permafrost in the past (French 2007). Boulders on the investigated landforms have an extensive lichen and moss cover. The landforms show no evidence of post-depositional disturbance or erratics transported by former glacier ice. Plant assemblages have partly developed in sheltered areas between rocks; trees are common in low lying areas. The environmental conditions and lithology of all control points and landforms are comparable. This is a critical prerequisite for successful SHD application (Matthews and Winkler 2011).

Blockfields were measured at the summits of Blåhø (BL-I) at 1617 m a.s.l. and Rundhø (BL-II, Figure 3b) at 1562 m a.s.l., with spatial extents of ~ 0.25 km² and ~ 0.06 km² respectively. The blockfields are characterized by in situ weathered angular blocks and boulders (Nesje et al. 1994a). The surface boulders cover a soil matrix of mixed grain sizes (Rea et al. 1996; Ballantyne 2010). Both blockfield surfaces are near horizontal and are 20-50 cm deep. Surface boulders have an average diameter of 30-70 cm. Downslope transport of boulders from BL-II has created blockstreams, which were also investigated in this study.

Sorted stone polygons (SP) are grouped on a plateau at an altitude of 1450 m a.s.l. and cover an area of ~ 2200 m². The stone gutters, where boulders were measured, were randomly selected. Most sorted polygons ($\sim 90\%$) are larger than two metres in diameter (Figure 3c). The average gutter width ranged from 20 cm to 50 cm (largest up to one metre), gutter depth from 20 cm to 40 cm, and average boulder sizes are generally of 20-60 cm. However, smaller (>10 cm) and larger (80-100 cm) boulders are also present. Boulders within the gutters are arranged predominantly on their edges and therefore are generally perpendicular to the surface gradient. Only smaller SP (<1 m diameter) can develop without permafrost in a short time (Feuillet and Mercier 2012), the influence of permafrost is highly likely when the diameter exceeds 2 m (Goldthwait 1976). Even though, permafrost is not necessary for SP development, although they mostly occur in cold environments (Washburn 1956).

Further, SHD was performed on bedrock (BR) outcrops on the western part of the Rundhø summit (1562 m a.s.l.). Blockstreams on the south east slope of Rundhø occur at the lower end of the blockfield at ~ 1500 m a.s.l. and extend down to ~ 1400 m a.s.l. with a length of about 140 m (Figure 3d). The transition zone between blockfield and blockstreams is characterized by typical periglacial morphologies, e.g. lobate fronts. The blockstreams occur on the same slope in parallel alignment but with varying lengths and widths. They appear to be relict due to the debris arrangement and the degree of lichen/ moss cover, which is consistent with other blockstream studies (e.g. Boelhouwers et al. 2002; Wilson et al. 2017). The selected blockstream was divided into an upper (BS-u) and lower part (BS-l). The upper part has a width of ~ 6 m and depth of ~ 30 cm. The blockstream narrows slightly to 4.5 m and depth reduces to 20 cm on the lower part. In both parts there was a limited number boulders for SH measurements, thus only 100 boulders were measured. The blockstream has an inclination of about 15° , with small surface lobes and steps evident. These may be

indicative of permafrost (Goldthwait 1976; Rixhon and Demoulin 2013; Wilson et al. 2017 and references therein), although it is not necessary for their development (Washburn 1956).

On the southern slope of Blåhø a rock-slope failure (RSF-I), ranging from ~550 m a.s.l. to 380 m a.s.l. was also investigated. This feature covers an area of 0.14 km² (Figure 3e) and due to abundant boulders, we measured more boulders here than on other landforms. The steep south-facing bedrock wall, with a typical failure scar (Wilson 2004) at ~1000 m a.s.l., was identified as the source area. The entire slope is inclined at ~25°. The average diameter of boulders ranged from 60 to 50 cm, but boulders with a diameter of >4-5 m were present as well. Most boulders within the rock-slope failure were stable. The thickness of the failed debris ranged between 1-3 m. Trees grow at the foot of the landform, grading into forest further downslope. At ~450 m a.s.l. an east-west oriented line of trees was observed, and may be an indication of relict solifluction. The second investigated rock-slope failure (RSF-II) is located between ~740 m a.s.l. and 500 m a.s.l. at the south eastern slope of Blåhø (Figure 3f). At ~1100 m a.s.l. a steep hillslope with a failure scar was identified as a possible source of debris. The entire landform comprises an area of ~0.25 km². Field observations indicate a relict status as many trees and boulders with extensive lichen and moss cover are present. The boulder sizes vary mostly from 30 cm to 150 cm a b axis, but larger boulders >2 m diameter are also present. The inclination is relatively flat at the foot with <10°, although the entire slope gradient averages ~25°.



Figure 3. (a) View east from Rundhø towards Blåhø. (b) View to the Rundhø blockfield towards the northwest. Note the Schmidt hammer is 20 cm long. (c) View of the sorted stone polygon plateau towards west. The pole is 2 m long. (d) Down-valley view towards the south of the blockstream. Note the car for scale. (e) The lower part of rock-slope failure I, view is towards the east, note the Schmidt hammer for scale. (f) View north east from the foot of rock-slope failure II.

Methods

Schmidt-hammer and sampling design

Originally, the Schmidt hammer was developed for in situ hardness testing of concrete (Schmidt 1950) but has since been applied in geomorphological research worldwide (see Goudie 2006; Shakesby et al. 2006), e.g. moraines (McCarroll 1989; Ffoulkes and Harrison 2014), snow avalanche impact ramparts (Matthews et al. 2015), rock glaciers (Aoyama 2005; Kellerer-Pirklbauer et al. 2008), and periglacial trimlines (Ballantyne et al. 1997; Rae et al. 2004). Schmidt hammer measurements provide data concerning the relative surface weathering of boulders, providing that lithology is uniform. The degree of surface weathering allows in turn estimates about the length of surface exposure (Černá and Engel 2011). This technique has been successfully

applied on coarse debris landforms in several parts of Norway (e.g. McCarroll and Nesje 1993; Nesje et al. 1994b; Shakesby et al. 2006; Matthews et al. 2011, 2013, 2014, 2017). Mostly, single landforms were studied, including patterned ground (Cook-Talbot 1991; Winkler et al. 2016) and alluvial fans (White et al. 1998). Few attempts have been made to investigate an assemblage of landforms (Wilson and Matthews 2016).

SHD and the application of a high-precision age calibration curve is a recently developed approach (Shakesby et al. 2011; Matthews and McEwen 2013; Wilson and Matthews 2016). The establishment of a reliable local calibration curve requires at least two control surfaces (young and old) of known age from the same lithology as the studied landforms, to successfully produce numerical age estimates (Matthews and Owen 2010; Winkler 2014; Matthews and Wilson 2015). The limitations of this approach are closely related to the reliability of the control sites. The calculation of 95% confidence intervals of the control points and sampled sites allows to estimation of SHD ages and their uncertainties. The age estimates from Schmidt hammer studies are largely in agreement with ages obtained by TCND (e.g. Matthews and Owen 2010), optically stimulated luminescence (e.g. White et al. 1998; Stahl et al. 2013), radiocarbon dating (e.g. Nesje et al. 1994b; Aa and Sjøstad 2000; Winkler 2005) and lichenometric dating (e.g. Evans et al. 1999).

In this study a N-Type electronic RockSchmidt (2.207 Nm impact energy) was used (Proceq 2014). The rebound (R)- values yielded by a RockSchmidt are obtained differently to those of mechanical Schmidt hammers and, therefore, not identical. Winkler and Matthews (2014) have, however, shown that these R-values are interconvertible and data series obtained by electronic and mechanical Schmidt hammers can be analysed in the same way.

Here, we sampled boulder surfaces at six different boulder-dominated landforms. We measured 200 boulders at each landform (when possible), with two impacts per boulder. Only stable boulders >30 cm diameter were measured. This was consistently applied throughout sampling. R-values obtained from one landform were initially treated as a homogeneous sample. This sampling design is similar to that applied by Wilson and Matthews (2016) and ensured representative and sufficient sample sizes (Shakesby et al. 2006; Niedzielski et al. 2009). A large number of impacts increases statistical significance, lowers the probability of outliers and the influence of lithological heterogeneities or micro-weathering (McCarroll 1989; Winkler 2009). However, certain lithological heterogeneity of the Precambrian rocks could theoretically have affected the R-values. The samples were obtained from visually homogeneous lithology and near horizontal, dry surfaces. Potential sources of error such as boulder edges, structural rock weaknesses, lichen or moss covered surfaces were avoided (McCarroll 1989; Wilson et al. 2017). As recommended by Černá and Engel (2011) for bedrock investigations, extensive areas of rock surfaces were sampled to avoid sub-horizontal cracks within bedrock as a source of error. The rock surfaces were not modified or prepared in any way before measurement. We consider the micro- and meso-topographic variabilities to average out due to the large sample sizes and therefore they are insignificant influences on our results (Matthews et al. 2015).

The R-values were statistically processed using R statistic software. Histograms were produced to show the R-value distributions, as bimodal distributions could be associated with relocation processes or different exposure history (McCarroll and Nesje 1993; Winkler 2014). The standard statistical analysis comprised the

calculation of the standard mean, standard error of the mean (SEM), 95% confidence interval, skewness, kurtosis and test of normality (Shapiro-Wilk-Test). Sites with an overlapping 95% confidence interval are interpreted on the premise that these sites are of the same population and therefore are of equal age (Shakesby et al. 2006; Winkler 2009). The Mann-Whitney test was used to determine statistical significance between pairs of sites.

Control points and calibration curve

On the basis of the young and old control points a high-precision calibration equation was derived. The young control R-values were obtained from boulders at a construction site. The old control points (1100 m a.s.l. and 1450 m a.s.l.) with ^{10}Be dates (11.400 ± 1.0 ka and 15.000 ± 1.1 ka) represent bedrock surfaces (Goehring et al. 2008). At each control point 200 measurements (R-values) were obtained.

Linear age-calibration curves from Little Ice Age (LIA) and late Preboreal surfaces were first presented by Shakesby et al. (2006). This approach was further developed by Matthews and Owen (2010) and resulted in a high-precision calibration curve. The approach has since been successfully applied by several authors (e.g. Matthews and Winkler 2011; Wilson and Matthews 2016). A linear relationship is a solid based assumption as: (1) former studies on granitic surface proved the linear relationship (e.g. Shakesby et al. 2011), and (2) hard crystalline rock types show slow and close to linear weathering characteristics when using the Holocene as a reference time frame (Colman 1981; André 1996). There is evidence that this linear relationship even goes beyond the Holocene timescale (Engel 2007; Sánchez et al. 2009; Klapyta 2013). Furthermore, Tomkins et al. (2016, 2018) show the R-value-age relationship to be linear during the transition from arctic to more temperate conditions (post-LGM to Lateglacial). For our calibration curve, we use a standard linear regression:

$$Y = a + bx \quad (1)$$

where y is the surface age in years, a is the intercept age (acquired by substitution in the calibration equation), b is the slope of the calibration curve and x is the mean R-value. The b coefficient is described as:

$$b = (y_1 - y_2) / (x_1 - x_2) \quad (2)$$

with y_1 and x_1 representing the age and mean R-value of the old control point. Whereas y_2 and x_2 represent the age and mean R-value of the young control point.

The 95% confidence interval for a SHD age, comprising the total error (C_t), consists of the error of the calibration curve at the point related to the dated sample (C_c) and to the sampling error of the sample itself (C_s):

$$C_t = \sqrt{(C_c^2 + C_s^2)} \quad (3)$$

The error of the calibration curve is represented by the errors of the control points and their age differences:

$$C_c = C_o - [(C_o - C_y) (R_s - R_o) / (R_y - R_o)] \quad (4)$$

with C_o expressing the 95% confidence interval of the old control point in years, C_y the 95% confidence interval of the young control point in years. R_o , R_y and R_s are associated with the mean R-value of the old and young control point and the sample. The sampling error of the sample itself is calculated incorporating the b coefficient, Student's t statistic, standard deviation (s) of the sample's R-value and the sample size (n):

$$C_s = b [ts / \sqrt{(n - 1)}] \quad (5)$$

Results

The Schmidt hammer results from the control sites and investigated landforms are shown as frequency distributions (Figure 4, Figure 6) and numerically Table 1.

Control sites

The mean R-values for the young (68.3 ± 0.45), old control point I at 1100 m a.s.l. (49.7 ± 0.92) and old control point II at 1450 m a.s.l. (40.1 ± 0.97) differ by about 20, and 30 units respectively (Table 1). The young control point value shows about half the confidence interval variability than of the old control points. Positive skewness and the small number of low R-values indicate, furthermore, that few boulders with a high degree of surface weathering are present at the site. Long-term exposure to weathering at the old control points leads to an increasing variability of R-values reflected in higher standard deviations as well as in the 95% confidence intervals.

Table 2. Schmidt hammer R-values and statistics for the control sites. Mean R-values are obtained from the means of two impacts on each of the sampled 200 boulders, 95% confidence intervals were calculated from n=200 boulders.

Control point	Age (in yr) ^a	Mean R-value	σ	95% CI ^b	Kurtosis	Skewness
Young	1	68.3	4.62	0.45	-0.45	0.52
Old I	11400 \pm 1.0	49.7	9.34	0.92	-0.31	-0.37
Old II	15000 \pm 1.1	40.1	9.84	0.97	-0.81	-0.15

^a Age of young control point from field observation. Ages from old control point I and II from Goehring et al. (2008).

^b Mean of R-values with 95% confidence intervals ($\alpha = 0.05$).

The histograms for the young control point and old control point I show unimodal distribution, whereas old control point II shows a polymodal distribution (Figure 4). Judging by the 95% confidence intervals, the old control points I and II differ significantly. Because of the uncertainties with the polymodal distribution of R-values of old control point II we base our calculation of the calibration curve on the young and old control point I only (see discussion) yielding the equation $y = 40467.6724 - 592.672414x$ (Figure 5).

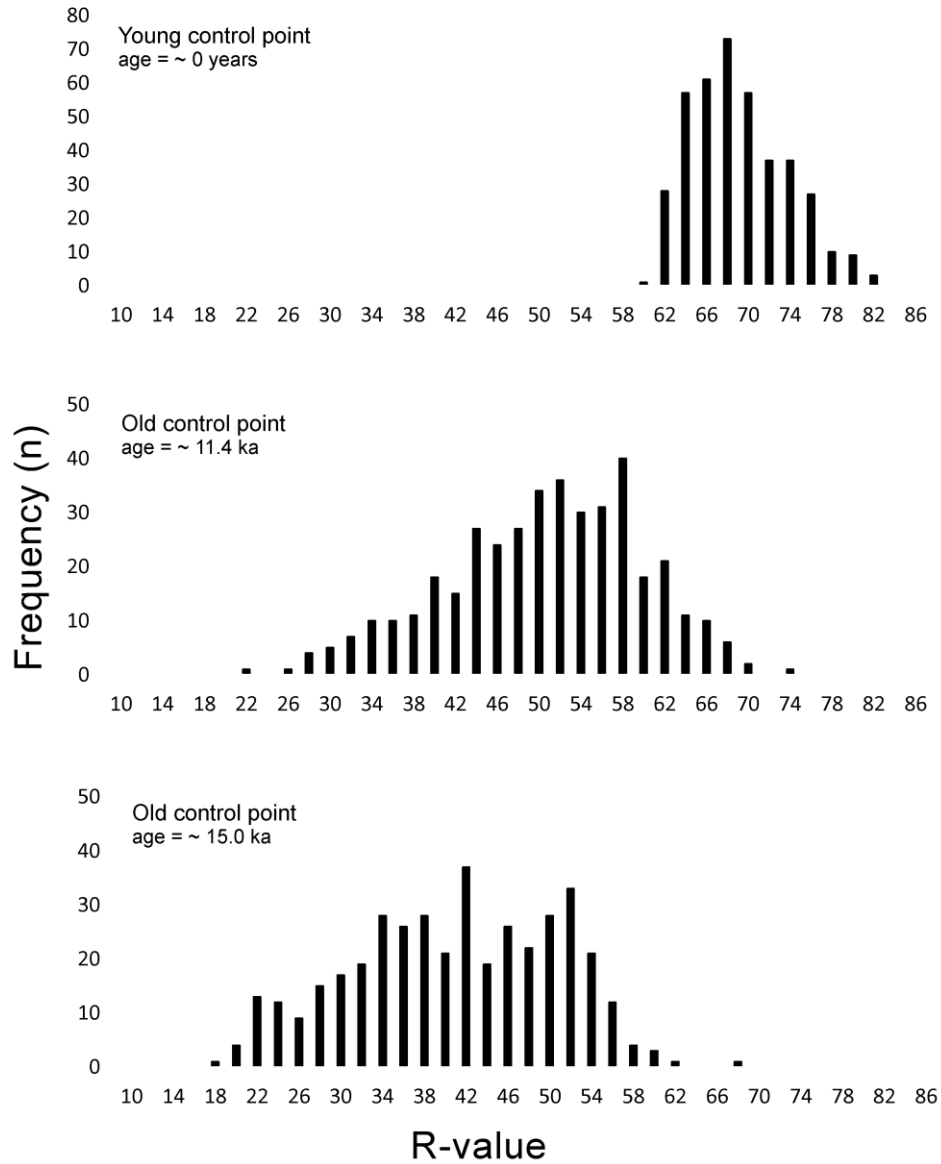


Figure 4. Frequency distributions of Schmidt hammer R-values of the young and the two old control points.

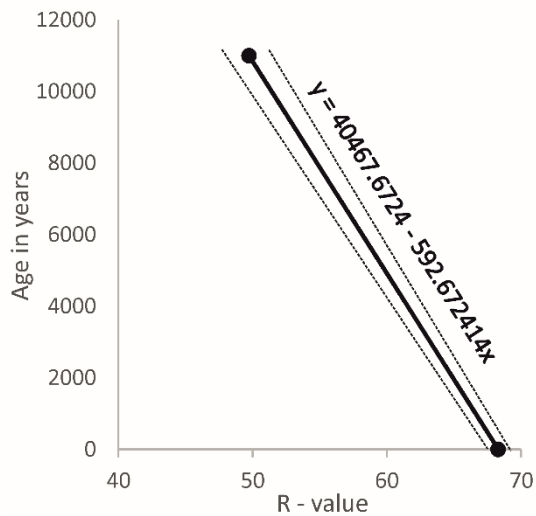


Figure 5. High-precision calibration curve and calibration equation for Blåhø calculated from the young control and the old control point I.

R-values of studied landforms

Most mean R-values of the investigated landforms are lower than old control point I, except for RSF-II. Yet, due to the inferred linear weathering relationship (see above) we consider the results to be plausible. The mean R-values from the different landforms on Blåhø are themselves consistent (Table 2), regardless of the rather high intra-site R-value variability represented by standard deviations and frequency distributions. However, the large sample size narrows the 95% confidence intervals. The standard deviation of most sites are in the same range (except RSF-I and RSF-II), largely with negative kurtosis and skewness. The lowest mean R-values were obtained from BL-II (35.99 ± 0.86), the highest values from RSF-I (59.31 ± 1.03). Overlapping confidence intervals for all landforms above 1450 m a.s.l. are noteworthy (except RSF-II and BL-II). Our histograms share rather platykurtic distributions with plateaus, wide R-value distributions, narrow tails and polymodal distributions (Figure 6). The SP and BS have no clear bi- or polymodal distribution. This is probably related to the formative processes and the nature of these landforms (see discussion). RSF-I has a high mode in the 50s, whereas RSF-II shows a high mode in the 60s. Both RSFs show the widest distribution of R-values, reflected in their standard deviations.

Table 3. Schmidt hammer R-values, standard deviation, kurtosis, skewness and n for the studied landforms.

Site	Mean \pm 95%CI ^a	σ	Kurtosis	Skewness	Boulders (n)
blockfield I	38.50 ± 0.88	8.96	-0.56	-0.31	200
blockfield II	35.99 ± 0.86	8.79	-0.64	-0.05	200
sorted polygon	37.49 ± 0.97	9.92	-0.37	0.16	200
bedrock	39.95 ± 1.04	9.15	-0.47	-0.40	150
blockstream (u)	38.05 ± 1.12	8.07	-0.61	-0.26	100
blockstream (l)	38.09 ± 1.31	9.43	-0.51	-0.37	100
rock-slope failure I	59.31 ± 1.03	12.86	0.25	-0.80	300
rock-slope failure II	46.19 ± 1.13	11.52	-0.26	-0.27	200

^a Mean of R-values with 95% confidence intervals ($\alpha = 0.05$).

u: upper site; l: lower site.

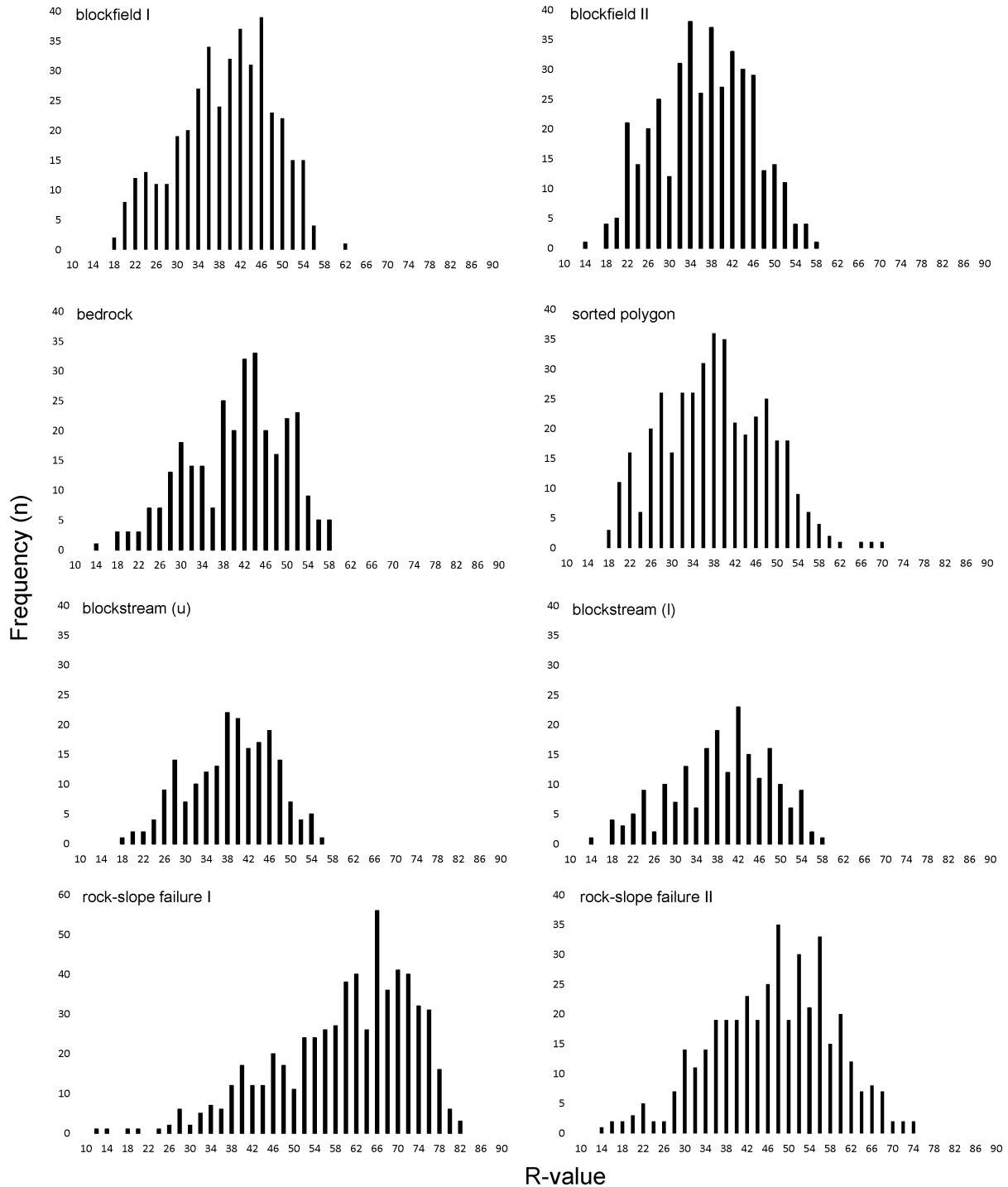


Figure 6. Frequency distributions of Schmidt hammer R-values from all investigated landforms.

All control sites and landforms fail the Shapiro-Wilk normality test. The upper and lower part of BS are not statistically different from each other, whereas BS differs from SP, BL-I and BL-II significantly. The positive skewness of SP suggests the possibility of somewhat less weathered boulders within the population. The other negatively skewed landforms probably include more weathered boulders in their population. The majority of pairs fail the Mann-Whitney test and are significantly different from each other (Table 3). The pairs of sites passing the Mann-Whitney test share a close spatial proximity (e.g. SP paired with BS) or are part of

the same landform (BS). However, BR and BL-II being statistically different to all other landforms in their proximity are somewhat unusual. Also note that BL-II is the feeder area of the BS and yet is a significantly different population.

Table 4. Results of Mann-Whitney tests of differences between pairs.

Pairs of sites	H ₀ ^a	α^b	Boulders (n)
SP – BL I	Retain	0.05649	400
SP – BL II	Reject	4.264e-05	400
SP – BS (u)	Retain	0.314	300
SP – BS (l)	Retain	0.2288	300
SP – BR	Reject	0.0001705	350
SP – RSF I	Reject	<2.2e-16	500
SP – RSF II	Reject	<2.2e-16	400
BL I – BL II	Reject	4.264e-05	400
BL I – BS (u)	Retain	0.4403	300
BL I – BS (l)	Retain	0.7095	300
BL I – BR	Reject	0.03391	350
BL I – RSF I	Reject	<2.2e-16	500
BL I – RSF II	Reject	<2.2e-16	400
BL II – BS (u)	Reject	0.004737	300
BL II – BS (l)	Reject	0.003916	300
BL II – BR	Reject	8.4e-09	350
BL II – RSF I	Reject	<2.2e-16	500
BL II – RSF II	Reject	<2.2e-16	400
BS (u) – BS (l)	Retain	0.717	200
BS (u) – BR	Reject	0.00876	250
BS (u) – RSF I	Reject	<2.2e-16	400
BS (u) – RSF II	Reject	<2.2e-16	300
BS (l) – BR	Reject	0.03271	250
BS (l) – RSF I	Reject	<2.2e-16	400

BS (l) – RSF II	Reject	2.38e-16	300
BR – RSF I	Reject	<2.2e-16	450
BR – RSF II	Reject	7.37e-14	350
RSF I – RSF II	Reject	<2.2e-16	500

^a H_0 = distribution of values is the same across both samples (decision at $\alpha = 0.05$).

^b Asymptotic significance level (two-tailed test).

Schmidt hammer exposure-age dating ages

The estimated SHD ages for different landforms are summarized in Table 4. There is an obvious difference in the SHD ages concerning the lower elevation RSFs and the landforms above 1450 m a.s.l. All landforms above this elevation yield SHD ages between 19137 ± 908 (BL-II) and 16790 ± 927 (BR) years based on our calibration curve and are statistically indistinguishable in age, except for BR and BL-II. The RSFs are significantly younger, with RSF-I (5316 ± 731 years) representing the youngest surveyed landform. It should be noted that the altitudinal relationship of all sites is statistically significant ($R^2=0.8337$). However, SHD ages do not necessarily increase with altitude (e.g. BL-I and BL-II).

Table 5. SHD ages from the sampled landforms. Each SHD age has a 95% confidence interval (C_i) derived from the sampling error of the landform sample (C_s) and the error of the calibration curve (C_c).

Landform	SHD age (years)	C_i (years)
blockfield I (1617 m a.s.l.)	17650	± 884
blockfield II (1562 m a.s.l.)	19137	± 908
sorted stone polygon (1450 m a.s.l.)	18248	± 928
bedrock (1562 m a.s.l.)	16790	± 927
blockstream (u) (1500 m a.s.l.)	17916	± 1059
blockstream (l) (1450 m a.s.l.)	17893	± 980
rock-slope failure I (550 m a.s.l.)	5316	± 731
rock-slope failure II (740 m a.s.l.)	13092	± 898

The SHD ages indicate three age groupings for the studied landforms. The age of RSF-I falls within the mid Holocene, RSF-II in the Bølling-Allerød interstadial and BL-I, BL-II, BR, SP, BS-u and BS-l in the end of the Late Weichselian.

Discussion

Schmidt hammer investigations from bedrock and coarse debris landforms have shown that the differing hardness properties revealed by R-values can be linked to different exposure time to subaerial weathering (Nesje et al. 1994b; Shakesby et al. 2006). SHD ages express the estimated age of boulders at the landform surface. All landforms show no indications of recent disturbance, therefore we assume no post-depositional boulder alteration. Consequently, our SHD ages indicate the maximum time since the boulders stabilized and the landforms became inactive. At all landforms, older boulders beneath those exposed at the surface are present. Hence, we consider that the SHD ages are minimum age estimates for the initiation of the landforms (Wilson and Matthews 2016).

Methodological implications

The range of the mean R-values between the young and the old control sites are comparable to other studies (e.g. Matthews et al. 2014; Wilson and Matthews 2016). High mean R-values and low variability of the young control site seem to be general characteristics of freshly exposed rocks (Matthews et al. 2013). In the same way as differences in surface weathering caused by minor lithological differences will become enhanced over time and cause standard deviation and confidence intervals to increase with older rocks that also have lower mean R-values (Aydin and Basu 2005; Matthews et al. 2013). Deriving our young control point from a construction site is acceptable, but not optimal. These boulders do not reflect fresh and unweathered material, because even recently excavated boulders are likely to have experienced some degree of subsurface weathering to an unknown extent. Furthermore, empirical studies have shown that freshly exposed bedrock does not necessarily give mean R-values expected for completely unweathered rock (Matthews et al. 2016). On the other hand, such exposed bedrock may more likely represent the initial conditions when boulders on the blockfield and other landforms became exposed for the first time (see discussion in Matthews et al. 2014, Winkler et al. 2016; Winkler and Lambiel 2018). Therefore, we rate the young control point as reasonably reliable despite a few older boulders with low R-values among the population and assign an age of zero to it.

For the old control point, two possible sites with documented ^{10}Be TCND ages were sampled. We used the old control point I at 1100 m a.s.l. for establishing the calibration curve, because of four reasons: (1) the better availability of material for sampling, (2) the smaller 95% confidence interval (Table 1), (3) the non-polymodal distribution suggesting no major post-depositional disturbance or polygenetic origin, and (4) the established linear weathering relationship during the Holocene and into the Late Glacial (Matthews and Owen 2010; Matthews and Wilson 2015; Winkler and Lambiel 2018). Although the old control points derived from bedrock and not individual boulders, we consider them as reliable because the differences of surface properties between boulders and bedrock tend to equalize over time (Matthews and Winkler 2011; Matthews et al. 2014).

The assumption of the linear relationship can largely be sustained by our results, despite a trend of slight decline with time (Figure 7). Černá and Engel (2011) show that linear weathering cannot be assumed prior

the Holocene, as weathering rates change throughout time. On the other hand, Tomkins et al. (2016, 2018) demonstrate that a quasi-linear relationship can be assumed for a period including the LGM. Because we consider old control point II as not entirely reliable (see above) we do not apply an alternative function for our linear calibration curve but instead have to consider pre-Holocene exposure ages as minimum ages when R-value decline by age is extrapolated beyond old control point I.

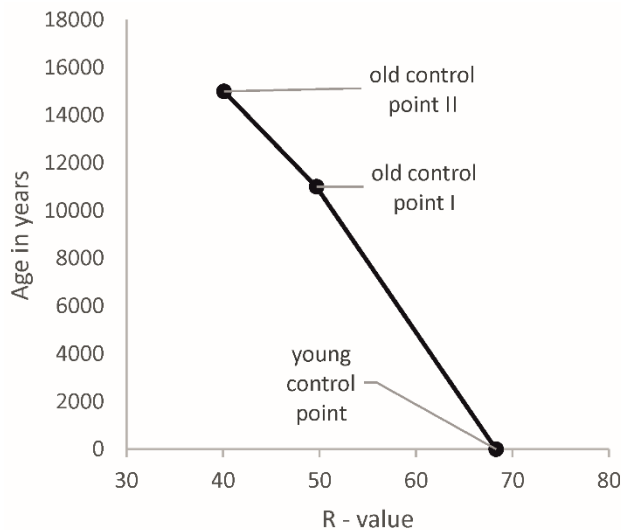


Figure 7. Calibration curve integrating the young control point and both two old control points.

The influence of snowpatches on weathering and their subsequent influence on Schmidt hammer results remains uncertain (see Ballantyne et al. 1989; Benedict 1993). Some studies (Ballantyne et al. 1989; Hall 1993) point to the fact, that late lying snow could enhance chemical weathering because of prolonged wetting. Other studies infer decreasing weathering due to the protective properties of snow (cf. Benedict 1993). Goudie (2006) states that the influence of snow should be reflected in high R-value variations, which is not detectable in our results. We consider weathering enhancement due to snow to be negligible, as all our sites have comparable annual snow coverage, limiting the influence on the relative ages. Additionally, aspect is considered to have an influence on weathering (Goudie 2006), but our localities share comparable southern aspect, thus we consider the relative effect negligible.

SHD landform ages and their interpretation

The mean R-values are estimates of the true age of landforms (Matthews et al. 2013). The consistency of our mean R-values between the different landforms, and within the same landform, confirm that the SHD ages are reliable estimates of the average boulder age. However, the interpretation of SHD ages from diachronous periglacial landforms are somewhat complicated (Washburn 1979; French 2007) compared to the interpretation of landforms linked to single, individual events like small rock slope failures (Matthews et al. submitted) or moraines (Winkler 2014). In such cases, mean R-values yield information on the exact timing of a specific depositional event, e.g. rockfall-avalanches (Nesje et al. 1994b). By contrast, some of our landforms share complex, long-term formation histories with variable time spans of disturbance, including subaerial exposure and burial of boulders. The complex dynamics and the role of non-climate related factors

on a local scale, makes drawing palaeoclimatic conclusions for patterned ground complicated (cf. Winkler et al. 2016).

The SHD exposure ages range from 19137 ± 908 to 5316 ± 731 years, reflecting the relict and inactive character of the landforms. The stability of the landforms is supported by blockfield depths of 1.60 m at Blåhø and 1.40 m at Rundhø showing differentiated stratigraphical layers, which indicate no profound post-depositional disturbance (Marr and Löffler 2017). This is supported by negative skewness (except SP), showing that the landforms were reactivated before final stabilization, as more weathered rocks are incorporated in the population. Negative skewness of R-values from periglacial landforms has been recorded previously (Rode and Kellerer-Pirklbauer 2011; Matthews et al. 2014). The estimated landform ages and their long period of formation is underpinned by the platykurtic nature of the histograms and the broad confidence intervals. The platykurtic histogram characteristics are in sharp contrast to those of landforms created by single events and distinct processes, which mostly have narrow peaks without plateaus like typical normal distributions (Aa and Sjästad 2000; Shakesby et al. 2004). Sorted circles studied by Winkler et al. (2016) show similar broad R-value distributions to those studied here. Comparable plateau-like histograms were reported from a relict pronival rampart (Matthews et al. 2011), ice-cored moraines (Matthews et al. 2014) and a relict blockfield (Wilson and Matthews 2016).

Permafrost presence can be inferred for all sites (except RSF-I and RSF-II) during most of the Holocene (Etzelmüller et al. 2003; Lilleøren and Etzelmüller 2011; Lilleøren et al. 2012). At present, permafrost is absent below 1450 m a.s.l. Farbrøt et al. (2011). The inactive status of the landforms above 1450 m a.s.l. raises the question whether they had also been inactive despite supposed presence of permafrost during several colder periods during the Late Glacial and the Holocene. Possible explanations include insufficient moisture supply in the active layer, changes in the freeze-thaw regime, decreasing frost susceptibility of fine (e.g. inner polygon) material leading to the termination of frost sorting (Winkler et al. 2016).

Climatic Implications

Plotting the SHD ages with established cold periods since the Late Weichselian confirms the general assumption that the landforms investigated responded to periods of colder climatic conditions (Figure 8). The development of the studied landforms is largely associated with permafrost, which often occurs after local deglaciation (Lilleøren et al. 2012). The SHD ages from landforms above 1450 m a.s.l. range between 19137 ± 908 (BL-II) and 16790 ± 927 years (BR). The 95% confidence intervals of these landforms are largely overlapping, indicating stabilization of all landforms during the same time period. Thus our results imply stabilization of the summit blockfields during severe periglacial conditions of the Karmøy/Bremanger readvance (~ 18.5 - 16.5 ka) observed in both western and southern Norway (Winguth et al. 2005; Olsen and Bergstrøm 2007) and coinciding with Heinrich event I at ~ 16.8 cal ka BP (Hemming 2004).

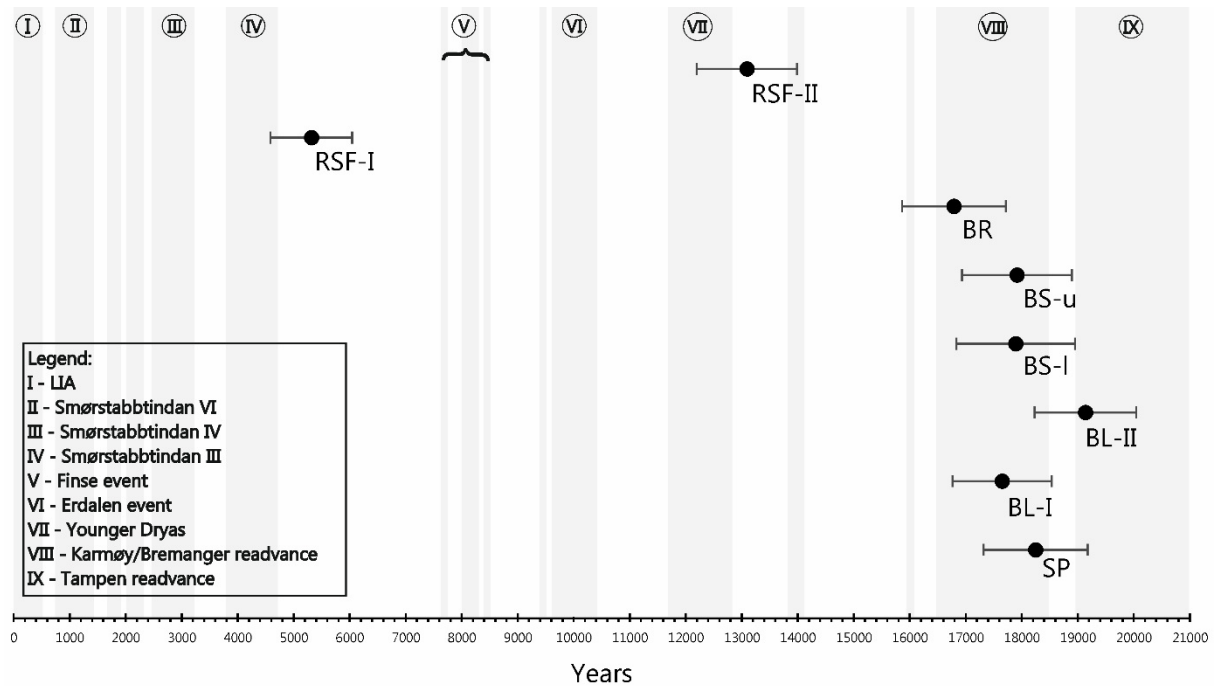


Figure 8. Plot integrating SHD ages and their total error for the studied landforms and intervals of documented climatic deteriorations during the late Quaternary. The major climatic deteriorations are displayed in grey (Data from Nygård et al. 2004; Winguth et al. 2005; Olsen and Bergström 2007; Matthews and Dresser 2008; Sejrup et al. 2009; Lohne et al. 2013).

According to Goehring et al. (2008), deglaciation started around 25.1 10Be ka at the Blåhø summit. They indicate slow ice thinning to ~1450 m a.s.l. until 15.0 10Be ka although the North Atlantic climate remained cold according to the GISP $\delta^{18}\text{O}$ proxy temperature record (Ritterknecht et al. 2006). Assuming the formation of the Blåhø blockfield started shortly after local deglaciation, it took ~6 ka for blockfield formation and stabilization. However, the blockfield appears to be much older (Marr and Löffler 2017). Blockfields may survive several glaciations, either by protective cold-based ice (Kleman 1994) or because of their position on nunataks (Landvik et al. 2003). The origin of some blockfields probably dates back to the Tertiary, the blocky material migrated to the surface through periglacial upfreezing (Rea et al. 1996). That the other studied landforms were also created before the LGM is implied by the negative skew of their R-values, supporting the reactivation of already existing landforms (Wilson and Matthews 2016).

Apart from the Karmøy/Bremanger readvance, BL-II and SP SHD ages would also fit within the age range of the Tampen readvance from ~22-19 ka (Sejrup et al. 2009). Due to the confidence intervals, we infer that the BL-II stabilized at the end of the Tampen readvance and the SP in the early phase of the Karmøy/Bremanger readvance. Possibly, the decline of temperatures and moisture supply during this early phase led to the cessation of frost sorting and the stabilization of the sorted polygons during ice-free and severe periglacial conditions. Our results do not support the findings of Goehring et al. (2008), who argue that the ice was at ~1450 m a.s.l. at 15.0 ± 1.0 10Be ka. In contrast, our SHD ages infer ice free conditions with a severe periglacial climate at least since ~19 ka.

The SHD ages of the blockstreams and bedrock on Rundhø, give indications about formation processes. It appears that the weathered bedrock formed the blockfield, which grades downslope to blockstreams. Despite their proximity, each of these landforms represents a different statistical population, and we interpret them as stabilizing at different times. The blockstreams probably stabilized during the Karmøy/Bremanger readvance. Blockstreams are accepted as products of cold climate processes which can also form over several cold periods (cf. Aldiss and Edwards 1999; Wilson et al. 2008). Uncertainty probably derives from various exposure times of boulders and the incorporation of older boulders, due to blockstream movement, internal mixing and sorting before they become stable. The broad confidence intervals and platycurtic histograms support the relatively long time for upfreezing and stabilization of the landforms. This is also particularly the case for the sorted polygons.

The age estimate for RSF-I points to the fact that the RSF event occurred during a period which was characterized by decreasing temperatures in western Norway and the onset of neoglaciation at the Jostedalbre Plateau (Nesje and Kvamme 1991; Nesje 2009) or during the preceding Holocene Thermal Maximum (HTM, ~8.0-5.0 ka; cf. Winkler et al. 2016). Such a timing would correspond to one peak of RSF activity in nearby Jotunheimen (Matthews et al. submitted).

The 95% confidence interval of the RSF-II age overlaps with one warmer period (Bølling-Allerød interstadial ~14.7-12.9 ka) and two climatic deteriorations, the Older Dryas between 14.1-13.8 ka (Olsen 2002) and the Younger Dryas (YD) 12.9-11.7 cal ka BP (Lohne et al. 2013). The negative skewness supports the cessation of rock falls and slope stabilization during the beginning of the YD. Due to the RSF size and the absence of other possible sources of boulders we consider the RSF to have occurred as a single event. The skewness however, leaves the possibility of several consecutive RSFs within a short time. Prolonged warm periods prior the YD probably led to permafrost degradation and weakening of the slope. McColl (2012) and Matthews et al. (submitted) point out that RSFs can also be connected to warming climate, when snow melt and permafrost degradation are enhanced.

Our SHD RSF ages support the findings of other studies that detail the occurrence of intensified (rock-)avalanche activity during the Lateglacial Interstadial, the YD and the second half of the Holocene (cf. Nesje et al. 1994b; Blikra et al. 2006; Longva et al. 2009). The recently reported causes of small rock-slope failures in the Holocene from Matthews et al. (submitted) in Jotunheimen, underpin the role of permafrost degradation in the context of warmer climate and lend support to our findings. Potential causes of RSFs are manifold and comprise glacial debuitressing, earthquakes or climate triggering, including permafrost degradation, enhanced precipitation, increased cleftwater pressure and freeze thaw activity (cf. Dawson et al. 1986; McColl 2012; Ballantyne et al. 2013; Wilson and Matthews 2016). All mentioned factors do not necessarily act in isolation, they may operate in various combination across longer time scales, where cause and effect are hard to distinguish (McColl 2012; Ballantyne and Stone 2013).

The results from this study indicate that RSFs do not necessarily occur shortly after deglaciation (Nesje et al. 1994b) as stated by others (e.g. Cruden and Hu 1993). Furthermore, we reject earthquakes as a major trigger because the magnitude of earthquakes appears to be too low to trigger small RSFs in inland Norway,

in contrast to the more active coastal regions (cf. Matthews et al. submitted). In concert with McColl (2012) and Pánek et al. (2016) we consider our RSFs to have occurred during warm phases in the Holocene and the Lateglacial, namely the HTM and the Bølling-Allerød interstadial. During these periods water pressures likely increased during snow melt periods, permafrost degradation and heavy precipitation (Blikra et al. 2006; cf. McColl 2012).

Several periods of climatic cooling, including the YD, the Erdalen event (9100 ± 200 14C yr BP), the Finse event (~ 7600 14C yr BP) and the Neoglacial (~ 6 ka) (Sejrup et al. 2000; Matthews and Dresser 2008; Nesje 2009), seem not to have triggered any activity at the studied landforms above 1450 m a.s.l. This is despite the occurrence of YD moraines at 1400/1500 m a.s.l. south of Lesjaskog, close to our study area (Foltestad 2007). Even during the Neoglacial maximum of the Little Ice Age, when most south Norwegian glaciers reached their maximum extent since deglaciation in the early Holocene (e.g. Matthews and Dresser 2008; Nesje 2009), the Blåhø landforms were not reactivated. However, Matthews et al. (2014) show that other landforms in the area, such as ice-cored ridges re-formed during this period. The non-reactivation of the studied landforms can only be explained by their strong structural stability, which was probably determined prior to the LGM.

Conclusion

This study gives first indications of geomorphic footprints of late Quaternary cold events in Ottadalen, Norway. This paper demonstrates that new local high-precision age-calibration equations are suitable for age determination of boulder-dominated landforms. We provide valuable insights into the environmental modifications between the LGM and the YD/early Holocene transition. By successfully applying high-precision SHD on a variety of periglacial landforms, we obtained exposure ages from 19137 ± 908 to 5316 ± 731 years. The following conclusions can be drawn from the present study:

- (1) The landforms above 1450 m a.s.l. most likely stabilized within the cold phase of the Karmøy/Bremanger readvance (~ 18.5 - 16.5 ka). Our results indicate severe periglacial conditions occurred ~ 19 ka, which is in contrast to the inferred ice coverage at that time.
- (2) The lower lying RSFs likely occurred during warm phases during the Holocene Thermal Maximum and the Bølling-Allerød interstadial (~ 14.7 - 12.9 ka). This does not support the general notion that rock-slope failures mostly occur a few millennia after deglaciation.
- (3) Late Glacial and Holocene cold periods affected those landforms in lower lying areas, but did not reactivate those above 1450 m a.s.l. It appears that climatic cooling, possibly assisted by limited moisture availability, was insufficient to reactivate or substantially modify those landforms within the last ~ 16 ka. We demonstrate that the landforms investigated are essentially relict, with only limited recent activity.
- (4) Our results have wider implications on the glaciation history of the area. Instead of the inferred ice coverage above 1450 m a.s.l. at 15.0 ± 1.0 10Be ka, it appears that the landforms at this elevation were

ice free since up to ~19 ka. We infer that the studied landforms were created before the LGM and either survived beneath cold-based ice or on nunataks.

Acknowledgements

We are thankful to Jenny Müller and Claire Pfalzner-Gibbon who contributed during the field work. This study was financed by the Friedrich-Ebert-Stiftung. We thank Peter Wilson and an anonymous reviewer for valuable comments on the manuscript.

Conflict of interest

The authors have no conflict of interest to disclose.

References

- Aa AR, Sjøstad JA. 2000. Schmidt hammer age evaluation of the moraine sequence in front of Bøyabreen, western Norway. *Norsk Geol Tidsskr.* 80(1):27–32.
- Aldiss DJ, Edwards EJ. 1999. The Geology of the Falkland Islands. Technical Report WC/99/10. Keyworth: British Geological Survey.
- André MF. 1996. Rock weathering rates in arctic and subarctic environments (Abisko Mts., Swedish Lapland). *Zeitschrift f Geomorph.* 40(4):499–517.
- André MF. 2003. Do periglacial landscapes evolve under periglacial conditions? *Geomorphology.* 52(1–2):149–164.
- Aoyama M. 2005. Rock glaciers in the northern Japanese Alps: palaeoenvironmental implications since the Late Glacial. *J Quaternary Sci.* 20(5):471–484.
- Aydin A, Basu A. 2005. The Schmidt Hammer in rock material characterization. *Eng Geol* 81(1):1–14.
- Ballantyne CK. 2010. A general model of autochthonous blockfield evolution. *Permafrost Periglac Proc.* 21(4):289–300.
- Ballantyne CK. 2013. Trimlines and paleonunataks. Elias SA, editor. *Encyclopedia of Quaternary Science.* 2nd ed. Volume 2. Amsterdam: Elsevier; p. 918–928.
- Ballantyne CK, Harris C. 1994. The periglaciation of Great Britain. Cambridge: Cambridge University Press.
- Ballantyne CK, Stone JO. 2013. Timing and periodicity of paraglacial rock-slope failures in the Scottish Highlands. *Geomorphology.* 186:150–161.
- Ballantyne CK, Black NM, Finlay DP. 1989. Enhanced boulder weathering under late-lying snowpatches. *Earth Surf Proc Land.* 14(8):745–750.
- Ballantyne CK, McCarroll D, Nesje A, Dahl SO. 1997. Periglacial trimlines, former nunataks and the altitude of the last ice sheet in Wester Ross, northwest Scotland. *J Quaternary Sci.* 12(3):225–238.
- Ballantyne CK, McCarroll D, Nesje A, Dahl SO, Stone JO. 1998. The last ice sheet in North-West Scotland: reconstruction and implications. *Quaternary Sci Rev.* 17(12):1149–1184.
- Ballantyne CK, Wilson P, Schnabel C, Xu S. 2013. Lateglacial rock slope failures in north-west Ireland: age, causes and implications. *J Quaternary Sci.* 28(8):789–802.
- Benedict JB. 1993. Influence of snow upon rates of grandiorite weathering, Colorado Front Range, USA. *Boreas.* 22(2):87–92.
- Blikra LH, Longva O, Braathen A, Anda E, Dehls JF, Stalsberg K. 2006. Rock slope failures in Norwegian fjord areas: examples, spatial distribution and temporal pattern. In: Evans SG, Mugnozsa GS, Strom A, Hermanns RL, editors. *Landslides from Massive Rock Slope Failure.* Dordrecht: Springer; p.475–496.
- Boelhouwers JC, Holness S, Meiklejohn I, Sumner P. 2002. Observations on a blockstream in the vicinity of Sani Pass, Lesotho highlands, Southern Africa. *Permafrost Periglac Proc.* 13(4):251–257.
- Brook EJ, Nesje A, Lehman SJ, Raisbeck GM, Yiou F. 1996. Cosmogenic nuclide exposure ages along a vertical transect in western Norway: Implications for the height of the Fennoscandian ice sheet. *Geology.* 24(3):207–210.

- Černá B, Engel Z. 2011. Surface and sub-surface Schmidt hammer rebound value variation for a granite outcrop. *Earth Surf Proc Land*. 36(2):170–179.
- Clark PU, Dyke AS, Shakun JD, Carlson AE, Clark J, Wohlfarth B, Mitrovica JX, Hostetler SW, McCabe AM. 2009: The last glacial maximum. *Science*. 325:710–714.
- Colman SM. 1981. Rock-weathering rates as functions of time. *Quaternary Res*. 15(3):250–264.
- Cook-Talbot JD. 1991. Sorted circles, relative-age dating and palaeoenvironmental reconstruction in an alpine periglacial environment, eastern Jotunheimen, Norway: lichenometric and weathering-based approaches. *Holocene*. 1(2):128–141.
- Cruden DM, Hu XQ. 1993. Exhaustion and steady state models for predicting landslide hazards in the Canadian Rocky Mountains. *Geomorphology*. 8(4):279–285.
- Dahl R. 1966. Block fields and other weathering forms in the Narvik mountains. *Geogr Ann Ser A Phys Geogr*. 48(4):224–227.
- Dahl SO, Nesje A, Øvstedal J. 1997. Cirque glaciers as morphological evidence for a thin Younger Dryas ice sheet in east-central southern Norway. *Boreas*. 26(3):161–180.
- Dawson AG, Matthews JA, Shakesby RA. 1986. A Catastrophic Landslide (Sturzstrom) in Verkildalen, Rondane National Park, Southern Norway. *Geogr Ann Ser A Phys Geogr*. 68(1–2):77–87.
- Engel Z. 2007. Measurement and age assignment of intact rock strength in the Krkonoše Mountains, Czech Republic. *Zeitschrift f Geomorph. N.F.* 51, Supplementary Issue 2:69–80.
- Etzelmüller B, Berthing I, Sollid JL. 2003. Aspects and concepts on the geomorphological significance of Holocene permafrost in southern Norway. *Geomorphology*. 52(1–2):87–104.
- Evans DJA, Archer S, Wilson DJH. 1999. A comparison of the lichenometric and Schmidt hammer dating techniques based on data from the proglacial areas of some Icelandic glaciers. *Quaternary Sci Rev*. 18(1):13–41.
- Fabel D, Stroeven A, Harbor J, Kleman J, Elmore D, Fink D. 2002. Landscape preservation under Fennoscandian ice sheets determined from in situ produced ¹⁰Be and ²⁶Al. *Earth Planet Sci Letters*. 201(2):397–406.
- Farbrot H, Hipp TF, Etzelmüller B, Isaksen K, Ødegård, RS, Schuler TV, Humlum O. 2011. Air and Ground Temperature Variations Observed along Elevation and Continentality Gradients in Southern Norway. *Permafrost Periglac Proc*. 22(4):343–360.
- Feuillet Th, Mercier D. 2012. Post-Little Ice Age patterned ground development on two Pyrenean proglacial areas: from deglaciation to periglaciation. *Geogr Ann Ser A Phys Geogr*. 94(3):363–376.
- Ffoulkes C, Harrison S. 2014. Evaluating the Schmidt hammer as a method for distinguishing the relative age of late Holocene moraines: Svellnosbreen, Jotunheimen, Norway. *Geogr Ann Ser A Phys Geogr*. 96(3):393–402.
- Fjellanger J, Sørbel L, Linge H, Brook EJ, Raisbeck GM, Yiou F. 2006. Glacial survival of blockfields on the Varanger Peninsula, northern Norway. *Geomorphology*. 82(3–4):255–272.
- Follestad BA. 2003. Development of minor late-glacial ice domes east of Oppdal, Central Norway. *Norges geologiske undersøkelse Bulletin*. 441:39–49.
- Follestad BA. 2007. Lesjaskog 1419 III. Preliminart kvartargeologisk kart M 1:50.000. *Norges geologiske undersøkelse*.
- French HM. 2007. *The Periglacial Environment*. 3rd ed. Chichester: Wiley.
- Goehring BM, Brook EJ, Linge H, Raisbeck GM, Yiou F. 2008. Beryllium-10 exposure ages of erratic boulders in southern Norway and implications for the history of the Fennoscandian Ice Sheet. *Quaternary Sci Rev*. 27(3–4):320–336.
- Goldthwait RP. 1976. Frost-sorted patterned ground: A review. *Quaternary Res*. 6(1):27–35.
- Goodfellow BW, Fredin O, Derron M-H, Stroeven AP. 2008. Weathering processes and Quaternary origin of an alpine blockfield in Arctic Sweden. *Boreas*. 38(2):379–398.
- Goudie AS. 2006. The Schmidt Hammer in geomorphological research. *Prog in Phy Geog*. 30(6):703–718.
- Hall K. 1993. Enhanced bedrock weathering in association with late-lying snowpatches: Evidence from Livingston Island, Antarctica. *Earth Surf Proc Land*. 18(2):121–129.

- Hemming SR. 2004. Heinrich events: Massive late Pleistocene detritus layers of the North Atlantic and their global climate imprint. *Rev Geophys.* 42(1):1–43.
- Hughes ALC, Gyllencreutz R, Lohne ØS, Mangerud J, Svendsen JI. 2016. The last Eurasian ice sheets – a chronological database and time-slice reconstruction, DATED-1. *Boreas.* 45(1):1–45.
- Juliussen H, Humlum O. 2007. Preservation of block fields beneath Pleistocene ice sheets on Solen and Elgahogna, central-eastern Norway. *Zeitschrift f Geomorph.* N.F 51, Supplementary Issue 2:113–138.
- Kellerer-Pirklbauer A, Wangensteen B, Farbrøt H, Etzelmüller B. 2008. Relative surface age-dating of rock glacier systems near Hólar in Hjaltadalur, northern Iceland. *J Quaternary Sci.* 23(2):137–151.
- Klapyta P. 2013. Application of Schmidt hammer relative age dating to Late Pleistocene moraines and rock glaciers in the Western Tatra Mountains, Slovakia. *Catena.* 111:104–121.
- Kleman J. 1994. Preservation of landforms under ice sheets and ice caps. *Geomorphology.* 9(1):19–32.
- Landvik JY, Brook EJ, Gualtieri L, Raisbeck G, Salvigsen O, Yiou F. 2003. Northwest Svalbard during the last glaciation: Ice-free areas existed. *Geology.* 31(10):905–908.
- Lilleøren KS, Etzelmüller, B. 2011. A regional inventory of rock glaciers and ice-cored moraines in Norway. *Geogr Ann Ser A Phys Geogr.* 93(3): 175–191.
- Lilleøren KS, Etzelmüller B, Schuler TV, Gislås K, Humlum O. 2012. The relative age of permafrost – estimation of Holocene permafrost limits in Norway. *Global Planet Change.* 92–93:209–223.
- Lohne ØS, Mangerud J, Birks HH. 2013. Precise ¹⁴C ages of the Vedde and Saksunarvatn ashes and the Younger Dryas boundaries from western Norway and their comparison with the Greenland Ice Core (GICC05) chronology. *J Quaternary Sci.* 28(5):490–500.
- Longva O, Blikra LH, Dehls JF. 2009. Rock avalanches: distribution and frequencies in the inner part of Storfjorden, Møre og Romsdal County, Norway. Report, Geological Survey of Norway.
- Marr P, Löffler J. 2017. Establishing a multi-proxy approach to alpine blockfield evolution in south-central Norway. *AUC Geogr.* 52(2):219–236.
- Matthews JA. 2013. Neoglaciation in Europe. In: Elias SA, editor. *Encyclopedia of Quaternary Science.* 2nd ed. Volume 2. Amsterdam: Elsevier; p. 257–268.
- Matthews JA, Dresser PQ. 2008. Holocene glacier variation chronology of Smørstabbtindan massif, Jotunheimen, southern Norway, and the recognition of century- to millennial-scale European Neoglacial Events. *Holocene.* 18(1):181–201.
- Matthews JA, Owen G. 2010. Schmidt hammer exposure-age dating: developing linear age-calibration curves using Holocene bedrock surfaces from the Jotunheimen-Jostedalbreen regions of southern Norway. *Boreas.* 39(1):105–115.
- Matthews JA, Winkler S. 2011. Schmidt-hammer exposure-age dating (SHD): application to early Holocene moraines and a reappraisal of the reliability of terrestrial cosmogenic-nuclide dating (TCND) at Austanbotnbreen, Jotunheimen, Norway. *Boreas.* 40(2):256–270.
- Matthews JA, McEwen LJ. 2013. High-precision Schmidt-hammer exposure-age dating of flood berms, Vetlestølsdalen, alpine southern Norway: first application and some methodological issues. *Geogr Ann Ser A Phys Geogr.* 95(2):185–195.
- Matthews JA, Wilson P. 2015. Improved Schmidt-hammer exposure ages for active and relict pronival ramparts in southern Norway, and their palaeoenvironmental implications. *Geomorphology.* 246:7–21.
- Matthews JA, Shakesby RA, Owen G, Vater AE. 2011. Pronival rampart formation in relation to snow-avalanche activity and Schmidt-hammer exposure-age dating (SHD): Three case studies from southern Norway. *Geomorphology.* 130(3–4):280–288.
- Matthews JA, Nesje A, Linge H. 2013. Relict Talus-Foot Rock Glaciers at Øyberget, Upper Ottadalen, Southern Norway: Schmidt hammer Exposure Ages and Palaeoenvironmental Implications. *Permafrost Periglac Proc.* 24(4):336–346.
- Matthews JA, Winkler S, Wilson P. 2014. Age and origin of ice-cored moraines in Jotunheimen and Breheimen, southern Norway: insights from Schmidt-Hammer exposure-age dating. *Geogr Ann Ser A Phys Geogr.* 96(4):531–548.
- Matthews JA, McEwen L, Owen G. 2015. Schmidt-hammer exposure-age dating (SHD) of snow-avalanche impact ramparts in southern Norway: approaches, results and implications for landform age, dynamics and development. *Earth Surf Proc Land.* 40(13):1705–1718.

- Matthews JA, Owen G, Winkler S, Vater AE, Wilson P, Mourne RW, Hill JL. 2016. A rock-surface micro-weathering index from Schmidt hammer R-values and its preliminary application to some common rock types in southern Norway. *Catena*. 143:35–44.
- Matthews JA, Wilson P, Mourne RW. 2017. Landform transitions from pronival ramparts to moraines and rock glaciers: a case study from the Smørbotn cirque, Romsdalsalpane, southern Norway. *Geogr Ann Ser A Phys Geogr*. 99(1):15–37.
- Matthews JA, Winkler S, Wilson P, Mourne RW, Hill JL, Owen G, Vater AE. Small rock-slope failures conditioned by Holocene permafrost degradation: a new approach and conceptual model based on Schmidt-hammer exposure-age dating in Jotunheimen, southern Norway. *Boreas*. (submitted).
- McCarroll D. 1989. Potential and Limitations of the Schmidt Hammer for Relative-Age Dating: Field Tests on Neoglacial Moraines, Jotunheimen, Southern Norway. *Arctic Alpine Res*. 21 (3):268–275.
- McCarroll D. 2016. Trimline Trauma: The Wider Implications of a Paradigm Shift in Recognising and Interpreting Glacial Limits. *Scottish Geogr J*. 132(2):130–139.
- McCarroll D, Nesje A. 1993. The vertical extent of ice sheets in Nordfjord, western Norway: measuring degree of rock surface weathering. *Boreas*. 22(3):255–265.
- McCull ST. 2012. Paraglacial rock-slope stability. *Geomorphology*. 153–154:1–16.
- Moen A. 1998. Nasjonalatlas for Norge: vegetasjon (National atlas of Norway: vegetation). Norwegian Mapping Authority. Hønefoss, Norway.
- Nesje A. 2009. Latest Pleistocene and Holocene alpine glacier fluctuations in Scandinavia. *Quaternary Sci Rev*. 28(21–22):2119–2136.
- Nesje A, Dahl SO. 1990. Autochthonous block fields in southern Norway: implications for the geometry, thickness, and isostatic loading of the Late Weichselian Scandinavian ice sheet. *J Quaternary Sci*. 5(3):225–234.
- Nesje A, Kvamme M. 1991. Holocene glacier and climate variations in western Norway: Evidence for early Holocene glacier demise and multiple Neoglacial events. *Geology*. 19(6):610–612.
- Nesje A, Dahl SO, Anda E, Rye N. 1988. Block fields in southern Norway: significance for the Late Weichselian ice sheet. *Norsk Geol Tidsskr*. 68:149–169.
- Nesje A, McCarroll D, Dahl SO. 1994a. Degree of rock surface weathering as an indicator of ice-sheet thickness along an east–west transect across southern Norway. *J Quaternary Sci*. 9(4):337–347.
- Nesje A, Blikra LH, Anda E. 1994b. Dating rockfall-avalanche deposits from degree of rock-surface weathering by Schmidt-hammer tests: a study from Norangsdalen, Sunnmøre, Norway. *Norsk Geol Tidsskr*. 74(2):108–113.
- Nesje A, Dahl SO, Linge H, Ballantyne CK, McCarroll D, Brook EJ, Raisbeck GM, Yiou, F. 2007. The surface geometry of the Last Glacial Maximum ice sheet in the Andøya-Skånland region, northern Norway, constrained by surface exposure dating and clay mineralogy. *Boreas*. 36(3):227–239.
- Niedzielski T, Migon P, Placek A. 2009. A minimum sample size required from Schmidt hammer measurements. *Earth Surf Proc Land*. 34(13):1713–1725.
- Nygård A, Sejrup HP, Hafliðason H, Cecchie M, Ottesen D. 2004. Deglaciation history of the southwestern Fennoscandian Ice Sheet between 15 and 13 ¹⁴C ka BP. *Boreas*. 33(1):1–17.
- Olsen L. 2002. Mid and Late Weichselian, ice-sheet fluctuations northwest of the Svartisen glacier, Nordland, northern Norway. *Norges geologiske undersøkelse Bulletin*. 440:39–51.
- Olsen L, Bergström B. 2007. Glacier variations during the LGM interval in the Karmøy – Jæren district, SW Norway. *NGF Abstracts and Proceedings*. 1:73–74.
- Pánek T, Engel Z, Metlík P, Braucher R, Břežný M, Škarpich V, Zondervan A. 2016. Cosmogenic age constraints on post-LGM catastrophic rock slope failures in the Tatra Mountains (Western Carpathians). *Catena*. 138:52–67.
- Pape R, Löffler J. 2017. Determinants of arctic-alpine pasture resources—The need for a spatially and functionally fine-scaled perspective. *Geografiska Annaler: Series A, Physical Geography*. 99:353–370.
- Pape R, Wundram D, Löffler J. 2009. Modelling Near-Surface Temperature Conditions in High Mountain Environments - An Appraisal. *Climate Res*. 39(2):99–109.
- Proceq. 2014. Operating instructions RockSchmidt and Rocklink. Proceq SA, Schwerzenbach.

- Rae AC, Harrison S, Mighall T, Dawson AG. 2004. Periglacial trimlines and nunataks of the Last Glacial Maximum: the Gap of Dunloe, southwest Ireland. *J Quaternary Sci.* 19(1):87–97.
- Rea BR. 2013. Blockfields (Felsenmeer). In: Elias SA, editor. *Encyclopedia of Quaternary Science*. 2nd ed. Volume 3. Amsterdam: Elsevier; p. 523–534.
- Rea BR, Whalley W, Rainey MM, Gordon JE. 1996. Blockfields, old or new? Evidence and implications from some plateaus in northern Norway. *Geomorphology*. 15(2):109–121.
- Ritterknecht VR, Clark PU, Raisbeck GM, Yiou F, Bitinas A, Brook EJ, Marks, L, Zelčs V, Lunkka JP, Pavlovskaya E, et al. 2006. The Last Deglaciation of the Southeastern Sector of the Scandinavian Ice Sheet. *Science*. 311(5766):1449–1452.
- Rixhon G, Demoulin A. 2013. Evolution of slopes in a cold climate. In: Shroder J, editor. *Treatise on Geomorphology*, volume 8 (glacial and periglacial geomorphology). Elsevier, Amsterdam, 392–415.
- Rode M, Kellerer-Pirklbauer A. 2011. Schmidt-hammer exposure-age dating (SHD) of rock glaciers in the Schöderkogel-Eisenhut area, Schladminger Tauern Range, Austria. *Holocene*. 22(7):761–771.
- Rudberg S. 1988. Gross morphology of Scandinavia—six complementary ways of explanation. *Geogr Ann Ser A Phys Geogr*. 70(3):135–167.
- Sánchez JS, Mosquera DF, Vidal Romani JRV. 2009. Assessing the age-weathering correspondence of cosmogenic ^{21}Ne dated Pleistocene surfaces by the Schmidt Hammer. *Earth Surf Proc Land*. 34(8):1121–1125.
- Schaefer MJ, Finkel RC, Balco G, Alley RB, Caffee MW, Briner JP, Young NE, Gow AJ, Schwartz R. 2016. Greenland was nearly ice-free for extended periods during the Pleistocene. *Nature*. 540:252–255.
- Schmidt E. 1950. Der Beton-Prüfhammer. *Schweizer Baublatt*, Zürich 68(28):378.
- Sejrup HP, Larsen E, Landvik J, King EL, Hafliðason H, Nesje A. 2000. Quaternary glaciations in southern Fennoscandia: evidence from southwestern Norway and the northern North Sea region. *Quaternary Sci Rev*. 19(7):667–685.
- Sejrup HP, Nygård A, Hall AM, Hafliðason H. 2009. Middle and Late Weichselian (Devensian) glaciation history of south-western Norway, North Sea and eastern UK. *Quaternary Sci Rev*. 28(3–4):370–380.
- Shakesby RA, Matthews JA, Winkler S. 2004. Glacier variations in Breheimen, southern Norway: relative-age dating of Holocene moraine complexes at six high-altitude glaciers. *Holocene*. 14(6):899–910.
- Shakesby RA, Matthews JA, Owen G. 2006. The Schmidt hammer as a relative-age dating tool and its potential for calibrated-age dating in Holocene glaciated environments. *Quaternary Sci Rev*. 25(21–22):2846–2867.
- Shakesby RA, Matthews JA, Karlén W, Los SO. 2011. The Schmidt hammer as a Holocene calibrated-age dating technique: Testing the form of the R-value-age relationship and defining the predicted age errors. *Holocene*. 21(4):615–628.
- Stahl T, Winkler S, Quigley M, Bebbington M, Duffy B, Duke D. 2013. Schmidt hammer exposure-age dating (SHD) of late Quaternary fluvial terraces in New Zealand. *Earth Surf Proc Land*. 38(15):1838–1850.
- Stroeven AP, Fabel D, Hättstrand C, Harbor J. 2002. A relict landscape in the centre of Fennoscandian glaciation: cosmogenic radionuclide evidence of tors preserved through multiple glacial cycles. *Geomorphology*. 44(1–2):145–154.
- Strømsøe JR, Paasche Ø. 2011. Weathering patterns in high-latitude regolith. *J Geophys Res*. 116(F3):1–17.
- Tomkins MD, Dortch JM, Hughes PD. 2016. Schmidt hammer exposure dating (SHED): Establishment and implications for the retreat of the last British Ice Sheet. *Quaternary Geochr*. 33:46–60.
- Tomkins MB, Hucka JJ, Dortch JM, Hughes PD, Kirbride MP, Barr ID. 2018. Schmidt Hammer exposure dating (SHED): Calibration procedures, new exposure age data and an online calculator. *Quaternary Geochr*. 44:55–62.
- Tveten E, Lutro O, Thorsnes T. 1998. *Geologisk kart over Norge [Geological map of Norway]* 1:250,000. Trondheim: Norges Geologiske Undersøkelse.
- Washburn AL. 1956. Classification of patterned ground and review of suggested origins. *Geol Soc America Bulletin*. 67(7):823–866.

- Washburn AL. 1979. *Geocryology. A survey of periglacial processes and environments*. London: Edward Arnold.
- Whalley WB, Rea BR, Rainey MM. 2004. Weathering, blockfields and fracture systems and the implications for long-term landscape formation: some evidence from Lyngen and Öksfjordjokelen areas in north Norway. *Polar Geogr.* 28:93–119.
- White K, Bryant R, Drake N. 1998. Techniques for measuring rock weathering: application to a dated fan segment sequence in southern Tunisia. *Earth Surf Proc Land.* 23(11):1031–1043.
- Wilson P. 2004. Relict rock glaciers, slope failure deposits, or polygenetic features? A re-assessment of some Donegal debris landforms. *Irish Geogr.* 37(1):77–87.
- Wilson P, Matthews JA. 2016. Age assessment and implications of late Quaternary periglacial and paraglacial landforms on Muckish Mountain, northwest Ireland, based on Schmidt-hammer exposure-age dating (SHD). *Geomorphology.* 270:134–144.
- Wilson P, Bentley MJ, Schnabel C, Clark R, Xu S. 2008. Stone run (block stream) formation in the Falkland Islands over several cold stages, deduced from cosmogenic isotope (^{10}Be and ^{26}Al) surface exposure dating. *J Quaternary Sci.* 23(5):461–473.
- Wilson P, Matthews JA, Mourné RW. 2017. Relict Blockstreams at Insteheia, Valdalen-Talfjorden, Southern Norway: Their Nature and Schmidt Hammer Exposure Age. *Permafrost Periglac Proc.* 28(1):286–297.
- Winguth C, Mickelson D, Larsen E, Darter JR, Moeller CA, Stalsberg K. 2005. Thickness evolution of the Scandinavian Ice Sheet during the Late Weichselian in Nordfjord, western Norway: evidence from ice-flow modeling. *Boreas.* 34(2):176–185.
- Winkler S. 2005. The Schmidt hammer as a relative-age dating technique: potential and limitations of its application on Holocene moraines in Mt Cook National Park, Southern Alps, New Zealand. *New Zealand J Geol Geophys.* 48(1):105–116.
- Winkler S. 2009. First attempt to combine terrestrial cosmogenic nuclide (^{10}Be and Schmidt hammer relative-age dating): Strauchon Glacier, Southern Alps, New Zealand. *Central Europ J Geosciences.* 1(3):274–290.
- Winkler S. 2014. Investigation of late-Holocene moraines in the western Southern Alps, New Zealand, applying Schmidt-hammer exposure-age dating. *Holocene.* 24(1):48–66.
- Winkler S, Matthews JA. 2014. Comparison of electronic and mechanical Schmidt hammers in the context of exposure-age dating: are Q- and R-values interconvertible? *Earth Surf Proc Land.* 39(8):1128–1136.
- Winkler S, Lambiel C. 2018. Age constraints of rock glaciers in the Southern Alps/New Zealand – exploring their palaeoclimatic potential. *Holocene* (published online – doi: 10.1177/0959683618756802).
- Winkler S, Matthews JA, Mourné RW, Wilson P. 2016. Schmidt-hammer exposure ages from periglacial patterned ground (sorted circles) in Jotunheimen, Norway, and their interpretative problems. *Geogr Ann Ser A Phys Geogr.* 98(3):265–285.

8 Schmidt-Hammer Exposure-Age Dating (SHD) Performed on Periglacial and Related Landforms in Opplendskedalen, Geirangerfjellet, Norway: Implications for Mid- and Late-Holocene Climate Variability

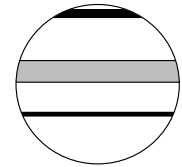
MARR, P., WINKLER, S. and LÖFFLER, J. (2019a): Schmidt-hammer exposure-age dating (SHD) performed on periglacial and related landforms in Opplendskedalen, Geirangerfjellet, Norway: Implications for mid- and late-Holocene climate variability. In: *The Holocene* 29, 97–109.

Abstract


Schmidt-hammer exposure-age dating (SHD) was applied to a variety of boulder-dominated periglacial landforms in an attempt to establish a local mid-/ late-Holocene chronology for the Geirangerfjellet in South Norway. Landform ages were obtained by application of a local calibration curve for Schmidt hammer R-values based on young and old control points comprising fresh road cuts and a bedrock surface in proximity to the study area, respectively. The area was deglaciated ~11.5 ka ago according to independent age information. Investigation of age, formation and stabilization of the periglacial landforms and processes involved allowed assessment of the underlying Holocene climate variability and its relationship to landform evolution. Our SHD ages range from 7.47 ± 0.73 ka for glacially abraded bedrock at the valley bottom to 2.22 ± 0.49 ka for surface boulders of a rock-slope failure. All landforms shared negative skewness and largely have narrow tailed frequency distributions of their R-values. This points to either substantial reworking of the boulders within a landform or continuous debris supply. Our results show that most landforms stabilized during the Holocene Thermal Maximum (~8.0 – 5.0 ka). The findings do not support the hypothesis that rock-slope failures predominately occur shortly after local deglaciation. Instead, it appears that they cluster during warm periods due to climate-driven factors, for example, decreasing permafrost depth or increasing cleft-water pressure leading to slope instabilities. Periglacial boulder-dominated landforms in the western maritime fjord region seem to react sensitively to Holocene climate variability and may constitute valuable but to date mostly unexplored sources of palaeoclimatic information.

Keywords

Holocene Thermal Maximum, landform evolution, mid-/late-Holocene climate variability, periglacial landforms, Schmidt-hammer exposure-age dating (SHD), South Norway



Schmidt-hammer exposure-age dating (SHD) performed on periglacial and related landforms in Opplendskedalen, Geirangerfjellet, Norway: Implications for mid- and late-Holocene climate variability

The Holocene
2019, Vol. 29(1) 97–109
© The Author(s) 2018
Article reuse guidelines:
sagepub.com/journals-permissions
DOI: 10.1177/0959683618804634
journals.sagepub.com/home/hol


Philipp Marr,¹  Stefan Winkler² and Jörg Löffler¹

Abstract

Schmidt-hammer exposure-age dating (SHD) was applied to a variety of boulder-dominated periglacial landforms in an attempt to establish a local mid-/late-Holocene chronology for the Geirangerfjellet in South Norway. Landform ages were obtained by application of a local calibration curve for Schmidt hammer R-values based on young and old control points comprising fresh road cuts and a bedrock surface in proximity to the study area, respectively. The area was deglaciated ~11.5 ka ago according to independent age information. Investigation of age, formation and stabilization of the periglacial landforms and processes involved allowed assessment of the underlying Holocene climate variability and its relationship to landform evolution. Our SHD ages range from 7.47 ± 0.73 ka for glacially abraded bedrock at the valley bottom to 2.22 ± 0.49 ka for surface boulders of a rock-slope failure. All landforms shared negative skewness and largely have narrow tailed frequency distributions of their R-values. This points to either substantial reworking of the boulders within a landform or continuous debris supply. Our results show that most landforms stabilized during the Holocene Thermal Maximum (~8.0–5.0 ka). The findings do not support the hypothesis that rock-slope failures predominately occur shortly after local deglaciation. Instead, it appears that they cluster during warm periods due to climate-driven factors, for example, decreasing permafrost depth or increasing cleft-water pressure leading to slope instabilities. Periglacial boulder-dominated landforms in the western maritime fjord region seem to react sensitively to Holocene climate variability and may constitute valuable but to date mostly unexplored sources of palaeoclimatic information.

Keywords

Holocene Thermal Maximum, landform evolution, mid-/late-Holocene climate variability, periglacial landforms, Schmidt-hammer exposure-age dating (SHD), South Norway

Received 5 July 2018; revised manuscript accepted 17 August 2018

Introduction

The glacial history of Scandinavia and the reconstruction of its past climate variability has been a research focus in excess of 100 years (e.g. Blytt, 1876; Hughes et al., 2016; Mangerud, 1991; Marr and Löffler, 2017; Patton et al., 2016, 2017; Stroeve et al., 2016). Much of the research conducted in (southern) Norway has explored glacier fluctuations aiming to understand climate variability since the Last Glacial Maximum (LGM, 26.5–20 ka, Clark et al., 2009; see Matthews, 2013; Nesje, 2009; Nesje and Dahl, 1993). Particular interest has been given to the Holocene and neoglacial events (or ‘Little Ice Age’-type events, see Matthews and Briffa, 2005) in order to improve our knowledge of the magnitude and frequency of glacier oscillations (Matthews and Dresser, 2008; Matthews et al., 2013; Nesje et al., 2008; Solomina et al., 2015; Wanner et al., 2008, 2011).

A variety of methods and approaches have been utilized for reconstructing Holocene cold events. Related studies often focus on establishing Holocene glacier chronologies, for example, by glaciolacustrine and glaciofluvial sediment stratigraphy (e.g. Matthews et al., 2000; Nesje et al., 2001), relative-age dating of moraine sequences using lichenometry or Schmidt hammer

(Bickerton and Matthews, 1993; Erikstad and Sollid, 1986; Evans et al., 1994; McCarroll, 1989a, 1989b; Matthews, 2005; Shakesby et al., 2004) or terrestrial cosmogenic nuclide dating (TCND; Böhme et al., 2015; Matthews et al., 2008; Shakesby et al., 2008). The recently developed Schmidt-hammer exposure-age dating (SHD) method offers the opportunity to accurately date boulder-dominated periglacial landforms (see Marr et al., 2018; Matthews and Owen, 2010; Wilson and Matthews, 2016; Winkler et al., 2016). By contrast to other dating methods such as TCND, the Schmidt hammer constitutes a cost-efficient, time-effective and reliable instrument for obtaining numerical ages from landforms using calibration curves based on control points of known age

¹Department of Geography, University of Bonn, Germany

²Department of Geography and Geology, University of Würzburg, Germany

Corresponding author:

Philipp Marr, Department of Geography, University of Bonn, Meckenheimer Allee 166, D-53115 Bonn, Germany.
Email: marr@uni-bonn.de

(Matthews and McEwen, 2013; Shakesby et al., 2011; Tomkins et al., 2018b). According to Shakesby et al. (2011), SHD is particularly suited for age assessment of Holocene landforms such as the ones investigated in this study.

Nevertheless, little attention has been given to the geomorphological impact of Holocene climate variability. Its heritage is retained in the form of periglacial boulder-dominated landforms that may act as tools for reconstruction of climatic fluctuations since the LGM (Matthews et al., 2013; Winkler et al., 2016). Determining the age of these landforms is, however, crucial in terms of correct assessment and interpretation of landscape development and relating any obtained age constraints for geomorphological processes to their inherited palaeoclimatologic signal (Matthews et al., 2013; Wilson and Matthews, 2016). Despite their reputation as valuable palaeoclimatic proxies for Holocene climate variations (Matthews et al., 2013; Winkler et al., 2016), this potential has been largely left unexplored in the northwestern fjord region of South Norway. Alongside few older studies on late-Holocene moraine sequences (e.g. Erikstad and Sollid, 1986; Evans et al., 1994), work on moraines and rock avalanches by Longva et al. (2009) and Böhme et al. (2015), as well as rock-slope failures and rock avalanches by Bøe et al. (2004), Blikra et al. (2006) and Hermanns et al. (2017), constitute few exceptions. The chronologies obtained remain, however, largely tentative and no numerical age data that could be used to reconstruct the Holocene landscape evolution of Geirangerfjord and its tributary valleys are available for our study area in Opplendskedalen.

Few studies on Holocene climate variability and related geomorphological activity have been carried out in the northwestern fjord areas of South Norway, especially in the (inner) Nordfjord (McCarroll and Nesje, 1993; Matthews et al., 2016; Rye et al., 1997), the Sognefjord (Nesje and Whillans, 1994) and other fjords (see Blikra et al., 2006). By contrast, Geirangerfjord and its tributary valley Opplendskedalen remain largely unexplored despite their high scenic and touristic value as a UNESCO world heritage site since 2005. Regional and local differences in frequency and magnitude of neoglacial events are to be expected, but their spatial and temporal relationships largely remain elusive (cf. Kirkbride and Winkler, 2012; Winkler and Matthews, 2010).

We conducted research on various boulder-dominated landforms, including small rock-slope failures (RSF), a pronival rampart (PR), a moraine ridge (MO) and bedrock outcrops (BR). With our aim to establish chronological control of small rock-slope failures, it is important to note that small events often remain unrecorded in comparable studies leading to their potential underrepresentation in related data collections (Matthews et al., 2018). In addition, only smaller events that occurred during the last 1000 years may be recorded because they are prone to erosional removal (Böhme et al., 2015). The glaciers in the region are relatively small meaning that they potentially respond rapidly to climate changes. This offers the possibility to detect smaller changes of glacier expansion (e.g. in form of moraines) and obtain a higher resolution than at larger glaciers (Dahl et al., 2003). Our specific study objectives were as follows:

1. To calculate an SHD calibration curve for Opplendskedalen and determine accurate and precise surface exposure ages for the landforms investigated;
2. To establish a mid-/late-Holocene chronology of cold events for Opplendskedalen;
3. To explore the regionally specific relationship between landform dynamics and palaeoclimatic conditions during the Holocene;
4. To assess the sensitivity of periglacial landforms in a maritime fjord region with regard to past and present climate change.

Study area

The studied landforms are located at or near Dalsnibba (1476 m a.s.l., Figure 1) in northwestern South Norway (62°4'43" N; 7°17'35" E). Dalsnibba is located in Opplendskedalen on Geirangerfjellet in southeastern Møre og Romsdal. It exhibits a prominent peak and is a tourist destination offering famous views towards Geirangerfjord. The gross morphology of the region was strongly affected by Quaternary glaciations. Well-developed glacial valleys and deep fjords are the dominant landforms (Böhme et al., 2015). The gentle paleic surfaces above deeply incised fjords and valleys with smooth mountain peaks ranging from ~1500 to 1800 m a.s.l. are considered to represent the preglacial land surface (Klemsdal and Sjulsen, 1988; Nesje and Whillans, 1994). Dalsnibba is characterized by gently undulating surfaces towards the north and east, an increasingly steep slope to the south and a very steep north-western slope.

The study area is located in the Precambrian basement and so-called Western Gneiss Region. The young and old control points and all landforms sampled in this study consist of metamorphic bedrock of granitic gneiss and migmatite (Tveten et al., 1998).

The climatic conditions are typical for the low-alpine and middle-alpine elevational belts in the maritime western part of Norway (Löffler et al., 2006). The mean annual temperature (MAAT) of 2.6°C (1961–1990) is derived from the closest climate station Grotli (872 m a.s.l.) about 20 km east of Dalsnibba (data: met.no). The 1 km gridded MAAT normal provided by the SeNorge Database for Dalsnibba suggest MAAT between 0.0°C and 2.0°C (1961–1990). The mean annual precipitation (1961–1990) ranged between 2000 and 3000 mm/yr (<http://www.senorge.no>). The mean number of days with a snow depth of >25 cm and >5 cm was 200–350 from 1971 to 2000 (<http://www.senorge.no>). Therefore, a somewhat mild periglacial climate with non-permafrost conditions is indicated.

The pattern of glacier retreat following the LGM in the study area is relatively well established. Deglaciation reached the inner parts of Storffjord during the Bølling-Allerød interstadial (~14.7–12.9 ka) where the glacier probably had several short-lived still stands in the Geirangerfjord (Longva et al., 2009). During the Younger Dryas (YD, 12.9–11.7 cal. ka BP, Lohne et al., 2013) glaciers readvanced and created prominent terminal moraines at the mouth of the Geirangerfjord (Longva et al., 2009). The maximum glacier extent was probably reached about 10.5 ± 0.2 ¹⁴C ka BP (Fareth, 1987). Subsequently, the glaciers retreated rapidly and the fjords were ice free around 500 years later (Longva et al., 2009). The time of deglaciation following the YD at the fjords in western Norway was generally between 11.2 ± 0.4 and 10.9 ± 0.2 cal. ka BP (cf. Nesje and Dahl, 1993; calibrated data from Hughes et al., 2016). Permafrost was present at high elevations during the LGM (Etzelmüller et al., 2003) and probably reached down to sea-level during the YD in western Norway (Blikra and Longva, 1995). Striations at the valley bottom (VB) of Opplendskedalen indicate that the latest ice flow was directed towards the fjord mouth. There are still small glaciers near the study area, the closest being Skjerdingsdalsbreen southwest of the investigated MO and VB bedrock (Erikstad and Sollid, 1986). However, there is only scarce information about Holocene climate variations after deglaciation and melting of the last ice sheet remnants in Opplendskedalen by comparison to the adjacent Jostedalbreen, Jotunheimen and Breheimen regions (e.g. Matthews, 2013; Matthews and Dresser, 2008; Nesje, 2009; Shakesby et al., 2004, 2007; Winkler et al., 2016).

Landforms

We investigated different periglacial boulder-related landforms of variable size and additionally bedrock and a moraine, none described or studied previously. Schmidt hammer measurements

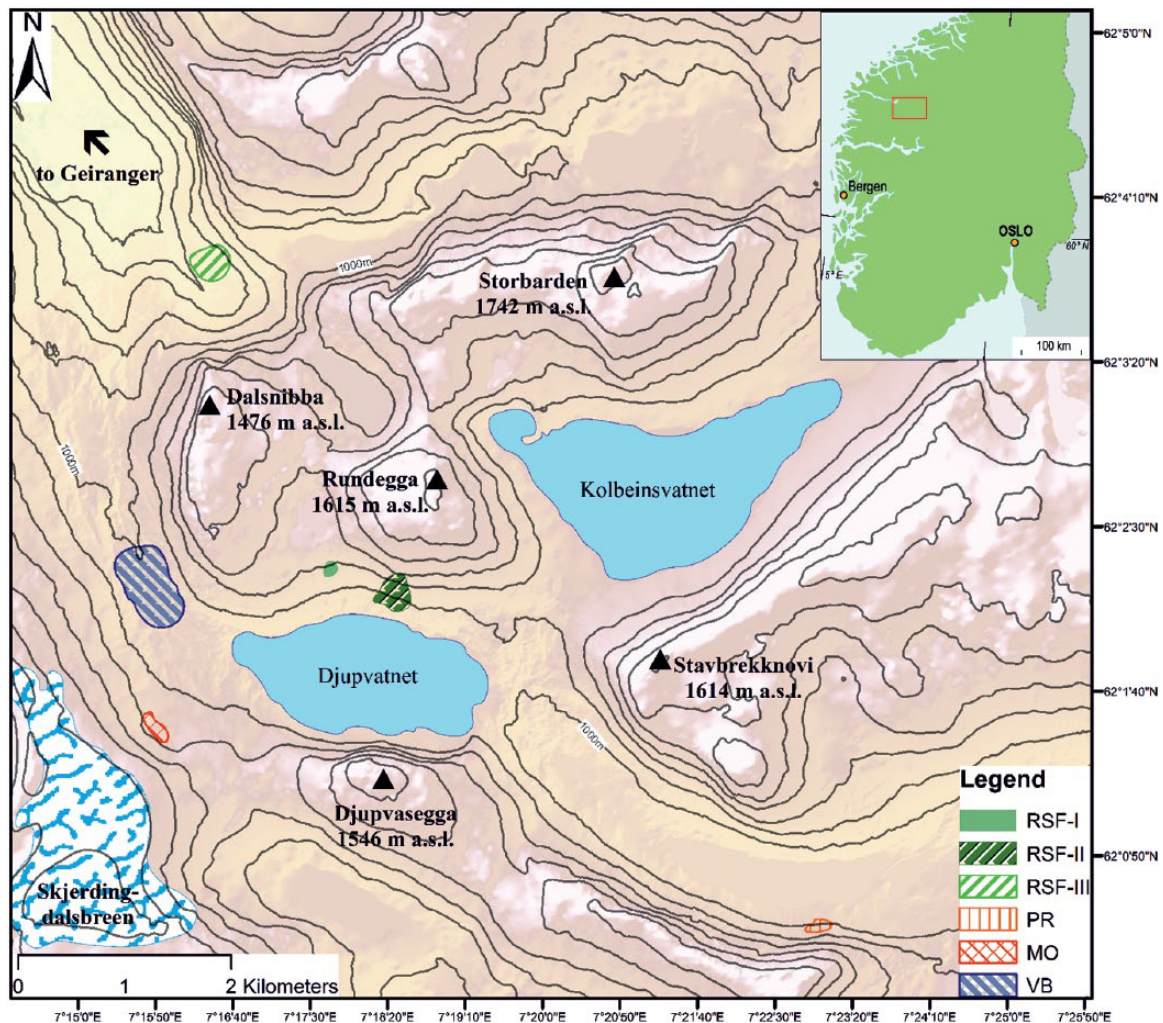


Figure 1. Rock-slope failures and other geomorphological features selected for SHD in the Geirangerfjellet, southeast Norway (source: <http://www.geonorge.no>).

were carried out at eight sites in an altitudinal range between 600 and 1230 m a.s.l. (Figure 2). The environmental and lithological conditions of these landforms and the control points are largely comparable promising successful application of SHD age assessment (Matthews and Winkler, 2011). The rock-slope failures investigated are small features matching the criteria of Matthews et al. (2018). The rock-slope failures shared compact and consistent depositional fans with coarse, angular boulders. The studied landforms did not show any evidence of post-depositional disturbance and are largely covered by mosses and lichens.

Small rock-slope failure I (RSF-I) is located at 1197 m a.s.l. ($62^{\circ}02'11''$ N; $7^{\circ}17'19''$ E) at the foot of a steep bedrock wall facing south with a typical failure scar (Wilson, 2004). A curved ridge-like boulder accumulation terminates the fan (snow covered in July 2017, Figure 2a) with a length of ~ 30 m, a width of ~ 7 m and a height of 1 m. The entire rock-slope failure zone covers an area of about 300 m². Boulder sizes are largely uniform (30–70 cm), although sizes on the distal slope are somewhat smaller. Proximal to the terminal ridge, larger boulders (> 2 m, up to 4 m in diameter) have been deposited.

Rock-slope failure II (RSF-II) is located slightly east of Dalsnibba ($62^{\circ}02'06''$ N, $7^{\circ}18'19''$ E) at an altitude between 1230 and 1050 m a.s.l. with a total size of RSF-II is ~ 0.3 km². The depositional fan was subdivided into three separate fans following visual appearance in the field and aerial image interpretation (Figures 2b and 3).

The uppermost, very steep ($\sim 36^{\circ}$) south-facing bedrock cliff is the source of the rock-slope failure. The first debris fan (RSF-II

first fan) consists of two debris areas (west and east) each with a length of ~ 80 m. The boulders were rather unstable, ranging from 5 cm to > 2 m in diameter and generally smaller than on the lower elevated fans. RSF-II first incorporates some visually fresher boulders by comparison to those on the older fans (~ 2 m thickness). This site was partly inaccessible and only 100 boulders could be measured.

The second bedrock cliff (1203 m a.s.l.) is intersected by two channels directing boulders into the second debris fan (RSF-II second fan). The eastern part of the fan is characterized by much larger blocks than its western counterpart albeit average boulder size is between 40 and 70 cm. These debris fans below this bedrock cliff have a length of ~ 70 m and a thickness of 2 m. The fan terminates at the third bedrock cliff which is at 1080 m a.s.l.

The third debris fan (RSF-II third fan) is located below a stable, vegetated ridge below the third bedrock cliff (1080 m a.s.l.). This cliff subdivides the debris into three smaller fans which we grouped together to RSF-II third fan. The debris fan terminates at an elevation of ~ 1050 m a.s.l. and is around 45 m long and 2 m thick. RSF-II third fan has mostly boulders between 50 and 70 cm, but the eastern part incorporates larger and fresher blocks (> 3 m). The fan terminates at a near-horizontal terrace which consists of stable boulders and bedrock.

RSF-III is located in a cirque next to a waterfall at the western foot of Dalsnibba ($62^{\circ}03'44''$ N; $7^{\circ}16'18''$ E) and stretches from ~ 700 to 600 m a.s.l. (Figure 2c). Above the small rock-slope failure, a bedrock cliff with a failure scar is visible, facing south west. The debris fan has a length of ~ 100 m and a thickness of ~ 1 –2 m.



Figure 2. (a) View of rock-slope failure I debris towards the east. (b) View of the rock-slope failure II towards the north. (c) View of rock-slope failure III towards the north-east. (d) View of down-valley into Opplendskedalen towards the east, with the moraine ridge in the centre of the picture. (e) View of pronival rampart with headwall. (f) View of down-valley into Opplendskedalen with the investigated valley bottom in the foreground.

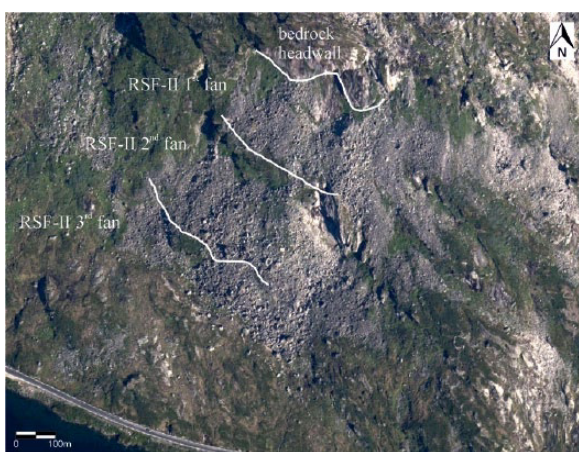


Figure 3. Aerial photo of rock-slope failure II (source: <http://www.norgebilder.no>). The boundary lines represent the transitions between the different debris fans of the rock-slope failure.

The debris fan is divided into two parts which are separated by a downslope aligned stable vegetation line. The average boulder size is between 30 and 80 cm. At the foot of the rock-slope failure, mostly bigger blocks with diameters of <math><3-4\text{ m}</math> are present. It seems that due to its steepness ($\sim 40^\circ$), boulders from the headwall

stabilize further downslope. A lobate form with a height of $\sim 1\text{ m}$ terminates the rock-slope failure debris.

The investigated MO is situated at the south western foot of Dalsnibba, about 1 km west of Djupvatnet ($62^\circ 01' 27\text{ N}$; $7^\circ 16' 01\text{ E}$) at 1166 m a.s.l. (Figure 2d). The moraine faces north-east has a length of $\sim 120\text{ m}$, a height of $\sim 2.5\text{ m}$ and a width of $\sim 10\text{ m}$. The proximal side of the moraine has a slope angle of $\sim 9^\circ$ and the distal side of $\sim 22^\circ$. MO is located in the foreland of an outlet of Skjerdingsdalsbreen which supposedly underwent an advance during the 'Little Ice Age' (LIA). Erikstad and Sollid (1986) licheno-metrically dated moraines at a different outlet of Skjerdingsdalsbreen $\sim 1.6\text{ km}$ south east of our study site and obtained an estimated age of $\sim 1750\text{ CE}$ for the maximum extent during the LIA. The moraine investigated is the one which is located closest to the valley head. Apparently judging from its position, MO is part of a moraine complex within the maximal LIA expansion. The moraine is characterized by a marked variability of boulder sizes. There is a large amount of small boulders, also pebbles and gravel; the average boulder size varies between 20 and 30 cm, and boulders greater than 60 cm are rare.

PR is located $\sim 7\text{ km}$ south east of Dalsnibba ($62^\circ 00' 26\text{ N}$; $7^\circ 23' 31\text{ E}$) at 964 m a.s.l. (Figure 2e). Here, we define PRs as debris ridges which form at the downslope limit of perennial or semi-perennial snowbeds at the foot of bedrock cliffs (Hedding, 2016). The bedrock cliff of 15 m height faces north-east and has a gradient of $\sim 40^\circ$. The debris fan (snow covered during field work

Table 1. Schmidt hammer R-values and statistics for the control sites. Mean R-values are obtained from the means of two impacts on each boulder, and 95% confidence intervals were calculated from the number (*n*) of sampled boulders.

Control point	Age (years) ^a	R-value	σ	95% CI ^b	Kurtosis	Skewness	Boulders (<i>n</i>)
Young I	2	70.97	5.51	0.77	-0.24	-0.54	100
Young II	4	69.65	4.84	0.67	-0.46	-0.25	100
Young mean	3	70.3	5.22	0.51	-0.37	-0.38	200
Old	11,500	40.3	–	2.4	–	–	–

CI: confidence interval.

^aAge of the young control point from field observation. Age of the old control point from Matthews et al. (2016).

^bMean of R-values with 95% confidence intervals ($\alpha = 0.05$).

in July 2017) has a length of ~100 m and a width of ~60 m. PR is located at the northwestern termination of the fan and has a length of about 90 m, width of ~15 m and height 3–4 m, with a proximal surface dip of 7–9° and a distal of 11–13°. The rampart appears to have been stable for a considerable time due to the weathered, lichen- and moss-covered boulders and the accumulation of fine matrix with plant communities at sheltered positions. Boulder sizes vary largely between 30 and 60 cm, less than 10 of the largest boulders observed were >2 m in diameter. Ten metres below, the snow fan solifluction lobes (facing north-east) indicate active slope processes.

From the VB area south east of Dalsnibba at ~1045 m a.s.l. (62°02'28 N; 7°15'01 E) in the centre of Opplandskedalen, several bedrock surfaces were measured (Figure 2f). The glacially abraded bedrock surfaces occur at an elevation of up to 50 m above the VB. Surfaces in the VB are largely horizontal but become steeper towards the Geirangerfjord and the valley-side-walls. The measurements at the VB were carried out ~1 km north of MO. The present watershed crosses the VB.

Methodology and research design

SHD

In this study, we used an electronic RockSchmidt N-Type (Proceq, 2014) with an impact energy of 2.207 Nm that was calibrated to the manufacturer's specifications. The rebound (R) values yielded by the RockSchmidt represent the measured rebound velocity of the plunger. On each control point and landform, we measured 150 boulders if possible, with two impacts on each. At least 10 different plots were used for measuring bedrock surfaces. Relatively large sample sizes help to minimize possible sources of error such as lithological heterogeneities, microclimatic variabilities, post-depositional disturbance or other factors, other than exposure to subaerial weathering, that influence the results obtained (Winkler, 2005, 2009). Impact points near cracks, edges, visible structural rock surface weaknesses, unusual lithology and cover by lichens or mosses were avoided (cf. Matthews and Owen, 2010; Shakesby et al., 2006). The measurements were carried out by a single operator during dry conditions on near-horizontal surfaces of stable boulders (>30 cm in diameter) which were not prepared before measuring.

The yielded R-values were statistically analysed applying R statistic software following standard statistical procedures. Frequency distributions were plotted to show R-value distribution, because bi- or polymodal distributions could be associated with post-depositional disturbance (McCarroll, 1989a; McCarroll and Nesje, 1993; Winkler, 2009). The standard statistical analysis comprised calculation of standard mean, standard error of the mean (SEM) at 95% confidence interval ($\alpha = 0.05$), skewness, kurtosis and test of normality (Shapiro–Wilk test). Sites with overlapping 95% confidence intervals were interpreted on the premise that their age does not significantly differ from each other (Wilson and Matthews, 2016). The Mann–Whitney test was applied to determine statistical significance between pairs of sites.

Control points and age calibration

Establishing a local calibration curve based on surfaces of known age allowed us to determine exposure ages for boulder surfaces of unknown age. Two road cuts at Dalsnibba at elevations of 1203 m a.s.l. (young control point I) and 1347 m a.s.l. (young control point II) served as our young control points. They were 2 and 4 years old, respectively. At each young control point, 100 boulders were measured. Due to the lack of existing numerical ages for landforms in Opplandskedalen, it was not possible to establish an old control point in close proximity to Dalsnibba. Therefore, data for the old control point were taken from a bedrock locality at Alnesdalen, ~50 km north-east from our study site, with a reported deglaciation age of ~11.5 cal. ka BP and a mean R-value of 40.3 ± 2.4 (cf. Matthews et al., 2016). However, these values were obtained by a mechanical Schmidt hammer and have to be converted to RockSchmidt R-values which are generally 9–10 units higher (Winkler and Matthews, 2014). This approach results in a mean R-value of 50.3 for the old control point used in this study. The magmatic gneiss bedrock at Alnesdalen exhibits similar lithological (modern) surface hardness as the migmatite gneiss at Dalsnibba.

Here, we assume a linear R-value age relationship between the young and old control points following similar studies applying high-precision calibration curves for SHD (e.g. Matthews and Owen, 2010; Matthews and Winkler, 2011; Shakesby et al., 2006; Wilson et al., 2017), all referring to Holocene (<11.7 ka) timescales. This linear relationship seems a valid presumption as former studies on gneiss bedrock confirmed such linear relationship (e.g. Matthews and Owen, 2010) and resistant rock types show slow and close to linear weathering characteristics in periglacial environments during the Holocene (André, 1996; Colman, 1981; Nicholson, 2008). There is evidence that this linear relationship may even extend beyond Holocene timescales (Kłapyta, 2013; Sánchez et al., 2009; Tomkins et al., 2016, 2018b; Winkler and Lambiel, 2018).

On the basis of the young and old control point values (Table 1), the local calibration equation was calculated, which is a standard linear regression:

$$y = a + bx \quad (1)$$

where *y* is the surface age in years, *a* is the intercept age (acquired by substitution in the calibration equation), *b* is the slope of the calibration curve and *x* is the mean R-value. The *b* coefficient is described as:

$$b = \frac{(y_1 - y_2)}{(x_1 - x_2)} \quad (2)$$

with *y*₁ and *x*₁ representing the age and mean R-value of the old control point, respectively, whereas *y*₂ and *x*₂ represent the age and mean R-value of the young control point, respectively.

The 95% confidence interval for a SHD age, comprising the total error (*C*), consists of the error of the calibration curve at the

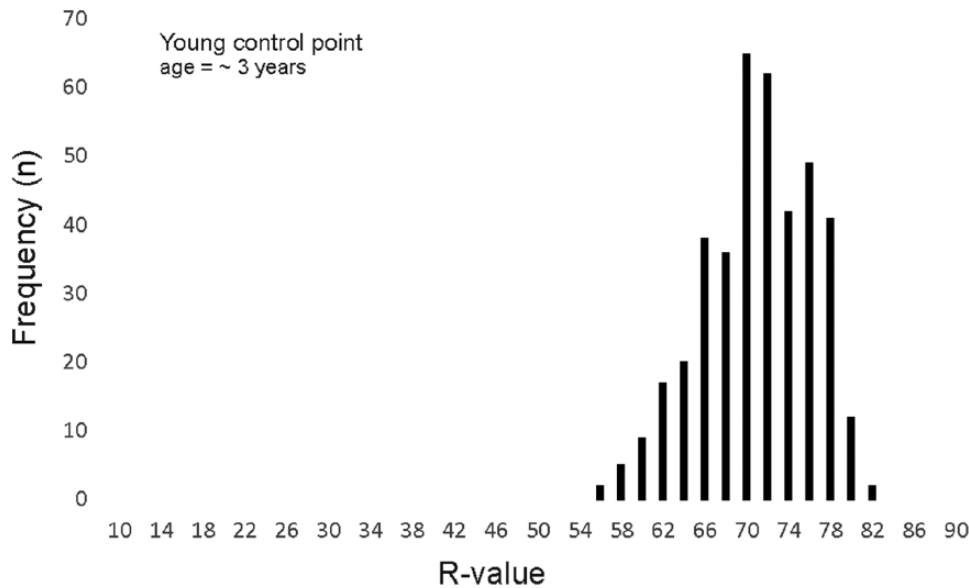


Figure 4. Frequency distributions of Schmidt hammer R-values of the (amalgamated) young control point.

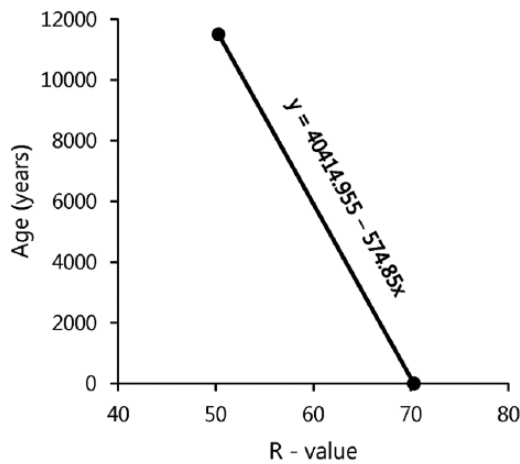


Figure 5. Calibration curve and calibration equation for the western fjord area calculated from the young and old control point.

point related to the dated sample (C_c) and to the sampling error of the sample itself (C_s):

$$C_t = \sqrt{C_c^2 + C_s^2} \quad (3)$$

The error of the calibration curve is represented by the errors of the control points and their age differences:

$$C_c = C_o - \left[\frac{(C_o - C_y)(R_s - R_o)}{(R_y - R_o)} \right] \quad (4)$$

with C_o expressing the 95% confidence interval of the old control point in years, C_y is the 95% confidence interval of the young control point in years. R_o , R_y and R_s are associated to the mean R-value of the old and young control points and the sample. The sampling error of the sample itself is calculated incorporating the b coefficient, Student's t statistic, standard deviation (s) of the sample's R-value and the sample size (n):

$$C_s = b \left[\frac{ts}{\sqrt{(n-1)}} \right] \quad (5)$$

Results

Control points

The Schmidt hammer results from the control sites are displayed in Table 1. The mean R-values for the young control point I and the young control point II are in close agreement. As both young control points share overlapping 95% confidence intervals, and fail the Mann–Whitney test ($p = 0.004$), they have no statistically significant difference allowing to amalgamate the data from both sites into a single young control point. This young control site has a mean R-value of 70.3 ± 0.5 and differs about 20 units from the old control site yielding a mean R-value of 50.3 ± 2.4 as reported by Matthews et al. (2016). The wider 95% confidence interval indicates greater variability in R-values because long-term exposure to surface weathering intensifies existing lithological inhomogeneities in comparison with young surfaces (Winkler and Matthews, 2014).

The frequency distributions of the R-values for the amalgamated young control point are shown in Figure 4. The histogram displays a small number of low R-values and a narrow tail that passes the Shapiro–Wilk test for normality. The calibration curve was derived from the equations given above with $y = 40,414.955 - 574.85x$ (Figure 5).

R-values and landforms

R-values for the investigated landforms are summarized in Table 2. All mean R-values fall between the young and old control points and are closer to the young control point. The R-values are generally consistent; they share low 95% confidence intervals and standard deviations. All R-value distributions fail the Shapiro–Wilk test for normality, are negatively skewed and show various degrees of kurtosis. The mean R-values with 95% confidence interval range from 66.4 ± 0.60 for RSF-II first fan to 57.3 ± 0.94 for VB. The 95% confidence intervals are largest for MO and smallest for PR. Notably, the three depositional fans of RSF-II (Figure 3) do not have overlapping confidence intervals. However, three rock-slope failures (RSF-I, RSF-II third fan and RSF-III) do have overlapping confidence intervals. The majority of pairs fail the Mann–Whitney test and are therefore significantly different from each other (Table 3). There appears to be no spatial relationship between the pairs passing the Mann–Whitney test. The three depositional fans of RSF-II represent significantly different age populations.

Table 2. Schmidt hammer R-values, standard deviation, kurtosis, skewness and *n* for the studied landforms.

Site	Mean \pm 95% CI ^a	σ	Kurtosis	Skewness	Boulders (<i>n</i>)
RSF-I	58.8 \pm 0.87	7.65	0.13	-0.34	150
RSF-II first	66.4 \pm 0.60	6.13	0.33	-0.54	200
RSF-II second	63.4 \pm 0.54	6.68	-0.04	-0.35	300
RSF-II third	60.1 \pm 0.53	8.18	-0.34	-0.40	450
RSF-III	58.0 \pm 1.11	9.76	-0.41	-0.32	150
MO	62.5 \pm 1.30	9.29	0.08	-0.7	100
PR	60.5 \pm 0.45	8.34	0.23	-0.59	150
VB	57.3 \pm 0.94	8.29	-0.2	-0.56	150

RSF: rock-slope failure; MO: moraine ridge; PR: pronival rampart; VB: valley bottom; CI: confidence interval.

^aMean of R-values with 95% confidence intervals ($\alpha = 0.05$).

Table 3. Results of Mann–Whitney tests of differences between pairs.

Pairs of sites	H_0^a	α^b	Boulders (<i>n</i>)
RSF-I – RSF-II first	Reject	<2.2e-16	350
RSF-I – RSF-II second	Reject	<2.2e-16	450
RSF-I – RSF-II third	Reject	0.0076	600
RSF-I – RSF-III	Retain	0.5354	300
RSF-I – MO	Reject	8.546e-08	250
RSF-I – PR	Reject	0.0027	300
RSF-I – VB	Retain	0.0874	300
RSF-II first – RSF-II second	Reject	4.195e-13	500
RSF-II first – RSF-II third	Reject	<2.2e-16	650
RSF-II first – RSF-III	Reject	<2.2e-16	350
RSF-II first – MO	Reject	2.007e-06	300
RSF-II first – PR	Reject	<2.2e-16	350
RSF-II first – VB	Reject	<2.2e-16	350
RSF-II second – RSF-II third	Reject	7.406e-14	750
RSF-II second – RSF-III	Reject	1.859e-15	450
RSF-II second – MO	Retain	0.9496	400
RSF-II second – PR	Reject	3.491e-06	450
RSF-II second – VB	Reject	<2.2e-16	450
RSF-II third – RSF-III	Reject	0.0027	600
RSF-II third – MO	Reject	2.845e-05	550
RSF-II third – PR	Retain	0.334	600
RSF-II third – VB	Reject	<3.1e-06	600
RSF-III – MO	Reject	<1.9e-07	250
RSF-III – PR	Reject	0.0016	300
RSF-III – VB	Retain	0.302	300
MO – PR	Reject	0.0026	250
MO – VB	Reject	1.922e-11	250
PR – VB	Reject	4.117e-06	300

RSF: rock-slope failure; MO: moraine ridge; PR: pronival rampart; VB: valley bottom.

^a H_0 = distribution of values is the same across both samples (decision at $\alpha = 0.05$).

^bAsymptotic significance level (two-tailed test).

The frequency distributions (Figure 6) largely show comparable characteristics for the different landforms. Most show narrow tails with one peak and few boulders with low R-values within the sample. In addition, most frequency distributions show near symmetry, although being negatively skewed (e.g. PR and RSF-II second fan). The three fans of RSF-II show the narrowest distributions, indicating that they were each most likely formed during one single event. RSF-III exhibits a rather platykurtic distribution with polymodal characteristics, also RSF-I shows more than one peak. Several histograms display

different distributions of low R-values and indicate the presence of more weathered boulders.

SHD and landform ages

By applying the local calibration curve (Figure 5), we obtain SHD ages with 95% confidence interval for the different landforms (Table 4, Figure 6). Landform ages vary between 7.47 ± 0.73 ka at VB and 2.22 ± 0.49 ka for RSF-II first fan. It is noteworthy that the ages of the depositional fans at RSF-II increases with greater distance from the headwall.

Discussion

Methodological considerations

The most severe limitation of the SHD approach is the construction of the calibration curve (Matthews et al., 2014). In order to ensure the reliability of the calibration curve, local control points are vital as only they can account for lithological differences. Even if regional control points are used in situations when lithological and surface roughness variations are comparable (Matthews et al., 2011), non-local control points appear to be a weakness of previous studies. The lack of a local old control site is, therefore, a potential weakness of our calibration curve.

The R-values for the old control point were taken from Matthews et al. (2016) and were obtained from a location with comparable lithology. Obtaining the old control point from a non-local, but regional source generally lowers the precision of SHD ages. Nonetheless, due to the lithological homogeneity and the demonstrated interconvertibility of R-values between the mechanical and electronic Schmidt hammer (Winkler and Matthews, 2014), we regard our approach as legitimate. The range of the mean R-values between the control sites is similar to other SHD studies (e.g. Matthews et al., 2014; Wilson and Matthews, 2016), we therefore consider our calibration curve as robust. In addition, Matthews et al. (2014) successfully applied SHD with a non-local old control point. The age error of the control points is considered insignificant compared with statistical and other inaccuracies connected to this method (see Matthews et al., 2014). The reliability of our calibration curve is supported by comparable results obtained for SHD control points at Tafjord with similar lithology (Wilson et al., 2017).

The negligible R-value divergence (Table 1) and the similar characteristics (Figure 4) between the two young control points justify the amalgamation of data from both control points. Obtaining the R-values for the young control points from road cuts is, however, not unproblematic. The R-values do not necessarily reflect fresh and unweathered material because subsurface weathering has to be taken into account (Winkler et al., 2016). Furthermore, empirical results show that freshly exposed bedrock at road cuts does not inevitably yield R-values expected from unweathered rock (Matthews et al., 2016). In turn, such freshly exposed bedrock may probably better reflect the original conditions when boulders become exposed for the first time (Matthews and McEwen, 2013; Matthews et al., 2014; Winkler et al., 2016). Therefore, we consider our young control site to be reasonably reliable despite a few weathered boulders and assign an age of 3 years for it. It appears to be a general characteristic that relatively freshly exposed rocks share narrow 95% confidence intervals and standard deviations. Lithological differences in older rocks become more exaggerated with longer exposure to surface weathering leading to a higher spread of R-values and reflected in wider 95% confidence intervals and higher standard deviations (Aydin and Basu, 2005; Matthews et al., 2013; Winkler and Matthews, 2014).

The effect of snow patches on rock weathering and its influence on Schmidt hammer results continues to be enigmatic (e.g.

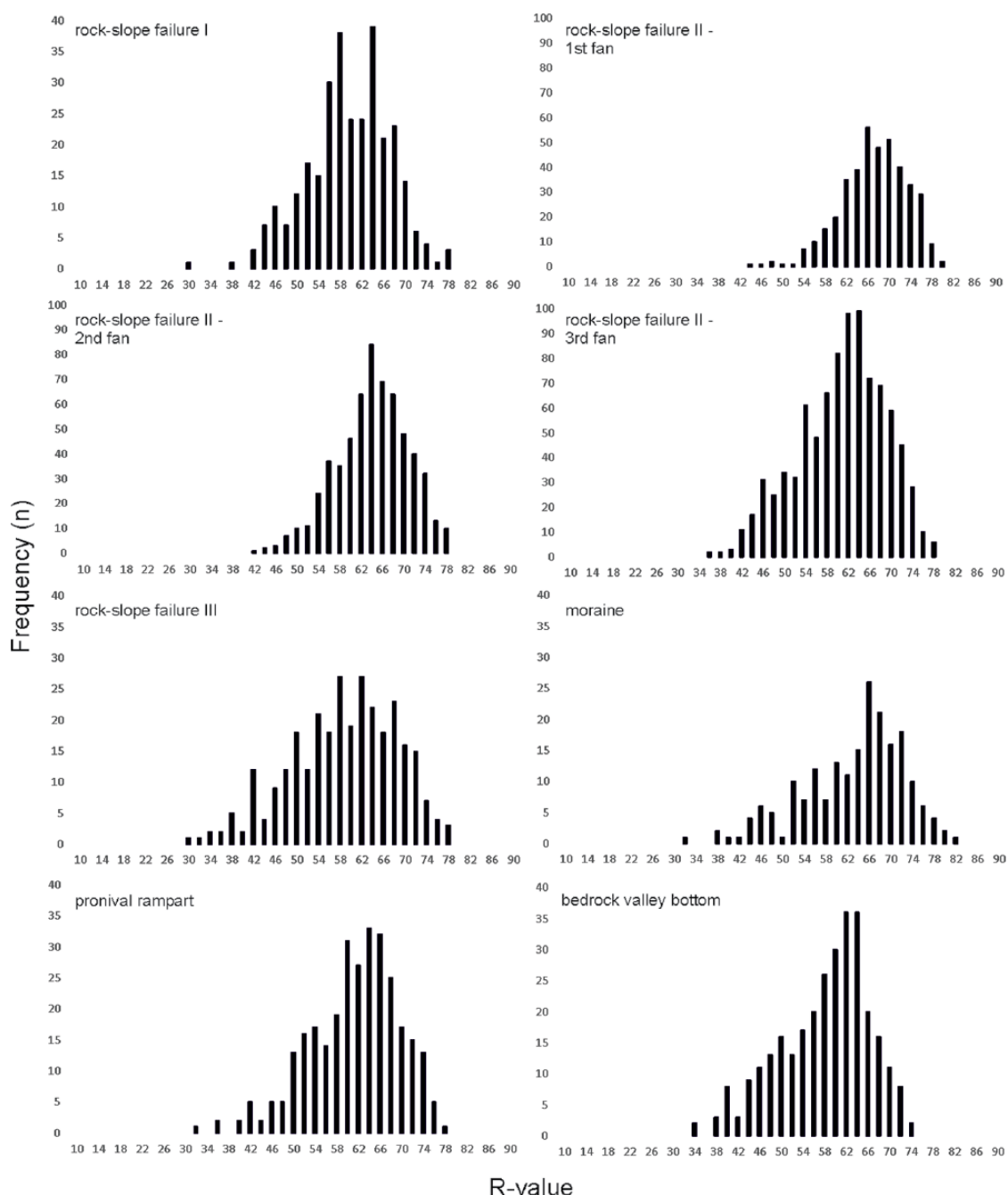


Figure 6. Frequency distributions of Schmidt hammer R-values from all investigated landforms. Note the different scale at rock-slope failure II histograms.

Table 4. SHD ages from the sampled landforms. Each SHD age has a 95% confidence interval (C_i) derived from the sampling error of the landform sample (C_s) and the error of the calibration curve (C_c).

Landform	SHD age (ka)	C_i (ka)
RSF-I	6.61	0.69
RSF-II first fan	2.22	0.49
RSF-II second fan	4.00	0.51
RSF-II third fan	5.89	0.54
RSF-III	7.10	0.80
MO	4.50	0.85
PR	5.64	0.51
VB	7.47	0.73

SHD: Schmidt-hammer exposure-age dating; RSF: rock-slope failure; MO: moraine ridge; PR: pronival rampart; VB: valley bottom.

Ballantyne et al., 1989; Benedict, 1993). On the one hand, studies show that snow patches can enhance chemical weathering (e.g. Hall, 1993) and could influence R-values. On the other hand, some studies report decreasing weathering (cf. Benedict, 1993) under snow patches. Regarding the comparable snow coverage between our study sites, we consider the effect of snow patches influencing our results to be insignificant.

SHD age interpretation and landform development

The exposure ages generated by SHD are considered robust estimates of the true landform age (Matthews et al., 2013). Landforms that are formed during one event and immediately stabilize, for example, flood berms (Matthews and McEwen, 2013) or most moraines (Winkler, 2014), facilitate the interpretation of the landform age. By contrast, SHD ages obtained from landforms showing non-uniform boulder age populations may either represent

complex diachronous formation histories (e.g. multiple events) or reflect the impact of post-depositional disturbance (French, 2007; Matthews et al., 2014). All landforms investigated seem to be currently inactive and field observations revealed no signs of post-depositional disturbance. The negatively skewed R-value distributions infer that some boulders were already exposed prior to the landforms becoming stable and indicate the dynamism of landform evolution. Therefore, we consider our SHD ages as maximum age estimates for landform stabilization. SHD ages consequently give minimum estimates for the onset of landform formation, as there were most likely older boulders beneath the surface boulders that we sampled (Wilson and Matthews, 2016).

Our SHD ages largely fall in the period of the Holocene Thermal Maximum (HTM, ~8.0–5.0 ka, Clark et al., 2009) and the following mid-/late-Holocene climate deterioration and range from 7.47 ± 0.73 ka at VB to 2.22 ± 0.49 ka at RSF-II first fan. The nature of the histograms (Figure 6) and the narrow confidence intervals point to the fact that most landforms formed during single events. The R-value histograms are comparable to those of many other landforms created by single events and distinct processes (Nesje et al., 1994; Winkler, 2014). Holocene moraine sequences studied by Aa and Sjøstad (2000) and Shakesby et al. (2004), as well as some of the snow-avalanche impact ramparts of Matthews et al. (2015) show comparable narrow-peak frequency distributions. Our frequency distributions are comparable to young ramparts investigated by Matthews and Wilson (2015). The somewhat platykurtic frequency distributions and broader confidence intervals at RSF-III, MO and PR may be explained by the reactivation and reworking of already formed landforms or a continuing supply of debris following the single-event origin (Wilson and Matthews, 2016; Winkler et al., 2016). The incorporation of pre-weathered boulders in reactivated landforms is a known phenomenon for moraines (McCarroll, 1989b). This scenario also seems to be possible for PRs (Matthews and Wilson, 2016) and for consecutive RSFs occurring on the same slope (El Bedoui et al., 2009). However, the smaller sample sizes on these landforms may be responsible for the larger confidence intervals and standard deviations (Matthews et al., 2015). In agreement with other studies (e.g. Rode and Kellerer-Pirklbauer, 2011), we find a consistent pattern of negative skewness for the landforms investigated. The reactivation of landforms is exhibited in the negative skewness as older boulders are re-mobilized by frost heave or other processes connected to renewed cooling (Wilson and Matthews, 2015). The SHD ages of VB have to be interpreted with caution as the R-values were obtained from different bedrock outcrops where the extent of surface exposure might have been heterogeneous.

The classification of RSF-II into three different units (RSF-II first fan, RSF-II second fan and RSF-II third fan) from morphological evidence proved to be consistent in terms of the statistically significant difference of the sampled boulders between the three debris fans as determined by the Mann–Whitney test (Table 3). Increasing SHD ages towards the foot of landform was also reported from rock glaciers and related to continuous development and movement (Frauenfelder et al., 2005; Winkler and Lambiel, 2018).

Climatic implications

Cold climate periods are considered to be a trigger for landscape transformation with respect to boulder-dominated periglacial landforms (e.g. Ballantyne and Harris, 1994). Therefore, we compare our results with the Smørstabbtindan cold event record presented by Matthews and Dresser (2008) for Jotunheimen (Figure 7). This represents the best mid-/late-Holocene palaeoclimatic reconstruction close to our study site.

According to the SHD ages and the 95% confidence limits of VB (7.47 ± 0.73 ka) and RSF-III (7.10 ± 0.80 ka), the stabilization of both landforms partly overlaps with climatic cooling

during the ‘Finse Event’ (~8.4–8.0 cal ka BP, Nesje and Dahl, 2001). This indicates that Opplendskedalen was ice covered until the end of this cold period that is recorded in several locations in Norway and in the Greenland ice cores (cf. Nesje, 2009). Opplendskedalen probably became ice free and subjected to subaerial weathering after the termination of the ‘Finse Event’. This is in agreement with diminishing glaciers in Norway (Nesje, 2009) and the most limited glacier extent in Scandinavia (cf. Solomina et al., 2015). Beside the surface exposure of the glacially abraded VB bedrock, the stabilization of RSF-III, RSF-I (6.61 ± 0.69 ka) and RSF-II third fan (5.89 ± 0.54 ka) also fall in the HTM. Böhme et al. (2015) report two failure surfaces of an HTM age of 7.01 ± 1.23 ka and 7.25 ± 1.14 ka ago which occurred at the spatial transition from the Geirangerfjord to the Korsfjord. This supports the occurrence of rock-slope failures in warm periods.

This climatic transition towards the HTM, with progressively higher summer temperatures (~0.7°C) and/or low winter precipitation (Dahl and Nesje, 1996) most likely caused permafrost degradation, increased cleft-water pressure and enhanced freeze-thaw activity (e.g. Ballantyne et al., 2013; McColl, 2012). Among others, these climatically induced factors are considered as important mechanisms triggering RSFs (Ballantyne et al., 2013; Blikra et al., 2006; McColl, 2012). But other potential RSF causes such as glacial debuiting or earthquakes need to be considered (Blikra et al., 2006; McColl, 2012). However, we reject earthquakes as a trigger for the rock-slope failures due to the lack of reliable evidence (Blikra et al., 2006). Glacial debuiting can also be ruled out as the main trigger due to the relatively low gradient of our RSF slopes. Monocausal explanations for RSF triggering are hard to determine, because all mentioned factors might act in distinct combinations over various time scales making it difficult to precisely indicate cause and effect in any case (Ballantyne and Stone, 2013; McColl, 2012).

We assume that these RSFs are most likely a coupling of long-term stress release from deglaciation combined with climatically induced factors related to warming as triggering mechanisms. Connecting RSFs to warming climate inducing decreasing permafrost depth, snow melt enhancement, increased precipitation and joint water pressure is in agreement with findings of Blikra et al. (2006), McColl (2012) and Matthews et al. (2018). The occurrence of RSFs during warm periods is supported by the timing of rock-slope failure frequency peaks reported by Matthews et al. (2018) at 7.38 ± 0.99 ka in Jotunheimen which corresponds with the ages of RSF-III and RSF-I. Also, the stabilization of RSF-II third fan is in agreement with a frequency peak of small rock-slope failures in Jotunheimen at 6.40 ± 0.77 ka (Matthews et al., 2018).

By contrast, RSF-II second fan and RSF-II first fan overlap with more than one cold events in the late Holocene. The surface boulders of RSF-II second fan probably stabilized during Smørstabbtindan III as inferred by their negative skewness. This timing corresponds with the highest frequency of RSFs during the Holocene observed by Matthews et al. (2018). The RSF-II first fan SHD age (2.22 ± 0.49 ka) overlaps with two warm and three cold periods (Figure 7). The relatively high number of surface boulders (>70) with an R-value higher than the young control point underlines the still ongoing debris supply from the source area. Due to the rather short time window for these events, we cannot conclusively state in which period the debris fan stabilized. However, other rock failures of similar average surface age (2.11 ± 0.31 ka) were reported from Blåhornet in the Storfjord (Böhme et al., 2015). In addition, Matthews et al. (2018) identified an intensity peak at ~2.6 ka. For RSF-II second fan and RSF-II first fan, we propose a delayed response to paraglacial stress release. The slope was probably weakened by prolonged warm periods throughout the Holocene, causing permafrost degradation (Cossart et al., 2014). Summarizing, our data from RSFs are in contrast to the concept of higher frequency in the first millennia

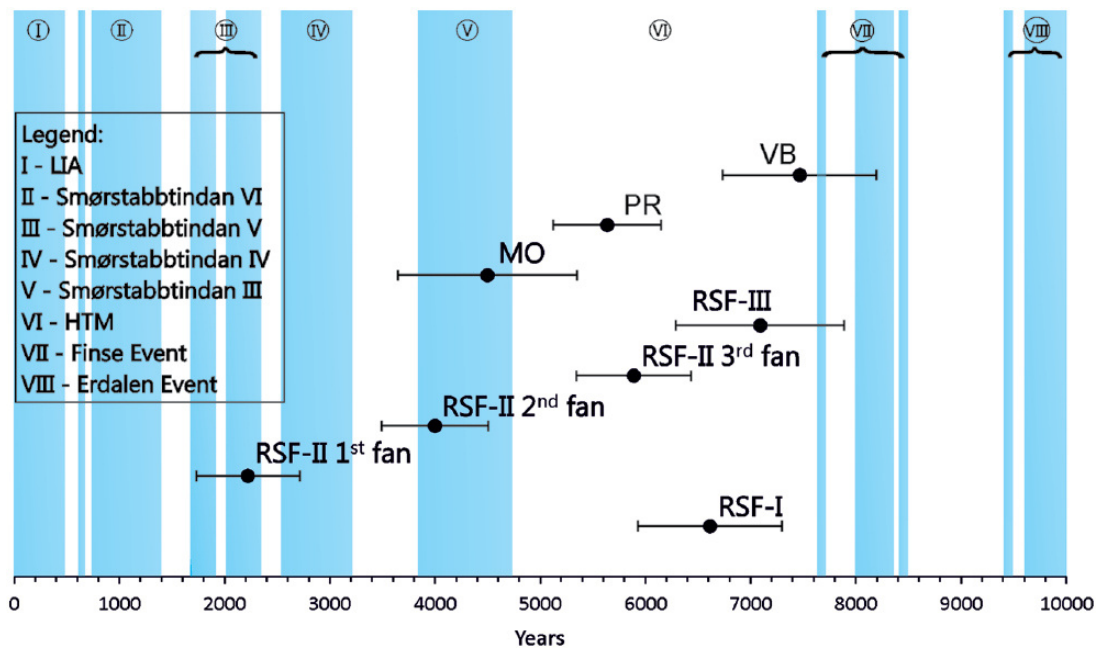


Figure 7. Plot integrating SHD ages and their total error for the studied landforms and intervals of documented climatic deteriorations since the early Holocene displayed in blue (data from Matthews and Dresser, 2008).

following deglaciation (Ballantyne et al., 2014) which is, for example, supported by Hermanns et al. (2017) in southwest Norway. The temporal similarity of four out of five RSFs to the SRSF-enhanced frequency distribution model in the Holocene reported by Matthews et al. (2018) points to a climatic control for causes of RSF triggering.

Given the negative skew, the high modal R-value at 66–62 (Figure 6), the PR investigated might have been ceasing its development prior 5.64 ± 0.51 ka ago (many R-values around 54) and then been reactivated (see Matthews and Wilson, 2015). Therefore, the rampart likely remained active for a considerable time and stabilized towards the termination of the HTM. Much of the accumulated coarse rock debris probably derived from the HTM when increased freeze-thaw activity, permafrost degradation and enhanced precipitation weakened the slope and increased the availability of debris. The mixed age of the rampart debris support the continuous build-up of the landform during the Holocene (Matthews and Wilson, 2015; Shakesby et al., 1999) and could have been initiated following demise of the YD glaciers. Hence, the rampart is significantly younger than those investigated by Matthews and Wilson (2015).

Following the HTM summer temperatures and precipitation decreased culminating in the Smørstabbtindan III cold event in which the SHD age of MO falls. The SHD age of the moraine of 4.50 ± 0.85 ka, however, is problematic. The moraine appears to have been reactivated, according to its negative skewness. The ridge was likely created prior to that time and then re-mobilized by neoglacial events. Accepting the lichenometric dating result of 1750 CE of Erikstad and Sollid (1986) for Skjerdingsdalsbreen, our SHD age of ~ 4.5 ka is not compatible because MO is located within the maximal LIA expansion of Skjerdingsdalsbreen. The overestimation of the SHD age is probably related to the reworking of the landform due of glacier advances and the incorporation of pre-weathered boulders, which is also reported from moraines elsewhere (McCarroll, 1989b; Tomkins et al., 2018a). As suggested by Wilson and Matthews (2016), significant landscape impact from Holocene cold periods like the Smørstabbtindan events can be inferred for former climate deteriorations. This would explain the presence of high and low R-values represented by fresh and older material. Though, the glacier outlet studied by Erikstad and Sollid (1986) is ~ 1.5 km south of the moraine

studied here, we correlated our moraine, based on aerial images, with an age of ~ 1750 CE. This, in turn, limits our understanding of the dynamics of Skjerdingsdalsbreen before the ‘Little Ice Age’.

Based on our results, we develop the first Holocene palaeoclimatic chronology for Opplendskedalen. Following YD deglaciation and the subsequent short warm interval, the ‘Finse Event’ resulted in climate deterioration in Opplendskedalen. Glaciers readvanced and covered the tributary valley of the Geirangerfjord until ~ 7.5 ka ago when the valley became ice free once more at the onset of the HTM. The HTM led to the thawing of permafrost and consequent slope weakening causing RSFs, processes that persisted also in the time periods following the HTM. The late-Holocene climate variability cannot reliably be explored based on our results. However, the LIA advance of Skjerdingsdalsbreen is represented by the overestimated age of our moraine in form of reworking an already existing moraine. In comparison with investigations on boulder-dominated landforms in the continental eastern part of southern Norway (Marr et al., 2018), the landforms studied here appear to have reacted more sensitively to Holocene climate variability. This is in agreement with Nesje et al. (2005) that state that landforms influenced by maritime climatic conditions and glaciers tend to be more sensitive to Holocene climate variability.

Conclusion

This study has explored the role of periglacial landforms as a palaeoclimatic proxy within the Holocene in the southwestern fjord region of Norway with the help of SHD for the first time. We draw the following conclusions:

1. With new age-calibration equations for Opplendskedalen in southern Norway, it was possible to determine ages of several periglacial landforms in this area. Road cuts with an age of 2–4 years and glacially scoured bedrock that became exposed ~ 11.5 ka ago were used as young and old control points for age calibration.
2. Our SHD ages suggest that all the landforms stabilized during the mid-/late-Holocene, the majority during the HTM. We obtained SHD ages ranging from 7.47 ± 0.73 ka from glacially abraded bedrock at the VB of Opplendskedalen to 2.22 ± 0.49 ka from a rock-slope failure.

This infers that glaciers re-advanced in Opplendskedalen during the 'Finse Event'. In addition, periglacial boulder-dominated landforms in the maritime fjord region seem to have reacted more dynamically to Holocene climate variability than those in continental Norway.

3. The view that rock-slope failures occur shortly after deglaciation is not supported by our SHD ages. The rock-slope failures studied here postdate YD deglaciation by at least ~4–9 ka and occurred during warm periods (e.g. HTM).
4. The PR was probably formed after deglaciation and was built up over the first part of the Holocene by continuous rock debris supplied by its bedrock cliff source which was weakened by permafrost degradation. The moraine material was likely reworked during several cold periods during the Holocene. During the LIA, an outlet of Skjerdingsdalsbreen overrode the area, leading to the incorporation of older (pre-weathered) boulders in the moraine within the LIA maximum expansion.
5. Finally, this study shows that small boulder-dominated landforms are a valuable source of palaeoclimatic information. Due to their small size and the absence of large glaciers in the area, it has been possible to gain insights into the response of the landscape to climate variability.

Acknowledgements

The authors are thankful to Jenny Müller and Claire Pflanzner-Gibbon who assisted with the field work. They also thank an anonymous reviewer for valuable comments on the manuscript.

Declaration of conflicting interests

The author(s) declared no potential conflicts of interest with respect to the research, authorship and/or publication of this article.

Funding

This study was financed by the Friedrich-Ebert-Stiftung.

ORCID iD

Philipp Marr  <https://orcid.org/0000-0002-8037-1017>

References

- Aa AR and Sjøstad JA (2000) Schmidt hammer age evaluation of the moraine sequence in front of Bøyabreen, western Norway. *Norsk Geologisk Tidsskrift* 80(1): 27–32.
- André MF (1996) Rock weathering rates in arctic and subarctic environments (Abisko Mts., Swedish Lapland). *Zeitschrift für Geomorphologie* 40(4): 499–517.
- Aydin A and Basu A (2005) The Schmidt hammer in rock material characterization. *Engineering Geology* 81(1): 1–14.
- Ballantyne CK and Harris C (1994) *The Periglaciation of Great Britain*. Cambridge: Cambridge University Press.
- Ballantyne CK and Stone JO (2013) Timing and periodicity of paraglacial rock-slope failures in the Scottish Highlands. *Geomorphology* 186: 150–161.
- Ballantyne CK, Black NM and Finlay DP (1989) Enhanced boulder weathering under late-lying snowpatches. *Earth Surface Processes and Landforms* 14(8): 745–750.
- Ballantyne CK, Sandeman GF, Stone JO et al. (2014) Rock-slope failure following Late Pleistocene deglaciation on tectonically stable mountainous terrain. *Quaternary Science Reviews* 86: 900–913.
- Ballantyne CK, Wilson P, Schnabel C et al. (2013) Lateglacial rock slope failures in north-west Ireland: Age, causes and implications. *Journal of Quaternary Science* 28(8): 789–802.
- Benedict JB (1993) Influence of snow upon rates of grandiorite weathering, Colorado Front Range, USA. *Boreas* 22(2): 87–92.
- Bickerton RH and Matthews JA (1993) 'Little Ice Age' variations of outlet glaciers from the Jostedalbreen ice-cap, southern Norway: A regional lichenometric dating study of ice-marginal moraine sequences and their climatic significance. *Journal of Quaternary Science* 8(1): 45–66.
- Blikra LH and Longva O (1995) Frost-shattered debris facies of Younger Dryas age in the coastal sedimentary successions in western Norway: Palaeoenvironmental implications. *Palaeogeography, Palaeoclimatology, Palaeoecology* 118(1–2): 89–110.
- Blikra LH, Longva O, Braathen A et al. (2006) Rock slope failures in Norwegian fjord areas: Examples, spatial distribution and temporal pattern. In: Evans SG, Mugnozsa GS, Strom A et al. (eds) *Landslides from Massive Rock Slope Failure*. Dordrecht: Springer, pp. 475–496.
- Blytt A (1876) *Immigration of the Norwegian Flora*. Christiania: Albert Cammermeyer.
- Bøe R, Longva O, Lepland A et al. (2004) Postglacial mass movements and their causes in fjords and lakes in western Norway. *Norwegian Journal of Geology* 84(1): 35–55.
- Böhme M, Oppikofer T, Longva O et al. (2015) Analyses of past and present rock slope instabilities in a Fjord valley: Implications for hazard estimations. *Geomorphology* 248: 464–474.
- Clark PU, Dyke AS, Shakun JD et al. (2009) The last glacial maximum. *Science* 325(5941): 710–714.
- Colman SM (1981) Rock-weathering rates as functions of time. *Quaternary Research* 15(3): 250–264.
- Cossart E, Mercier D, Decaulne A et al. (2014) Impacts of postglacial rebound on landslide spatial distribution at a regional scale in northern Iceland (Skagafjörður). *Earth Surface Processes and Landforms* 39(3): 336–353.
- Dahl SO and Nesje A (1996) A new approach to calculating Holocene winter precipitation by combining glacier equilibrium-line altitudes and pine-tree limits: A case study from Hardangerjøkulen, central southern Norway. *The Holocene* 6(4): 381–398.
- Dahl SO, Bakke J, Lie Ø et al. (2003) Reconstruction of former glacier equilibrium-line altitudes based on proglacial sites: An evaluation of approaches and selection of sites. *Quaternary Science Reviews* 22(2–4): 275–287.
- El Bedoui S, Guglielmi Y, Lebourg T et al. (2009) Deep-seated failure propagation in a fractured rock slope over 10,000 years: The La Clapière slope, the south-eastern French Alps. *Geomorphology* 105(3–4): 232–238.
- Erikstad L and Sollid JL (1986) Neoglaciation in South Norway using lichenometric methods. *Norsk Geografisk Tidsskrift* 40(2): 85–105.
- Etzel Müller B, Berthing I and Sollid JL (2003) Aspects and concepts on the geomorphological significance of Holocene permafrost in Southern Norway. *Geomorphology* 52(1–2): 87–104.
- Evans DJA, Butcher C and Kirthisingha AV (1994) Neoglaciation and an early 'Little Ice Age' in western Norway: Lichenometric evidence from the Sandane area. *The Holocene* 4(3): 278–289.
- Fareth OW (1987) *Glacial geology of Middle and Inner Nordfjord, western Norway*. Technical Report 408. Trondheim: Geological Survey of Norway.
- Frauenfelder R, Laustela RA and Kääh A (2005) Relative age-dating of Alpine rockglacier surfaces. *Zeitschrift für Geomorphologie* 49(2): 145–166.
- French HM (2007) *The Periglacial Environment*. Chichester: Wiley.
- Hall K (1993) Enhanced bedrock weathering in association with late-lying snowpatches: Evidence from Livingston Island, Antarctica. *Earth Surface Processes and Landforms* 18(2): 121–129.

- Hedding DW (2016) Pronival ramparts: Origin and development of terminology. *Erdkunde* 70(2): 141–151.
- Hermanns RL, Schleier M, Böhme M et al. (2017) Rock-Avalanche activity in W and S Norway peaks after the retreat of the Scandinavian ice sheet. In: Mikoš M, Vilímek V, Yin Y and et al. (eds) *Advancing Culture of Living with Landslides* (WLF 2017). Cham: Springer, pp. 331–338.
- Hughes ALC, Gyllencreutz R, Lohne ØS et al. (2016) The last Eurasian ice sheets – A chronological database and time-slice reconstruction, DATED-1. *Boreas* 45(1): 1–45.
- Kirkbride MP and Winkler S (2012) Correlation of Late Quaternary moraines: Impact of climate variability, glacier response, and chronological resolution. *Quaternary Science Reviews* 46: 1–29.
- Klapyta P (2013) Application of Schmidt hammer relative age dating to Late Pleistocene moraines and rock glaciers in the Western Tatra Mountains, Slovakia. *Catena* 111: 104–121.
- Klemsdal T and Sjulsen E (1988) The Norwegian macro-landforms: Definition, distribution and system of evolution. *Norsk Geografisk Tidsskrift* 42(2–3): 133–147.
- Löffler J, Pape R and Wundram D (2006) The climatologic significance of topography, altitude and region in high mountains – A survey of oceanic-continental differentiations of the Scandes. *Erdkunde* 60(1): 15–24.
- Lohne ØS, Mangerud J and Birks HH (2013) Precise 14C ages of the Vedde and Saksunarvatn ashes and the Younger Dryas boundaries from western Norway and their comparison with the Greenland Ice Core (GICC05) chronology. *Journal of Quaternary Science* 28(5): 490–500.
- Longva O, Blikra LH and Dehls JF (2009) *Rock avalanches: Distribution and frequencies in the inner part of Storfjorden, Møre og Romsdal County, Norway*. Technical Report 2009.002. Trondheim: Geological Survey of Norway.
- McCarroll D (1989a) Potential and limitations of the Schmidt hammer for relative-age dating: Field tests on Neoglacial Moraines, Jotunheimen, southern Norway. *Arctic and Alpine Research* 21(3): 268–275.
- McCarroll D (1989b) Schmidt hammer relative-age evaluation of a possible pre-‘Little Ice Age’ Neoglacial moraine, Leirbreen, southern Norway. *Norsk Geologisk Tidsskrift* 69: 125–130.
- McCarroll D and Nesje A (1993) The vertical extent of ice sheets in Nordfjord, western Norway: Measuring degree of rock surface weathering. *Boreas* 22(3): 255–265.
- McCull ST (2012) Paraglacial rock-slope stability. *Geomorphology* 153–154: 1–16.
- Mangerud J (1991) The last ice age in Scandinavia. In: Andersen BG and Königsson L-K (eds) *Late Quaternary Stratigraphy in the Nordic Countries 150,000–15,000 B.P.* Uppsala: Striae, pp. 15–30.
- Marr P and Löffler J (2017) Establishing a multi-proxy approach to alpine blockfield evolution in south-central Norway. *AUC Geographica* 52(2): 219–236.
- Marr P, Winkler S and Löffler J (2018) Investigations on blockfields and related landforms at Blåhø (Southern Norway) using Schmidt-hammer exposure-age dating (SHD): Palaeoclimatic and morphodynamic implications. *Geografiska Annaler: Series A, Physical Geography* 100: 285–306.
- Matthews JA (2005) ‘Little Ice Age’ glacier variations in Jotunheimen, southern Norway: A study in regionally-controlled lichenometric dating of recessional moraines with implications for climate and lichen growth rates. *The Holocene* 15(1): 1–19.
- Matthews JA (2013) Neoglaciation in Europe. In: Elias SA (ed.), *Encyclopedia of Quaternary Science*. Amsterdam: Elsevier, pp. 257–268.
- Matthews JA and Briffa KR (2005) The ‘Little Ice Age’: Re-evaluation of an evolving concept. *Geografiska Annaler: Series A, Physical Geography* 87(1): 17–36.
- Matthews JA and Dresser PQ (2008) Holocene glacier variation chronology of Smørstabbtindan massif, Jotunheimen, southern Norway, and the recognition of century- to millennial-scale European Neoglacial Events. *The Holocene* 18(1): 181–201.
- Matthews JA and McEwen LJ (2013) High-precision Schmidt-hammer exposure-age dating of flood berms, Vetleløsdalen, alpine southern Norway: First application and some methodological issues. *Geografiska Annaler: Series A, Physical Geography* 95(2): 185–195.
- Matthews JA and Owen G (2010) Schmidt hammer exposure-age dating: Developing linear age-calibration curves using Holocene bedrock surfaces from the Jotunheimen-Jostedalbreen regions of southern Norway. *Boreas* 39(1): 105–115.
- Matthews JA and Wilson P (2015) Improved Schmidt-hammer exposure ages for active and relict pronival ramparts in southern Norway, and their palaeoenvironmental implications. *Geomorphology* 246: 7–21.
- Matthews JA and Winkler S (2011) Schmidt-hammer exposure-age dating (SHD): Application to early Holocene moraines and a reappraisal of the reliability of terrestrial cosmogenic-nuclide dating (TCND) at Austanbotnbreen, Jotunheimen, Norway. *Boreas* 40(2): 256–270.
- Matthews JA, Dahl SO, Nesje A et al. (2000) Holocene glacier variations in central Jotunheimen, southern Norway based on distal glaciolacustrine sediment cores. *Quaternary Science Reviews* 19(16): 1625–1647.
- Matthews JA, McEwen L and Owen G (2015) Schmidt-hammer exposure-age dating (SHD) of snow-avalanche impact ramparts in southern Norway: Approaches, results and implications for landform age, dynamics and development. *Earth Surface Processes and Landforms* 40(13): 1705–1718.
- Matthews JA, Nesje A and Linge H (2013) Relict talus-foot rock glaciers at Øyberget, Upper Ottadalen, southern Norway: Schmidt hammer exposure ages and palaeoenvironmental implications. *Permafrost and Periglacial Processes* 24(4): 336–346.
- Matthews JA, Owen G, Winkler S et al. (2016) A rock-surface microweathering index from Schmidt hammer R-values and its preliminary application to some common rock types in southern Norway. *Catena* 143: 35–44.
- Matthews JA, Shakesby RA, Owen G et al. (2011) Pronival rampart formation in relation to snow-avalanche activity and Schmidt-hammer exposure-age dating (SHD): Three case studies from southern Norway. *Geomorphology* 130(3–4): 280–288.
- Matthews JA, Shakesby RA, Schnabel C et al. (2008) Cosmogenic ¹⁰Be and ²⁶Al ages of Holocene moraines in southern Norway I: Testing the method and confirmation of the date of the Erdalen event (c. 10 ka) at its type-site. *The Holocene* 18(8): 1155–1164.
- Matthews JA, Winkler S and Wilson P (2014) Age and origin of ice-cored moraines in Jotunheimen and Breheimen, southern Norway: Insights from Schmidt-hammer exposure-age dating. *Geografiska Annaler: Series A, Physical Geography* 96(4): 531–548.
- Matthews JA, Winkler S, Wilson P et al. (2018) Small rock-slope failures conditioned by Holocene permafrost degradation: A new approach and conceptual model based on Schmidt-hammer exposure-age dating in Jotunheimen, southern Norway. *Boreas* 47: 1144–1169.
- Nesje A (2009) Latest Pleistocene and Holocene alpine glacier fluctuations in Scandinavia. *Quaternary Science Reviews* 28(21–22): 2119–2136.
- Nesje A and Dahl SO (1993) Lateglacial and Holocene glacier fluctuations and climatic variations in western Norway: A review. *Quaternary Science Reviews* 12(4): 255–261.

- Nesje A and Dahl SO (2001) The Greenland 8200 cal. yr BP event detected in loss-on-ignition profiles in Norwegian lacustrine sediment sequences. *Journal of Quaternary Science* 16(2): 155–166.
- Nesje A and Whillans IM (1994) Erosion of Sognefjord, Norway. *Geomorphology* 9(1): 33–45.
- Nesje A, Bakke J, Dahl SO et al. (2008) Norwegian mountain glaciers in the past, present and future. *Global and Planetary Change* 60(1–2): 10–27.
- Nesje A, Blikra LH and Anda E (1994) Dating rockfall-avalanche deposits from degree of rock-surface weathering by Schmidt-hammer tests: A study from Norangsdalen, Sunnmøre, Norway. *Norsk Geologisk Tidsskrift* 74(2): 108–113.
- Nesje A, Jansen E, Birks HJB et al. (2005) Holocene climate variability in the Northern North Atlantic region: A review of terrestrial and marine evidence. In: Drange H, Dokken T, Furevik T et al. (eds) *The Nordic Seas: An Integrated Perspective* (Geophysical Monograph Series 158). New York: Wiley, pp. 89–322.
- Nesje A, Matthews JA, Dahl SO et al. (2001) Holocene glacier fluctuations of Flatebreen and winter precipitation changes in the Jostedalbreen region, western Norway, based on glaciolacustrine records. *The Holocene* 11(3): 267–280.
- Nicholson DT (2008) Rock control in microweathering of bedrock surfaces in a periglacial environment. *Geomorphology* 101(4): 655–665.
- Patton H, Hubbard A, Andreassen K et al. (2016) The build-up, configuration, and dynamical sensitivity of the Eurasian ice-sheet complex to Late Weichselian climatic and oceanic forcing. *Quaternary Science Reviews* 153: 97–121.
- Patton H, Hubbard A, Andreassen K et al. (2017) Deglaciation of the Eurasian ice sheet complex. *Quaternary Science Reviews* 169: 148–172.
- Proceq (2014) *Operating Instructions RockSchmidt & Rocklink*. Schwerzenbach: Proceq.
- Rode M and Kellerer-Pirklbauer A (2011) Schmidt-hammer exposure-age dating (SHD) of rock glaciers in the Schöderkogel-Eisenhut area, Schladminger Tauern Range, Austria. *The Holocene* 22(7): 761–771.
- Rye N, Nesje A, Lien R et al. (1997) Glacial geology and deglaciation chronology of the area between inner Nordfjord and Jostedalbreen – Strynefjellet, western Norway. *Norsk Geologisk Tidsskrift* 77: 51–63.
- Sánchez JS, Mosquera DF and Vidal Romání JRV (2009) Assessing the age-weathering correspondence of cosmogenic ²¹Ne dated Pleistocene surfaces by the Schmidt hammer. *Earth Surface Processes and Landforms* 34(8): 1121–1125.
- Shakesby RA, Matthews JA and Owen G (2006) The Schmidt hammer as a relative-age dating tool and its potential for calibrated-age dating in Holocene glaciated environments. *Quaternary Science Reviews* 25(21–22): 2846–2867.
- Shakesby RA, Matthews JA and Schnabel C (2008) Cosmogenic ¹⁰Be and ²⁶Al ages of Holocene moraines from southern Norway II: Evidence for individualistic responses of high-altitude glaciers to millennial-scale climatic fluctuations. *The Holocene* 18(8): 1165–1177.
- Shakesby RA, Matthews JA and Winkler S (2004) Glacier variations in Breheimen, southern Norway: Relative-age dating of Holocene moraine complexes at six high-altitude glaciers. *The Holocene* 14(6): 899–910.
- Shakesby RA, Matthews JA, Karlén W et al. (2011) The Schmidt hammer as a Holocene calibrated-age dating technique: Testing the form of the R-value-age relationship and defining the predicted age errors. *The Holocene* 21(4): 615–628.
- Shakesby RA, Matthews JA, McEwen LF et al. (1999) Snow-push processes in pronival (protalus) rampart formation: Geomorphological evidence from Smørbotn, Romsdalsalpane, Southern Norway. *Geografiska Annaler: Series A, Physical Geography* 81(1): 31–45.
- Shakesby RA, Smith JG, Matthews JA et al. (2007) Reconstruction of Holocene glacier history from distal sources: Glaciofluvial streambank mires and a glaciolacustrine sediment core near Sota Sæter, Breheimen, southern Norway. *The Holocene* 17(6): 729–745.
- Solomina ON, Bradley RS, Hodgson DA et al. (2015) Holocene glacier fluctuations. *Quaternary Science Reviews* 111: 9–34.
- Stroeven AP, Hättestrand C, Kleman J et al. (2016) Deglaciation of Fennoscandia. *Quaternary Science Reviews* 147: 91–121.
- Tomkins MB, Dortch JM, Hughes PD et al. (2018a) Rapid assessment of glacial landforms in the Pyrenees using Schmidt hammer exposure dating (SHED). *Quaternary Research*. Epub ahead of print 2 April. DOI: 10.1017/qua.2018.12.
- Tomkins MB, Hucka JJ, Dortch JM et al. (2018b) Schmidt hammer exposure dating (SHED): Calibration procedures, new exposure age data and an online calculator. *Quaternary Geochronology* 44: 55–62.
- Tomkins MD, Dortch JM and Hughes PD (2016) Schmidt hammer exposure dating (SHED): Establishment and implications for the retreat of the last British Ice Sheet. *Quaternary Geochronology* 33: 46–60.
- Tveten E, Lutro O and Thorsnes T (1998) *Geologisk kart over Norge, 1:250,000*. Trondheim: Norges Geologiske Undersøkelse.
- Wanner H, Beer J, Bütikofer J et al. (2008) Mid- to Late-Holocene climate change: An overview. *Quaternary Science Reviews* 27: 1791–1828.
- Wanner H, Solomina O, Grosjean M et al. (2011) Structure and origin of Holocene cold events. *Quaternary Science Reviews* 30: 3109–3123.
- Wilson P (2004) Relict rock glaciers, slope failure deposits, or polygenetic features? A re-assessment of some Donegal debris landforms. *Irish Geography* 37(1): 77–87.
- Wilson P and Matthews JA (2016) Age assessment and implications of late Quaternary periglacial and paraglacial landforms on Muckish Mountain, northwest Ireland, based on Schmidt-hammer exposure-age dating (SHD). *Geomorphology* 270: 134–144.
- Wilson P, Matthews JA and Mourne RW (2017) Relict block-streams at Insteheia, Valldalen-Talfjorden, southern Norway: Their nature and Schmidt hammer exposure age. *Permafrost and Periglacial Processes* 28(1): 286–297.
- Winkler S (2005) The Schmidt hammer as a relative-age dating technique: Potential and limitations of its application on Holocene moraines in Mt Cook National Park, Southern Alps, New Zealand. *Journal of Geology and Geophysics* 48(1): 105–116.
- Winkler S (2009) First attempt to combine terrestrial cosmogenic nuclide (¹⁰Be) and Schmidt hammer relative-age dating: Strauchon Glacier, Southern Alps, New Zealand. *Central European Journal of Geosciences* 1(3): 274–290.
- Winkler S (2014) Investigation of late-Holocene moraines in the western Southern Alps, New Zealand, applying Schmidt-hammer exposure-age dating. *The Holocene* 24(1): 48–66.
- Winkler S and Lambiel C (2018) Age constraints of rock glaciers in the Southern Alps/New Zealand – Exploring their palaeoclimatic potential. *The Holocene* 28: 778–790.
- Winkler S and Matthews JA (2010) Holocene glacier chronologies: Are ‘high-resolution’ global and inter-hemispheric comparisons possible? *The Holocene* 20(7): 1137–1147.
- Winkler S and Matthews JA (2014) Comparison of electronic and mechanical Schmidt hammers in the context of exposure-age dating: Are Q- and R-values interconvertible? *Earth Surface Processes and Landforms* 39(8): 1128–1136.
- Winkler S, Matthews JA, Mourne RW et al. (2016) Schmidt-hammer exposure ages from periglacial patterned ground (sorted circles) in Jotunheimen, Norway, and their interpretative problems. *Geografiska Annaler Series A, Physical Geography* 98(3): 265–285.

9 ¹⁰Be-Based Exploration of the Timing of Deglaciation in Two Selected Areas of Southern Norway

MARR, P., WINKLER, S., BINNIE, S. A. and LÖFFLER, J. (2019b): ¹⁰Be-based exploration of the timing of deglaciation in two selected areas of southern Norway. In: E&G Quaternary Science Journal 68, 165–176.

Abstract

We present new ¹⁰Be surface exposure ages from two selected locations in southern Norway. A total of five ¹⁰Be samples allow a first assessment of local deglaciation dynamics of the Scandinavian Ice Sheet at Dalsnibba (1476 m a.s.l.) in southwestern Norway. The bedrock ages from the summit of Dalsnibba range from 13.3 ± 0.6 to 12.7 ± 0.5 ka and probably indicate the onset of deglaciation as a glacially transported boulder age (16.5 ± 0.6 ka) from the same elevation likely shows inheritance. These ages indicate initial deglaciation commencing at the end of the Bølling–Allerød interstadial (~14.7 – 12.9 kyr BP) and ice-free conditions at Dalsnibba's summit during the Younger Dryas. Bedrock samples at lower elevations imply vertical ice surface lowering down to 1334 m a.s.l. at 10.3 ± 0.5 ka and a longer overall period of downwasting than previously assumed. Two further ¹⁰Be samples add to the existing chronology at Blåhø (1617 m a.s.l.) in south-central Norway. The ¹⁰Be erratic boulder sample on the summit of Blåhø yields 20.9 ± 0.8 ka, whereas a ¹⁰Be age of 46.4 ± 1.7 ka for exposed summit bedrock predates the Late Weichselian Maximum. This anomalously old bedrock age infers inherited cosmogenic nuclide concentrations and suggests low erosive cold-based ice cover during the Last Glacial Maximum. However, due to possible effects of cryoturbation and frost heave processes affecting the erratic boulder age and insufficient numbers of ¹⁰Be samples, the glacial history on Blåhø cannot conclusively be resolved. Comparing the different timing of deglaciation at both locations in a rather short west–east distance demonstrates the complex dynamics of deglaciation in relation to other areas in southern Norway.



¹⁰Be-based exploration of the timing of deglaciation in two selected areas of southern Norway

Philipp Marr¹, Stefan Winkler², Steven A. Binnie³, and Jörg Löffler¹

¹Department of Geography, University of Bonn, Meckenheimer Allee 166, 53115 Bonn, Germany

²Department of Geography and Geology, University of Würzburg, Am Hubland, 97074 Würzburg, Germany

³Institute for Geology and Mineralogy, University of Cologne, Zùlpicherstr., 49B, 50674 Cologne, Germany

Correspondence: Philipp Marr (marr@uni-bonn.de)

Relevant dates: Received: 18 January 2019 – Revised: 2 May 2019 – Accepted: 13 June 2019 –
Published: 30 July 2019

How to cite: Marr, P., Winkler, S., Binnie, S. A., and Löffler, J.: ¹⁰Be-based exploration of the timing of deglaciation in two selected areas of southern Norway, *E&G Quaternary Sci. J.*, 68, 165–176, <https://doi.org/10.5194/egqsj-68-165-2019>, 2019.

Abstract: We present new ¹⁰Be surface exposure ages from two selected locations in southern Norway. A total of five ¹⁰Be samples allow a first assessment of local deglaciation dynamics of the Scandinavian Ice Sheet at Dalsnibba (1476 m a.s.l.) in southwestern Norway. The bedrock ages from the summit of Dalsnibba range from 13.3 ± 0.6 to 12.7 ± 0.5 ka and probably indicate the onset of deglaciation as a glacially transported boulder age (16.5 ± 0.6 ka) from the same elevation likely shows inheritance. These ages indicate initial deglaciation commencing at the end of the Bølling–Allerød interstadial (~ 14.7 – 12.9 kyr BP) and ice-free conditions at Dalsnibba’s summit during the Younger Dryas. Bedrock samples at lower elevations imply vertical ice surface lowering down to 1334 m a.s.l. at 10.3 ± 0.5 ka and a longer overall period of downwasting than previously assumed. Two further ¹⁰Be samples add to the existing chronology at Blåhø (1617 m a.s.l.) in south-central Norway. The ¹⁰Be erratic boulder sample on the summit of Blåhø sample yields 20.9 ± 0.8 ka, whereas a ¹⁰Be age of 46.4 ± 1.7 ka for exposed summit bedrock predates the Late Weichselian Maximum. This anomalously old bedrock age infers inherited cosmogenic nuclide concentrations and suggests low erosive cold-based ice cover during the Last Glacial Maximum. However, due to possible effects of cryoturbation and frost heave processes affecting the erratic boulder age and insufficient numbers of ¹⁰Be samples, the glaciation history on Blåhø cannot conclusively be resolved. Comparing the different timing of deglaciation at both locations in a rather short west–east distance demonstrates the complex dynamics of deglaciation in relation to other areas in southern Norway.

Kurzfassung: Es werden neue ¹⁰Be Oberflächenexpositionsdatierungsalter zweier ausgewählter Lokalitäten in Südnorwegen vorgestellt. Insgesamt fünf ¹⁰Be Altersdatierungen erlauben eine erste Bewertung der lokalen Deglaziationsdynamiken des Skandinavischen Eisschildes auf Dalsnibba (1476 m ü.d.M., über dem Meeresspiegel) im westlichen Südnorwegen. Die Expositionsalter des anstehenden Grundgesteins zwischen 13.3 ± 0.6 und 12.7 ± 0.5 ka vom Gipfel der Dalsnibba indizieren den Beginn der Deglaziation, da das Alter des glazial transportierten Blocks (16.5 ± 0.6 ka) von ähnlicher Höhenlage stammt und dieser wahrscheinlich eine ererbte kosmogene Nuklidkonzentration besitzt. Dies

deutet auf eine beginnende initiale Deglaziation am Ende des Bølling–Allerød interstadial (~ 14.7 – 12.9 kyr BP) und einen eisfreien Gipfel der Dalsnibba während der Jüngerer Dryas hin. Expositionsalter für Grundgestein in niedrigerer Höhenlage weisen auf ein anschließendes Absinken der vertikalen Eisausdehnung auf 1334 m ü.d.M. um 10.3 ± 0.5 ka sowie auf eine länger anhaltende Eisschmelzperiode als bisher angenommen hin. Es werden zwei zusätzliche Datierungen zur bereits bestehenden Deglaziationschronologie von Blåhø (1617 m ü.d.M.) im zentralen Südnorwegen präsentiert. Das ¹⁰Be Alter eines erratischen Blocks auf Blåhø ergibt 20.9 ± 0.8 ka und das erzielte Alter von 46.4 ± 1.7 ka eines Grundgesteinsaufschlusses am Gipfel liegt zeitlich vor dem Spätweichsel-Maximum (LGM). Das ungewöhnlich hohe Grundgesteinssalter lässt sich auf eine ererbte kosmogene Nuklidkonzentration sowie eine Bedeckung mit wenig erosivem, kaltbasalen Eis auf Blåhø während des LGM schließen. Allerdings ist eine abschließende Bewertung der Vergletscherungsgeschichte Blåhø schwierig, da mögliche Effekte von Kryoturbation und Frosthebungsprozessen das Alter des Blocks beeinflussen haben könnten und die Anzahl der Expositionsdatierungen unzureichend ist. Der Vergleich des unterschiedlichen Beginns der Deglaziation in beiden Untersuchungsgebieten in geringer West–Ost Distanz deutet auf komplexe dynamische Deglaziationsprozesse in Relation zu anderen Gebieten in Südnorwegen hin.

1 Introduction

The growth and decay of Quaternary glaciers and ice sheets has had fundamental implications for environmental changes worldwide (Ehlers and Gibbard, 2007). Based on numerical terrestrial or marine radiocarbon and cosmogenic nuclide surface exposure ages in addition to pollen stratigraphy, the chronology of the last deglaciation of the Scandinavian Ice Sheet (SIS) following the Last Glacial Maximum (LGM, 26.5 – 20 kyr; Clark et al., 2009) and related ice marginal positions in Norway are generally perceived as well constrained (Hughes et al., 2016; Stroeven et al., 2016; Patton et al., 2017). The detailed vertical extent of the SIS in Norway for this period remains, however, uncertain over large areas. Scenarios ranging from maximum models with a central ice dome (Sollid and Reite, 1983; Mangerud, 2004) to minimum models implying a thin multi-domed ice sheet and larger ice-free areas (Dahl et al., 1997; Wohlfarth, 2010) are the topic of ongoing discussion. The knowledge of the vertical dimension of the LGM ice sheet could provide crucial information on palaeoenvironmental factors like sea-level changes, atmospheric and oceanic circulation, (de-)glaciation patterns, ice-sheet erosion rates, landscape evolution, and englacial thermal boundaries (Winguth et al., 2005; Rinterknecht et al., 2006; Goehring et al., 2008). The interpretation of bedrock with different degree of weathering in mountain areas affected by Quaternary glaciation can, therefore, be important for determining ice-sheet behaviour and thickness during the last glaciation periods (Brook et al., 1996; Briner et al., 2006; McCarroll, 2016). There are several concepts to explain the limit between differently weathered bedrock (trimline) separating highly weathered uplands comprising blockfields and tors from relatively unweathered lower exposures of freshly eroded glacial features (Rea et al., 1996; Briner et al., 2006). The two most discussed scenarios suggest on the one hand

the preservation of highly weathered uplands by a cover of non-erosive cold-based ice; thus the trimline would reflect an englacial thermal boundary. The alternative explanation suggests that the trimline represents the true upper vertical ice surface and erosional limit of a former warm-based ice sheet with ice-free nunatak areas above that boundary (Stroeven et al., 2002).

The rise of terrestrial cosmogenic nuclides (TCNs) for surface exposure dating as a key tool to yield numerical ages of landforms and bedrock surfaces representing specific glacier and ice sheet dynamics has revolutionized deglaciation chronologies (Dunai, 2010), especially for settings where organic material is not available for dating. TCNs have been frequently used to reconstruct glacial chronologies worldwide, often utilizing ages derived from erratic boulders or bedrock surfaces (Dunai, 2010; Stroeven et al., 2016, and references therein). To successfully apply TCNs and to establish timing and rates of the last deglaciation, it is necessary that any cosmogenic nuclide produced prior to the last deglaciation has been removed by erosion (Briner et al., 2006; Dunai, 2010). Consequently, the erosive capacity of an ice sheet is mirrored in the concentration of cosmogenic nuclides, as the degree of erosion governs the level of inheritance (Harbor et al., 2006). Erosive capacity is largely causally connected to the basal temperature regime of the ice and its related ability to move by basal sliding. Therefore, cosmogenic nuclide concentrations may also serve as a tool to identify englacial thermal boundaries between warm-based and cold-based zones or estimate palaeo-ice thickness of entirely warm-based glaciers (Kleman, 1994).

The SIS constituted the largest unit of the Eurasian ice sheet (Hughes et al., 2016). Despite the progress with reconstructing volume, margins and timing, the information from terrestrial sources about the former ice cover is limited (Patton et al., 2016). Only a few deglaciation studies have

been carried out in the Geiranger Fjord area in southwestern Norway, where our first selected site, Dalsnibba, is located (e.g. Fareth, 1987; Aarseth et al., 1997). These studies have mostly relied on ¹⁴C dates which have repeatedly been questioned (e.g. Donner, 1996). Hence, only limited numerical age data are available and there is a need for more reliable data for a better understanding of deglaciation dynamics in this area. Our second selected site at Blåhø was previously studied by several authors focussing on deglaciation following the LGM (e.g. Nesje et al., 1994; Goehring et al., 2008; Marr et al., 2018). We provide additional ages from an erratic boulder and from a bedrock outcrop to improve the image of the glacial history.

In the wake of growing evidence for a more dynamic SIS through the last glacial cycle (Rinterknecht et al., 2006; Mangerud et al., 2010), it is essential to establish a robust deglaciation chronology, particularly for its inner mountainous region, to understand landform evolution and ice sheet dynamics. Given the importance of ice sheets with respect to the climate system, a better understanding of their evolution and the rate and timing of their ice retreat across the mountainous parts of southern Norway is necessary. Here, we report cosmogenic ¹⁰Be surface exposure ages from boulder and bedrock surfaces of two selected mountain sites in southwestern and south-central Norway to improve our knowledge on the (de)glaciation history (Fig. 1). Our main study objectives were as follows:

1. to apply terrestrial cosmogenic ¹⁰Be dating and to determine ¹⁰Be surface exposure ages from the collected boulder and bedrock samples
2. to present the first estimate for the timing of initial local deglaciation for Dalsnibba in Opplendskedalen based on ¹⁰Be
3. to assess and further improve the existing deglaciation chronology for Blåhø in the light of new ¹⁰Be ages presented in this study
4. to explore the ice sheet dynamics and characteristics during the deglaciation in the selected areas in southern Norway.

2 Study area

2.1 Dalsnibba

Dalsnibba (62°4′43 N, 7°17′35 E; 1476 m a.s.l.) is located in Opplendskedalen on the Geirangerfjellet in the western part of south-central Norway. The summit area is dominated by glacially eroded bedrock outcrops which are moderately weathered, but there is no blockfield on Dalsnibba. The general morphology was strongly influenced by Quaternary glaciations with well-developed glacial valleys and deep fjords constituting prevailing macro-landforms (Holstedahl, 1967; Klemsdal and Sjulsen, 1988). Four bedrock samples

from glacially eroded bedrock surfaces and one glacially transported boulder sample taken at four elevations ranging from 1334 to 1476 m a.s.l. were analysed. We aimed for sampling along a vertical transect from Dalsnibba to the valley bottom of Opplendskedalen at ~ 1050 m a.s.l. However, inaccessibility and/or inappropriate sampling sites prohibited us from doing so. Sub-oceanic climatic conditions prevail at the site with mean annual air temperature between 0 and 2 °C (1971–2000) and mean annual precipitation between 2000 and 3000 mm a⁻¹ (1971–2000) (<http://www.senorge.no>, last access: 18 April 2019). The gneiss bedrock is mainly quartz dioritic to granitic and partly migmatitic and is part of the so-called Western Gneiss Region (Tveten et al., 1998). The sampled boulder had the equivalent lithological composition.

The ice retreat following the LGM probably saw the ice margin approaching the inner parts of Storfjorden during the Bølling–Allerød interstadial (~ 14.7–12.9 kyr BP; Patton et al., 2017) when the glacier probably experienced several short standstills in the Geiranger Fjord (Longva et al., 2009). Glaciers readvanced during the Younger Dryas (YD, 12.9–11.7 cal. kyr BP; Lohne et al., 2013) and created moraines at the fjord mouth (Longva et al., 2009). Little is known about the vertical ice limit during the YD; Andersen et al. (1995) suggest a thickness of 800–1200 m in fjords that became ice-free during the Bølling–Allerød interstadial. The final deglaciation following the YD in the fjords in western Norway generally falls between 11.2 ± 0.4 and 10.9 ± 0.2 cal. kyr BP (cf. Nesje and Dahl, 1993; calibration from Hughes et al., 2016, applied).

2.2 Blåhø

Blåhø (61°53′51 N, 9°16′58 E; 1617 m a.s.l.) is located in Otadalen in the central part of southern Norway. Smooth undulating surfaces at summit level are present, with three lower peaks – Rundhø (1556 m a.s.l.), Veslrundhø (1514 m a.s.l.) and Storhøi (1455 m a.s.l.) – part of the mountain ridge. The Blåhø summit is covered by an autochthonous blockfield extending down to a trimline at ~ 1500 m a.s.l. (Nesje et al., 1994). Two samples were collected at the summit: one from a bedrock slab at the eastern edge of the blockfield and one from an erratic boulder. Climatic conditions are continental, with a mean annual temperature of –2 to –1 °C and a mean annual precipitation of 750–1000 mm a⁻¹ at the summit and less than 500 mm a⁻¹ (1971–2000) in the valley (<http://www.senorge.no>); it is among the driest areas in Norway. The area is dominated by quartz-rich Precambrian bedrock. The summit itself is dominated by meta-conglomerate and meta-sandstone on higher and lower slopes, respectively (Tveten et al., 1998). The sampled erratic boulder from the summit is quartz pegmatite.

The (de)glaciation history of Blåhø has attracted researchers' attention for decades (e.g. Nesje et al., 1994; Goehring et al., 2008; Marr and Löffler, 2017). It has been debated whether the summit was covered by cold-based ice

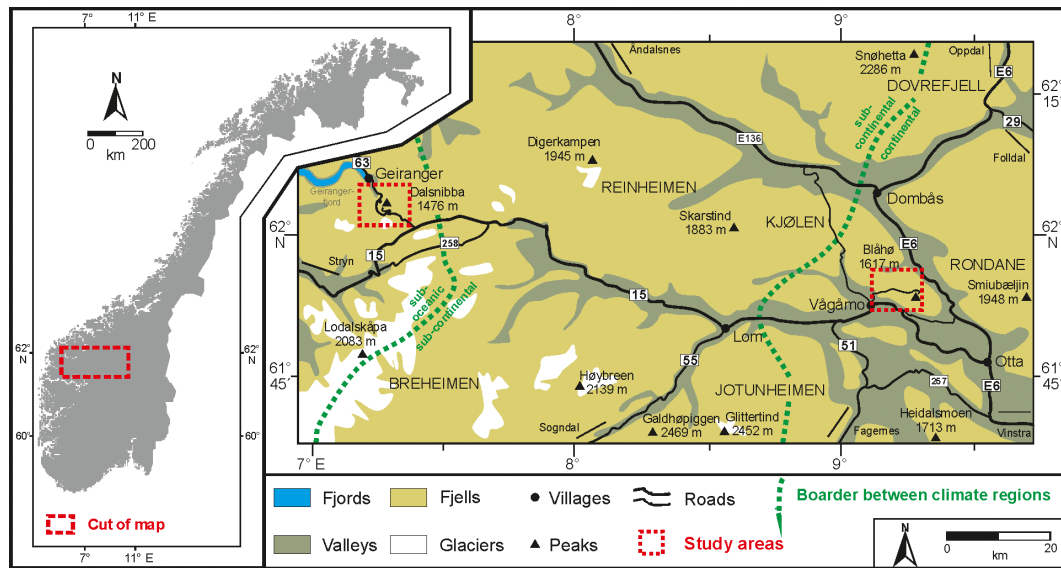


Figure 1. Study areas in southern Norway and the location of Dalsnibba in the west and Blåhø in the east (modified after Löffler and Pape, 2004).

(Goehring et al., 2008) or remained ice-free during the LGM (Nesje et al., 1994). Goehring et al. (2008) established a deglaciation chronology following the LGM, commencing at 25.1 ± 1.8 ka based on a ¹⁰Be age from an erratic boulder at the summit to 11.7 ± 1.0 ka at the lowermost sample (1086 m a.s.l.).

3 Methods

3.1 Material and measurement

Surface exposure dating utilizes the in situ build-up of cosmogenic nuclides like ¹⁰Be, ²⁶Al or ³⁶Cl by secondary cosmic rays to assess the duration of surface exposure at or near the earth's surface (Balco et al., 2008). The calculation of surface exposure ages using cosmogenic nuclide concentrations from glacial landforms is based on several assumptions. Exposure ages obtained using a single nuclide species are often considered minimum ages, as it is assumed that the samples were constantly exposed at the surface during one single period only, and that they neither contain an inherited nuclide concentration nor were they affected by significant snow shielding or erosion (Stroeven et al., 2002; Briner et al., 2006). In this study, we measured the ¹⁰Be concentration of five bedrock (-bed) and two boulder (-bo) samples (Fig. 2). We targeted bedrock outcrops to provide additional new data to existing datasets (Goehring et al., 2008) and to explore the potential thermal and erosional properties of the ice sheet (Harbor et al., 2006; Dunai, 2010) because erratics on top of (glacially modified) bedrock may (Fabel et al., 2002; Dunai, 2010), but not necessarily, provide deglaciation ages (cf. Heymann et al., 2011). It has to be acknowledged, however, that our limited ¹⁰Be ages ($n = 7$), especially in the

eastern study area, allow us to improve and assess the existing deglaciation chronology rather than construct an independent one.

The samples were collected by hammer and chisel, and only boulders broader than 20 cm in diameter were selected for measurement to minimize the probability of post-depositional disturbance. All samples were obtained from flat surfaces (dip < 5°) with at least 25 cm distance from any edges for the large boulder and the longest distance possible from the edges of the smaller boulder. Both bedrock samples were obtained from locations with weathered surfaces and/or lichen cover to avoid surfaces so intensively weathered that slabs had potentially broken off the boulder surfaces (Fig. S5 in the Supplement). We sampled from local topographic highs to minimize the influence of snow cover. Geographical coordinates and elevations of sampling locations were recorded with a handheld GPS. Topographic shielding was derived from compass and clinometer measurements at each sample site.

After crushing and sieving, between ca. 10 to 44 g of purified quartz was extracted from the rock samples using the approach of Kohl and Nishiizumi (1992). Quartz samples were spiked with around 300 µg of a commercial beryllium solution (Scharlab, 1000 mg L⁻¹, density 1.02 g cm⁻³) before being dissolved in a concentrated HF/HNO₃ mixture. Preparation of the purified quartz as AMS (accelerator mass spectrometry) targets was undertaken in tandem with a reagent blank. Target preparation chemistry was undertaken in the clean laboratory at the University of Cologne using the single-step column approach described by Binne et al. (2015). Beryllium hydroxide was co-precipitated with Ag, according to Stone et al. (2004), for pressing

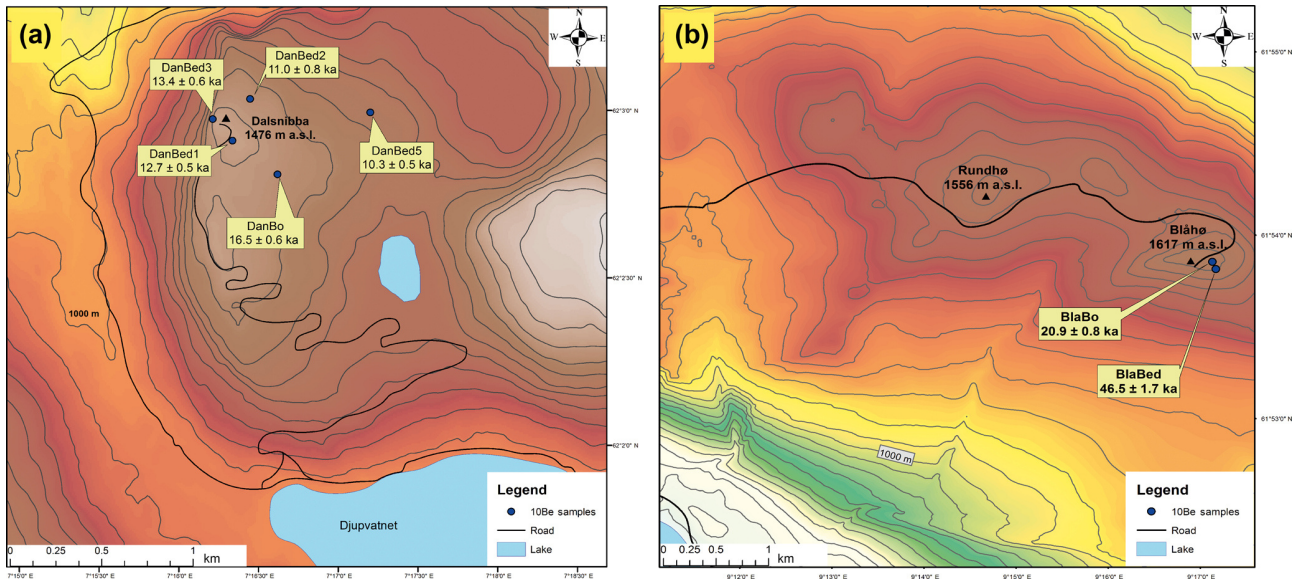


Figure 2. Detailed sampling locations at (a) Dalsnibba and (b) Blåhø. The bedrock samples in both study areas are labelled as -bed, the boulder samples as -bo. The calculated ^{10}Be ages of every sample are reported with 1σ uncertainty in ka. The contour line intervals are a distance of 50 m (source: <http://www.kartverket.no>, last access: 14 January 2019).

into AMS targets. Measurements of $^{10}\text{Be}/^9\text{Be}$ were undertaken at CologneAMS (Dewald et al., 2013), normalized to the revised standard values reported by Nishiizumi et al. (2007). Uncertainties in the blank-corrected ^{10}Be concentrations were derived by propagating (summing in quadrature) the 1 SD uncertainties in the AMS measurements of the blanks and the samples along with an estimated 1 % uncertainty (1 SD) in the mass of ^9Be added as a carrier.

3.2 Exposure age calculations

The ^{10}Be surface exposure ages were calculated with the on-line exposure age calculator version 3, formerly known as the CRONUS-Earth online exposure age calculator (Balco et al., 2008; Balco, 2017; <http://hess.ess.washington.edu/>, last access: 30 April 2019). The spallation-induced regional production rate for western Norway (normalized to sea-level high latitude) was used, as surfaces of unknown age can be dated more precisely due to the proximity of the calibration site (Goehring et al., 2012a, b). We applied the time-dependent LSD scaling model of Lifton et al. (2014) and used the 07KNSTD flag in the online calculator. A rock density of 2.6 g cm^{-3} was applied for all samples. We did not correct our ages for atmospheric pressure anomalies, temporal shielding by snow, sediment or vegetation. Erosion of 1 mm kyr^{-1} was applied in the online calculator, a comparable erosive capacity in summit areas as presented by Andersen et al. (2018a) for Reinheimen, close to Blåhø.

One parameter required within the calibration process for calculating ^{10}Be age is the elevation of the sampled bedrock or boulder surface. Any correction for the effect of post-

glacial glacio-isostatic uplift is, however, quite challenging. No detailed local uplift data for Dalsnibba are available, but an estimate of ca. 100 m total uplift based on reports of former shoreline displacement or modelling attempts seems reasonable (Svendsen and Mangerud, 1987; Fjeldskaar et al., 2000; Steffen and Wu, 2011). For Blåhø, the total postglacial uplift is estimated at around 300 m (Morén and Pässe, 2001). However, this postglacial uplift cannot be described as a linear function as data from other localities in western Norway highlight (e.g. Fjeldskaar, 1994; Helle et al., 2007). An initial strong uplift during Allerød halted during the Younger Dryas and resumed after its termination with high uplift rates in the Early Holocene that subsequently significantly decreased (Lohne et al., 2007). According to newest modelling by Fjeldskaar and Amatonov (2018) the calculated uplift between Allerød and Younger Dryas at around Dalsnibba would summarize to around 50 m, i.e. half of the suggested total postglacial glacio-isostatic uplift. Because postglacial uplift first becomes relevant for ^{10}Be age calculation after exposure of the sampled surface, a circular reference emerges as surface exposure age (the unknown factor itself) needed to be known to precisely determine the amount of uplift that had already occurred according to established models (cf. Jones et al., 2019). To resolve this problem and simplify the correction for postglacial uplift, we assume initial fast uplift between 13 and 11.5 kyr totaling 50 m following Fjeldskaar and Amatonov (2018), followed by linear uplift during the Holocene that accounts for the remaining 50 m. The resulting reduction for sample elevation is ca. 30 m for Dalsnibba. Following similar considerations for Blåhø, a maximum reduction of 150 m in relation to modern elevation is

considered. However, the alternative influence of ca. 100 m reduction and no uplift correction are also assessed because of a likely non-linear uplift function, with maximum uplift during or immediately following deglaciation. The results of different uplift scenarios on Blåhø ages are presented in Table S3 in the Supplement. A reduction of sample elevation of ca. 100 m averaged over the entire surface exposure time seems reasonable and needs to be treated as a maximum value as Early Holocene uplift rates may be underestimated. Finally, with respect to all potential uncertainties with the calculation and calibration of ¹⁰Be surface exposure age estimates (production rates, selected scaling schemes, etc.), our simplified postglacial uplift correction appears appropriate.

4 Results

AMS analysis gave ¹⁰Be/⁹Be ratios ranging from 1.65×10^{-12} to 8.69×10^{-14} . The reagent blank prepared alongside the samples gave a ¹⁰Be/⁹Be value of 6.47×10^{-15} , and the blank subtractions were < 4 % of the total number of ¹⁰Be atoms measured in the samples, aside from sample DanBed2, which yielded less quartz, resulting in a blank subtraction that was 7.5 % of the total.

The cosmogenic exposure ages calculated for all samples from Dalsnibba and Blåhø are shown in Fig. 2 and Table 1. The boulder sample from the summit of Dalsnibba (DanBo) was the oldest from this site at 16.5 ± 0.6 ka. The ¹⁰Be ages from Blåhø are 46.4 ± 1.7 ka (BlaBed) for the bedrock from the blockfield, whereas the boulder resting on the blockfield gave 20.9 ± 0.8 ka (BlaBo). The recalculated ages for Goehring et al. (2008) are presented in Table S4. Results for the effect of different glacio-isostatic uplift rates for Dalsnibba and Blåhø are presented in Tables S2 and S3. The considered uplift of 30 m vs. no uplift for Dalsnibba results in a ~ 3 % age increase. An uplift of 100 m at Blåhø leads to ~ 9 % older ages if compared to no correction for no uplift. For the maximum scenario of 150 m uplift the corresponding value is a ~ 14 % age increase.

5 Discussion

5.1 Methodological considerations and processes affecting ¹⁰Be concentrations

We collected our rock samples from three different settings: bedrock outcrops from weathered debris/blockfields, glacially eroded bedrock surfaces, and boulders. Erosion of the sampled surfaces or undetected shielding (e.g. snow or vegetation cover) would lower the nuclide concentrations and consequently lead to underestimated ages (Stroeven et al., 2002; Hughes et al., 2016). Further, samples collected above the weathering limit, where outcrops are prone to surface degradation by severe frost weathering, also result in an underestimation of the true surface exposure (Brook et al., 1996).

The uplift model used by Goehring et al. (2008) applied on Blåhø reveals ~ 22 % older ages from high-elevation samples (> 1400 m a.s.l.). The recalculated data from Goehring et al. (2008) applying our uplift correction approach (with 100 m) give an estimated age difference of ~ 9 %. A total uplift of 150 m results in ~ 14 % older ages, which is closer to the value obtained by Goehring et al. (2008). For further discussion we rely on the most realistic option with a total uplift of 100 m for Blåhø.

The impact of snow cover on the ¹⁰Be ages was estimated on the basis of Gosse and Philipps (2001) with recent snow conditions (data from <http://www.senorge.no>, averaged 1958–2019). By assuming 150 cm during 9–10 months in the west and 40 cm for 7–8 months (snow density 0.3 g cm^{-3}) in the east are representative of this interglacial, the ¹⁰Be calculations could result in 18 %–20 % too young ages in the west and 4.2 %–4.8 % in the east. It needs, however, to be pointed out that it is impossible to assess whether modern snow conditions are representative of the conditions during the entire Holocene with its known climate variability (Nesje, 2009). We are aware that due to our limited dataset it is impossible to make conclusive statements about the glaciation history, especially for Blåhø, and to definitively identify geological bias and sample outliers (Stroeven et al., 2016). Furthermore, our restrictions to a single cosmogenic nuclide (¹⁰Be) does not allow us to obtain information on any complex burial history that would require pairing ¹⁰Be with other nuclides like ²⁶Al (Fabel et al., 2002). Nevertheless, we assume our results to have the capacity to contribute to the discussion of the timing of deglaciation in both areas because of their generally coherent ages in relation to previously published timings of deglaciation between 11.2 ± 0.4 and 10.9 ± 0.2 cal. kyr BP (cf. Nesje and Dahl, 1993; calibration from Hughes et al., 2016, applied) in the west and 21.8 ± 1.6 ka (Goehring et al., 2008, recalculated) in the east. Recent findings indicate the timing of the last deglaciation at 11 ± 0.2 ka in Reinheimen, located between our study areas (Andersen et al., 2018a).

5.2 Timing of deglaciation at Dalsnibba

The obtained ¹⁰Be surface exposure ages from Dalsnibba offer the possibility of presenting the first age constraints for local deglaciation based on cosmogenic nuclides. The internal consistency of our ¹⁰Be exposure ages from glacially eroded bedrock surfaces with their post-LGM age implies that glacial erosion was sufficient to remove any inherited nuclide concentration, and that the bedrock had been continuously exposed since. This supports the concept that glaciers in fjord landscapes were highly effective erosional agents and consequently warm-based (Aarseth et al., 1997; Matthews et al., 2017), especially in the valleys. This is in agreement with Landvik et al. (2005), who claim that frozen-bed conditions throughout the growth and decay of glaciers in coastal environments are unlikely. However, there are blockfield-covered summits between the fjords which are mostly located at a

Table 1. Sample and laboratory data and calculated ¹⁰Be surface exposure ages.

Sample ID	Sample type	Latitude (°)	Longitude (°)	Altitude (m a.s.l.)	Sample thickness (cm)	Topographic shielding	Blank-corrected ¹⁰ Be conc. (10 ⁵ at g ⁻¹)	Uncertainty (1σ) blank-corrected ¹⁰ Be conc. (10 ³ at g ⁻¹)	External uncertainty (year)	Exposure age (year)
DanBed1	Bedrock	62.047639	7.274044	1476	4.8	0.999935	2.04	8	1100	12700 ± 500
DanBed2	Bedrock	62.049925	7.275275	1418	3.5	0.999997	1.70	13	1200	11000 ± 800
DanBed3	Bedrock	62.049314	7.270258	1464	5.9	0.999976	2.10	8	1200	13300 ± 600
DanBed5	Bedrock	62.048295	7.287856	1334	4.7	0.999544	1.48	6	900	10300 ± 500
DanBo	Boulder	61.897524	9.282407	1438	6.5	1	2.60	10	1500	16500 ± 600
BlaBed	Bedrock	61.897700	9.284238	1615	2.4	1	7.49	26	4200	46400 ± 1700
BlaBo	Boulder	62.044505	7.274839	1617	2.8	1	3.59	14	1900	20900 ± 800

All ages are calculated using version 3 of the calculator code found at <https://hess.ess.washington.edu/> (last access: 30 April 2019) (Balco et al., 2008; Balco, 2017). The western Norway ¹⁰Be production rate (Goehring et al., 2012a, b) is applied with standard atmosphere and pressure “std” and a rock density of 2.6 g cm⁻³. The time-dependent LSD scaling model of Lifton et al. (2014) was used. An uplift for 30 m for Dalsnibba and 100 m for Blåhø was assumed as well as an erosion of 1 mm kyr⁻¹.

higher altitude above the blockfield boundary, indicating that they were potentially protected by cold-based ice (Brook et al., 1996). The two uppermost bedrock ages and the glacial boulder are from comparable altitudinal settings, whereas the boulder is ~ 3.8 to 3.2 ka older than the bedrock samples. This points to inherited cosmogenic nuclide inventory, and we therefore interpret the uppermost bedrock ages ranging from 13.3 ± 0.6 to 12.7 ± 0.5 ka as the timing of deglaciation on Dalsnibba. The bedrock ages mark the subsequent lowering of the ice surface; by plotting sample age with altitude (Fig. S4, $R^2 = 0.91$) the dynamics of ice surface lowering through time becomes clear. As the lowermost sample in this study is at 1334 m a.s.l. (which cannot cover the spectrum until the final downmelt of the ice), the exposure age of the valley bottom of Opplendskedalen (7.47 ± 0.73 ka at 1045 m a.s.l.; Marr et al., 2019) is used to determine the ice surface lowering rate. This gives an ice surface lowering of about 430 m within ~ 5.8 ka. We calculate a thinning rate of ~ 7.3 cm a⁻¹, which is comparable to the inland thinning rate determined by Linge et al. (2007) of 5 cm a⁻¹. We explain this with the persistence of a small ice cap on Dalsnibba and/or glacial readvances (with related fluctuations of the vertical ice limit) as the YD in the valleys probably led to a prolonged ice coverage. Our results from the western study site have three important implications in terms of the local glaciation history:

1. We suggest that the vertical ice limit must have exceeded 1476 m a.s.l. to be able to transport and deposit the boulder at its location. This contrasts to some extent with the view that ice thickness in coastal areas was supposed to be relatively thin due to effective ice drainage (Nesje et al., 1987), but it needs to be considered that Dalsnibba is located at the innermost fjord head of the Geiranger Fjord. Some authors anyway infer the possibility of nunataks on high coastal surfaces in western Norway (Mangerud, 2004; Winguth et al., 2005). In the light of our results, we have to reject the possibility that

Dalsnibba was a nunatak during the LGM but suggest that the summit was covered by warm-based ice.

2. The timing of deglaciation between 13.3 ± 0.6 and 12.7 ± 0.5 ka overlaps with the Bølling–Allerød interstadial, during which the summit of Dalsnibba was probably ice-free, and coincides with when the deglaciation reached Storfjord (Longva et al., 2009). Subsequently, Dalsnibba was not affected by the Younger Dryas readvance. Our results indicate that the deglaciation on Dalsnibba began at the end of the Bølling–Allerød or later, and Dalsnibba constituted a nunatak during the Younger Dryas.
3. There is only sparse information on the final deglaciation in the Scandinavian mountains; it is supposed to have commenced shortly after ~ 10 ka (cf. Hughes et al., 2016). In Reinheimen, east of Dalsnibba, Andersen et al. (2018a) suggest 11 ± 0.2 ka as the timing of the last deglaciation. With our ¹⁰Be results it is difficult to constrain the final deglaciation as our lowermost sample was collected at 1334 m a.s.l. However, we can clearly state that the ice persisted at ~ 1330 m a.s.l. until 10.3 ± 0.5 ka when the final local deglaciation was partly inferred for the region 11.2 ± 0.4 and 10.9 ± 0.2 cal. kyr BP (cf. Nesje and Dahl, 1993; calibration from Hughes et al., 2016, applied). Therefore, our results open up the possibility that the ice coverage at Dalsnibba lasted longer than previously anticipated and also longer than in the Reinheimen area, unless the last part of deglaciation was characterized by a sudden collapse of the remaining ice.

5.3 Implications of ¹⁰Be exposure ages from Blåhø

The ¹⁰Be ages from the blockfield support the overall interpretation that these relict features have survived glaciation with little or no erosion, which indicates long-term landform preservation (Rea et al., 1996; Linge et al., 2006). By acknowledging the widely accepted scenario that anoma-

lously high ^{10}Be concentrations of bedrock samples, such as BlaBed, are the consequence of cold-based ice cover, the blockfield boundary might represent the former englacial boundary between cold-based and warm-based ice (Fabel et al., 2002; Marquette et al., 2004). This implies that the bedrock sample is likely compromised by inherited ^{10}Be from previous exposure followed by preservation beneath cold-based ice (Linge et al., 2006). This scenario appears realistic for the Blåhø bedrock sample, which, consequently, confirms the presence of non-erosive cold-based ice in line with several models suggesting thick ice coverage for this part of Norway (Stroeven et al., 2002; see Goehring et al., 2008). Notably, few of the weighted average bedrock ages from Reinheimen (Andersen et al., 2018a) show inheritance and provide ages of ~ 11 ka. This may point towards different thermal basal ice conditions within a short distance. Cosmogenic ^{10}Be and ^{26}Al nuclide concentration data indicate that some repeatedly glaciated sites have experienced negligible glacial erosion over the entire Quaternary (Briner et al., 2006; Harbor et al., 2006). Therefore, the inherited cosmogenic nuclides must have accumulated during multiple phases of exposure and have subsequently been preserved by cold-based ice (Hughes et al., 2016). Subtracting the exposure age since deglaciation (~ 21 ka) the surface experienced ~ 25 kyr of prior exposure. By using the ice coverage modelled by Mangerud et al. (2010) and Hughes et al. (2016), we evaluate the ^{10}Be concentration accumulation over time (Stroeven et al., 2002). With this approach it seems possible that the bedrock sample on Blåhø was first exposed at the surface during the Early Weichselian or the Eemian interglacial. Some authors suggest even older blockfield ages (e.g. Linge et al., 2006). In this scenario, boulder ages are often considered to reflect the timing of deglaciation (Marquette et al., 2004; Goehring et al., 2008). Following this, our boulder age of 20.9 ± 0.8 ka reflects the beginning of deglaciation, which agrees with the termination of the LGM (Fig. 3). This and the recalculated boulder age of 21.8 ± 1.6 ka (Goehring et al., 2008) supports their statement of the onset of deglaciation around this time. However, alternative interpretations of these boulder ages cannot be rejected, e.g. age overestimation due to post-depositional shielding by burial and subsequent exhumation by frost heave, deposition prior to LGM followed by long-term shielding, or deposition during a readvance following LGM (Briner et al., 2006; Heymann et al., 2011). But Marr et al. (2018) show evidence that the blockfield stabilized ~ 18 ka during severe periglacial conditions, which indicates the absence of ice cover close to the inferred time of boulder deposition.

The alternative interpretation of the bedrock ^{10}Be nuclide concentration assumes continuous surface exposure since at least 46.4 ± 1.7 ka. Geomorphic evidence, such as periglacial activity of the summit blockfield until 18 ka, challenges the inferred presence of cold-based ice on Blåhø during the LGM (Marr et al., 2018). Recently, Andersen et al. (2018b) stated that high-elevation low-relief areas in south-central Norway

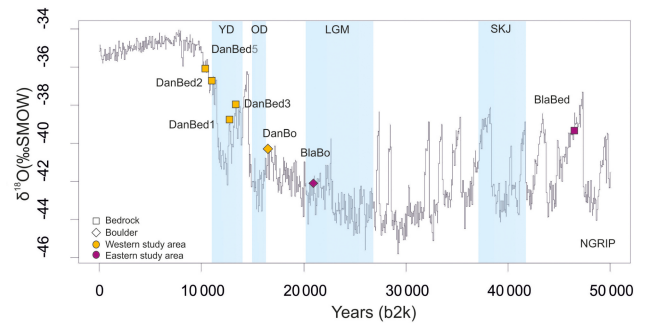


Figure 3. The ages are plotted against the North Greenland Ice Core Project (North Greenland Ice Core Project members, 2004) $\delta^{18}\text{O}$ with ^{10}Be ages. The key cold climate events are the Younger Dryas (YD), Older Dryas (OD), Last Glacial Maximum (LGM) and Skjoghelleren Stadial (SKJ); data are from Clark et al. (2009), Mangerud et al. (2010), Lohne et al. (2013) and Hughes et al. (2016).

were not covered by cold-based but warm-based ice as they calculated significant erosion rates. Therefore, whether the consistent trimline represents an englacial boundary remains ambiguous as englacial thermal boundaries may change frequently and may be unstable over long time periods (Nesje et al., 1987). However, decisive statements on glaciation history based on a single age are not possible; to resolve this issue on Blåhø, more numerical age data are necessary.

5.4 Implications for the regional glaciation history

The time difference of about 6–9 kyr for deglaciation between Dalsnibba and Blåhø is noteworthy. Taking into account the timing of deglaciation at 11 ± 0.2 ka in Reinheimen (Andersen et al., 2018a), located between our study areas, the deglaciation pattern in southern Norway was spatially and temporally variable. In relation to these ages the summit of Blåhø became apparently ice-free relatively early during deglaciation, whereas Dalsnibba at the inner fjord head of Geiranger Fjord became ice-free around 2 kyr later than the Reinheimen plateau. This means that during the YD readvance Reinheimen must have still been ice-covered, but the summit of Dalsnibba was already ice-free.

6 Conclusion

In this paper we present seven in situ cosmogenic ^{10}Be surface exposure ages from two selected mountain locations in southern Norway. Despite uncertainties related to the uncertainties of our ^{10}Be surface exposure ages and the limited dataset, we can delineate age constraints for the timing of deglaciation in the Geirangerfjellet in southwestern Norway. Further, we contribute new age estimates to the previously established deglaciation chronology for Blåhø in south-central Norway. The following conclusions can be drawn from this study:

1. According to the summit bedrock exposure ages ranging from 13.3 ± 0.6 to 12.7 ± 0.5 ka, deglaciation of the summit of Dalsnibba in Opplandskedalen commenced during the termination of the Bølling–Allerød interstadial. The summit successively remained ice-free during the Younger Dryas. However, the ice cover in the valley below the summit lasted longer (until 10.3 ± 0.5 ka) than previously assumed. In contrast to other studies, our results conclude that Dalsnibba was not a nunatak but covered by warm-based ice during the LGM.
2. The bedrock age from Blåhø (46.4 ± 1.7 ka) indicates long-term weathering history and exposure predating the LGM. Most likely, inherited cosmogenic nuclides preserved through shielding by non-erosive cold-based ice are responsible for its old age. However, possible post-depositional disturbance of the boulder and the lack of larger suitable datasets restrict its interpretation.
3. The different timing of deglaciation in both selected sites and in nearby Reinheimen implies complex deglaciation patterns within a spatially limited area. The vertical extent of the Younger Dryas readvance seems to have been less pronounced in the inner fjord areas.

Data availability. All data sources are publicly accessible online; supporting ground imagery can be found in the Supplement.

Supplement. The supplement related to this article is available online at: <https://doi.org/10.5194/egqsj-68-165-2019-supplement>.

Author contributions. PM prepared the manuscript with contributions from all co-authors. SAB was responsible for the ¹⁰Be measurements at CologneAMS.

Competing interests. The authors declare that they have no conflict of interest.

Special issue statement. This article is part of the special issue “Connecting disciplines – Quaternary archives and geomorphological processes in a changing environment”. It is a result of the First Central European Conference on Geomorphology and Quaternary Sciences, Gießen, Germany, 23–27 September 2018.

Acknowledgements. We thank Peter Wilson and one anonymous reviewer for very constructive and thoughtful comments that helped to improve the manuscript. We also thank Tibor Dunai for his expertise and his help. We further acknowledge permission to conduct field work in the Geiranger World Natural Heritage and Landscape Protection Area for over 20 years.

Financial support. This research has been supported by the Friedrich-Ebert-Stiftung (PhD scholarship grant).

References

- Aarseth, I., Austbo, P. K., and Risnes, H.: Seismic stratigraphy of Younger Dryas ice-marginal deposits in western Norwegian fjords, *Norsk Geol. Tidsskr.*, 77, 65–85, 1997.
- Andersen, B. G., Mangerud, J., Sørensen, R., Reite, A., Sveian, H., Thoresen, M., and Bergström, B.: Younger Dryas ice-marginal deposits in Norway, *Quatern. Int.*, 28, 147–169, [https://doi.org/10.1016/1040-6182\(95\)00037-J](https://doi.org/10.1016/1040-6182(95)00037-J), 1995.
- Andersen, J. L., Egholm, D. L., Knudsen, M. F., Linge, H., Jansen, J. D., Goodfellow, B. W., Pedersen, V. K., Tikhomirov, D., Olsen, J., and Fredin, O.: Pleistocene Evolution of a Scandinavian Plateau Landscape, *J. Geophys. Res.-Earth*, 123, 3370–3387, <https://doi.org/10.1029/2018JF004670>, 2018a.
- Andersen, J. L., Egholm, D. L., Knudsen, M. F., Linge, H., Jansen, J. D., Pedersen, V. K., Nielsen, S. B., Tikhomirov, D., Olsen, J., Fabel, D., and Xu, S.: Widespread erosion on high plateaus during recent glaciations in Scandinavia, *Nat. Commun.*, 9, 830, <https://doi.org/10.1038/s41467-018-03280-2>, 2018b.
- Balco, G.: Production rate calculations for cosmic-ray-muon-produced ¹⁰Be and ²⁶Al benchmarked against geological calibration data, *Quat. Geochronol.*, 39, 150–173, <https://doi.org/10.1016/j.quageo.2017.02.001>, 2017.
- Balco, G., Stone, J. O., Lifton, N. A., and Dunai, T. J.: A complete and easily accessible means of calculating surface exposure ages or erosion rates from ¹⁰Be and ²⁶Al measurements, *Quat. Geochronol.*, 3, 174–195, <https://doi.org/10.1016/j.quageo.2007.12.001>, 2008.
- Binnie, S. A., Dunai, T. J., Voronina, E., Goral, T., Heinze, S., and Dewald, A.: Separation of Be and Al for AMS using single-step column chromatography, *Nucl. Instrum. Methods Phys. Res. Sect. B Beam Interact. Mater. Atoms*, 361, 397–401, <https://doi.org/10.1016/j.nimb.2015.03.069>, 2015.
- Briner, J. P., Miller, G. H., Thompson Davis, P., and Finkel, R. C.: Cosmogenic radionuclides from fiord landscapes support differential erosion by overriding ice sheets, *Geol. Soc. Am. B.*, 118, 406–420, <https://doi.org/10.1130/B25716.1>, 2006.
- Brook, E. J., Nesje, A., Lehman, S. J., Raisbeck, R. M., and Yiou, F.: Cosmogenic nuclide exposure ages along a vertical transect in western Norway: Implications for the height of the Fennoscandian ice sheet, *Geology*, 24, 207–210, [https://doi.org/10.1130/0091-7613\(1996\)024<0207:CNEAAA>2.3.CO;2](https://doi.org/10.1130/0091-7613(1996)024<0207:CNEAAA>2.3.CO;2), 1996.
- Clark, P. U., Dyke, A. S., Shakun, J. D., Carlson, A. E., Clark, J., Wohlfarth, B., Mitrovica J. X., Hostetler, S. W., and McCabe, A. M.: The last glacial maximum, *Science*, 325, 710–714, <https://doi.org/10.1126/science.1172873>, 2009.
- Dahl, S. O., Nesje, A., and Øvstedal, J.: Cirque glaciers as morphological evidence for a thin Younger Dryas ice sheet in east-central southern Norway, *Boreas*, 26, 161–180, <https://doi.org/10.1111/j.1502-3885.1997.tb00850.x>, 1997.
- Dewald, A., Heinze, S., Jolie, J., Zilges, A., Dunai, T., Rethemeyer, J., Melles, M., Staubwasser, M., Kuczewski, B., Richter, J., Radtke, U., von Blanckenburg, F., and Klein, M.: CologneAMS, a dedicated center for accelerator mass spectrometry in Germany,

- Nucl. Instrum. Methods Phys. Res. Sect. B Beam Interact. Mater. Atoms, 294, 18–23, <https://doi.org/10.1016/j.nimb.2012.04.030>, 2013.
- Donner, J.: The early and middle Weichselian Interstadials in the central area of the Scandinavian glaciations, *Quaternary Sci. Rev.*, 15, 471–479, [https://doi.org/10.1016/0277-3791\(96\)00002-9](https://doi.org/10.1016/0277-3791(96)00002-9), 1996.
- Dunai, T. J.: *Cosmogenic Nuclides: Principles, Concepts and Applications in the Earth Surface Sciences*, Cambridge University Press, Cambridge, <https://doi.org/10.1017/CBO9780511804519>, 2010.
- Ehlers, J. and Gibbard, P. L.: The extent and chronology of Cenozoic Global Glaciation, *Quatern. Int.*, 164–165, 6–20, <https://doi.org/10.1016/j.quaint.2006.10.008>, 2007.
- Fabel, D., Stroeven, A. P., Harbor, J., Kleman, J., Elmore, D., and Fink, D.: Landscape preservation under Fennoscandian ice sheets determined from in situ produced ¹⁰Be and ²⁶Al, *Earth Planet. Sc. Lett.*, 201, 397–406, [https://doi.org/10.1016/S0012-821X\(02\)00714-8](https://doi.org/10.1016/S0012-821X(02)00714-8), 2002.
- Fareth, O. W.: *Glacial geology of Middle and Inner Nordfjord, western Norway*, Technical Report 408, Geological Survey of Norway, Trondheim, 1987.
- Fjeldskaar, W.: Viscosity and thickness of the asthenosphere detected from the Fennoscandian uplift, *Earth Planet. Sc. Lett.*, 126, 399–410, [https://doi.org/10.1016/0012-821X\(94\)90120-1](https://doi.org/10.1016/0012-821X(94)90120-1), 1994.
- Fjeldskaar, W. and Amatonov, A.: Younger Dryas transgression in western Norway: a modelling approach, *Norsk Geol. Tidsskr.*, 98, 127–139, <https://doi.org/10.17850/njg98-1-08>, 2018.
- Fjeldskaar, W., Lindholm, C., Dehls, J. F., and Fjeldskaar, I.: Post-glacial uplift, neotectonics and seismicity in Fennoscandia, *Quaternary Sci. Rev.*, 19, 1413–1422, [https://doi.org/10.1016/S0277-3791\(00\)00070-6](https://doi.org/10.1016/S0277-3791(00)00070-6), 2000.
- Goehring, B. M., Brook, E. J., Linge, H., Raisbeck, G. M., and Yiou, F.: Beryllium-10 exposure ages of erratic boulders in Southern Norway and implications for the history of the Fennoscandian Ice Sheet, *Quaternary Sci. Rev.*, 27, 320–336, <https://doi.org/10.1016/j.quascirev.2007.11.004>, 2008.
- Goehring, B. M., Lohne, Ø. S., Mangerud, J., Svendsen, J. I., Gyllencreutz, R., Schaefer, J., and Finkel, R.: Late glacial and Holocene ¹⁰Be production rates for western Norway, *J. Quaternary Sci.*, 27, 89–96, <https://doi.org/10.1002/jqs.2548>, 2012a.
- Goehring, B. M., Lohne, Ø. S., Mangerud, J., Svendsen, J. I., Gyllencreutz, R., Schaefer, J., and Finkel, R.: Erratum. Late glacial and Holocene ¹⁰Be production rates for western Norway, *J. Quaternary Sci.*, 27, 544, <https://doi.org/10.1002/jqs.2548>, 2012b.
- Gosse, J. C. and Phillips, F. M.: Terrestrial in situ cosmogenic nuclides: theory and application, *Quaternary Sci. Rev.*, 20, 1475–1560, [https://doi.org/10.1016/S0277-3791\(00\)00171-2](https://doi.org/10.1016/S0277-3791(00)00171-2), 2001.
- Harbor, J., Stroeven, A. P., Fabel, D., Clarhäll, A., Kleman, J., Li, Y., Elmore, D., and Fink, D.: Cosmogenic nuclide evidence for minimal erosion across two subglacial sliding boundaries of the late glacial Fennoscandian ice sheet, *Geomorphology*, 75, 90–99, <https://doi.org/10.1016/j.geomorph.2004.09.036>, 2006.
- Helle, S. K., Rye, N., Stabell, B., Prösch-Danielsen, L., and Hoel, C.: Neotectonic faulting and the Late Weichselian shoreline gradients in SW Norway, *J. Geodyn.*, 44, 96–128, <https://doi.org/10.1016/j.jog.2007.01.001>, 2007.
- Heymann, J., Stroeven, A. P., Harbor, J. M., and Caffee, M. W.: Too young or too old: Evaluating cosmogenic exposure dating based on an analysis of compiled boulder exposure ages, *Earth Planet. Sc. Lett.*, 302, 71–80, <https://doi.org/10.1016/j.epsl.2010.11.040>, 2011.
- Holtedahl, H.: Notes on the formation of fjord and fjord-valleys, *Geogr. Ann. A.*, 49, 188–203, <https://doi.org/10.1080/04353676.1967.11879749>, 1967.
- Hughes, A. L. C., Gyllencreutz, R., Lohne, Ø. S., Mangerud, J., and Svendsen, J. I.: The last Eurasian ice sheets – a chronological database and time-slice reconstruction, *DATED-1, Boreas*, 45, 1–45, <https://doi.org/10.1111/bor.12142>, 2016.
- Jones, R. S., Whitehouse, P. L., Bentley, P. M., Small, S., and Dalton, A. S.: Impact of glacial isostatic adjustment on cosmogenic surface-exposure dating, *Quaternary Sci. Rev.*, 212, 206–212, <https://doi.org/10.1016/j.quascirev.2019.03.012>, 2019.
- Kleman, J.: Preservation of landforms under ice sheets and ice caps, *Geomorphology*, 9, 19–32, [https://doi.org/10.1016/0169-555X\(94\)90028-0](https://doi.org/10.1016/0169-555X(94)90028-0), 1994.
- Klemsdal, T. and Sjulsen, E.: The Norwegian macro-landforms: Definition, distribution and system of evolution, *Norsk Geogr. Tidsskr.*, 42, 133–147, <https://doi.org/10.1080/00291958808552192>, 1988.
- Kohl, C. P. and Nishiizumi, K.: Chemical isolation of quartz for measurement of in-situ produced cosmogenic nuclides, *Geochim. Cosmochim. Ac.*, 56, 3583–3587, 1992.
- Landvik, J. Y., Ingólfsson, Ó., Mienert, J., Lehman, S. J., Solheim, A., Elverhøi, A., and Ottesen, D.: Rethinking Late Weichselian ice-sheet dynamics in coastal NW Svalbard, *Boreas*, 34, 7–24, <https://doi.org/10.1111/j.1502-3885.2005.tb01001.x>, 2005.
- Lifton, N., Sato, T., and Dunai, T. J.: Scaling in situ cosmogenic nuclide production rates using analytical approximations to atmospheric cosmic-ray fluxes, *Earth Planet. Sc. Lett.*, 386, 149–160, <https://doi.org/10.1016/j.epsl.2013.10.052>, 2014.
- Linge, H., Brook, E. J., Nesje, A., Raisbeck, G., Yiou, F., and Clark, H.: In situ ¹⁰Be exposure ages from southeastern Norway: implications for the geometry of the Weichselian Scandinavian ice sheet, *Quaternary Sci. Rev.*, 25, 1097–1109, <https://doi.org/10.1016/j.quascirev.2005.10.007>, 2006.
- Linge, H., Olsen, L., Brook, E. J., Darter, J. R., Mickelson, D. M., Raisbeck, G. M., and Yiou, F.: Cosmogenic nuclide surface exposure ages from Nordland, northern Norway: implications for deglaciation in a coast to inland transect, *Norsk Geol. Tidsskr.*, 87, 269–280, 2007.
- Löffler, J. and Pape, R.: Across scale temperature modelling using a simple approach for the characterization of high mountain ecosystem complexity, *Erdkunde*, 58, 331–348, <https://doi.org/10.3112/erdkunde.2004.04.04>, 2004.
- Lohne, Ø. S., Bondevik, S., Mangerud, J., and Svendsen, J. I.: Sea-level fluctuations imply that the Younger Dryas ice-sheet expansion in western Norway commenced during the Allerød, *Quaternary Sci. Rev.*, 26, 2128–2151, <https://doi.org/10.1016/j.quascirev.2007.04.008>, 2007.
- Lohne, Ø. S., Mangerud, J., and Birks, H. H.: Precise ¹⁴C ages of the Vedde and Saksunarvatn ashes and the Younger Dryas boundaries from western Norway and their comparison with the Greenland Ice Core (GICC05) chronology, *J. Quaternary Sci.*, 28, 490–500, <https://doi.org/10.1002/jqs.2640>, 2013.
- Longva, O., Blikra, L. H., and Dehls, J. F.: Rock avalanches: distribution and frequencies in the inner part of Storfjorden, Møre og

- Romsdal County, Norway, Technical Report 2009.002, Geological Survey of Norway, Trondheim, 2009.
- Mangerud, J.: Ice sheets limits in Norway and on the Norwegian continental shelf, in: Quaternary Glaciations Extent and Chronology, edited by: Ehlers, J. and Gibbard, P. L., Elsevier, Amsterdam, 271–294, 2004.
- Mangerud, J., Gulliksen, S., and Larsen, E.: ¹⁴C-dated fluctuations of the western flank of the Scandinavian Ice Sheet 45–25 kyr BP compared with Bølling–Younger Dryas fluctuations and Dansgaard–Oeschger events in Greenland, *Boreas*, 39, 328–342, <https://doi.org/10.1111/j.1502-3885.2009.00127.x>, 2010.
- Marquette, G. C., Gray, J. T., Gosse, J. C., Courchesne, F., Stockli, L., Macpherson, G., and Finkel, R.: Felsenmeer persistence under non-erosive ice in the Tornгат and Kaumajet mountains, Quebec and Labrador, as determined by soil weathering and cosmogenic nuclide exposure dating, *Can. J. Earth Sci.*, 41, 19–38, <https://doi.org/10.1139/e03-072>, 2004.
- Marr, P. and Löffler, J.: Establishing a multi-proxy approach to alpine blockfield evolution in south-central Norway, *AUC Geogr.*, 52, 219–236, <https://doi.org/10.14712/23361980.2017.18>, 2017.
- Marr, P., Winkler, S., and Löffler, J.: Investigations on blockfields and related landforms at Blåhø (Southern Norway) using Schmidt-hammer exposure-age dating: palaeoclimatic and morphodynamic implications, *Geogr. Ann. A.*, 100, 285–306, <https://doi.org/10.1080/04353676.2018.1474350>, 2018.
- Marr, P., Winkler, S., and Löffler, J.: Schmidt-hammer exposure-age dating (SHD) performed on periglacial and related landforms in Opplandskedalen, Geirangerfjellet, Norway: Implications for mid- and late-Holocene climate variability, *Holocene*, 29, 97–109, <https://doi.org/10.1177/0959683618804634>, 2019.
- Matthews, J. A., Shakesby, R. A., and Fabel, D.: Very low inheritance in cosmogenic surface exposure ages of glacial deposits: A field experiment from two Norwegian glacier forelands, *Holocene*, 27, 1406–1414, <https://doi.org/10.1177/0959683616687387>, 2017.
- McCarroll, D.: Trimline trauma: the wider implications of a paradigm shift in recognising and interpreting glacial limits, *Scottish Geogr. J.*, 132, 130–139, <https://doi.org/10.1080/14702541.2016.1157203>, 2016.
- Morén, L. and Pässe, T.: Climate and shoreline in Sweden during Weichsel and the next 150,000 years, SKB Technical Report 01-19, Swedish Nuclear Fuel and Waste Management Co., Stockholm, 67, 2001.
- Nesje, A.: Late Pleistocene and Holocene alpine glacier fluctuation in Scandinavia, *Quaternary Sci. Rev.*, 28, 2119–2136, <https://doi.org/10.1016/j.quascirev.2008.12.016>, 2009.
- Nesje, A. and Dahl, S. O.: Lateglacial and Holocene glacier fluctuations and climatic variations in western Norway: A review, *Quaternary Sci. Rev.*, 12, 255–261, [https://doi.org/10.1016/0277-3791\(93\)90081-V](https://doi.org/10.1016/0277-3791(93)90081-V), 1993.
- Nesje, A., Anda, E., Rye, N., Lien, R., Hole P. A., and Blikra, H.: The vertical extent of the Late Weichselian ice sheet in the Nordfjord-Møre area, western Norway, *Norsk Geol. Tidsskr.*, 67, 125–141, 1987.
- Nesje, A., McCarroll, D., and Dahl, S. O.: Degree of rock surface weathering as an indicator of ice-sheet thickness along an east–west transect across Southern Norway, *J. Quaternary Sci.*, 9, 337–347, <https://doi.org/10.1002/jqs.3390090404>, 1994.
- Nishiizumi, K., Imamura, M., Caffee, M. W., Southon, J. R., Finkel, R. C., and McAninch, J.: Absolute calibration of ¹⁰Be AMS standards, *Nucl. Instrum. Methods Phys. Res. Sect. B Beam Interact. Mater. Atoms*, 258, 403–413, <https://doi.org/10.1016/j.nimb.2007.01.297>, 2007.
- North Greenland Ice Core Project members: High-resolution record of Northern Hemisphere climate extending into the last interglacial period, *Nature*, 431, 147–151, <https://doi.org/10.1038/nature02805>, 2004.
- Patton, H., Hubbard, A., Andreassen, K., Winsborrow, M., and Stroeven, A. P.: The build-up, configuration, and dynamical sensitivity of the Eurasian ice-sheet complex to Late Weichselian climatic and oceanic forcing, *Quaternary Sci. Rev.*, 154, 97–121, <https://doi.org/10.1016/j.quascirev.2016.10.009>, 2016.
- Patton, H., Hubbard, A., Andreassen, K., Auriac, A., Whitehouse, P. L., Stroeven, A. P., Shackleton, C., Winsborrow, M., Heyman, J., and Hall, A. M.: Deglaciation of the Eurasian ice sheet complex, *Quaternary Sci. Rev.*, 169, 148–172, <https://doi.org/10.1016/j.quascirev.2017.05.019>, 2017.
- Rea, B. R., Whalley, W., Rainey, M. M., and Gordon, J. E.: Blockfields, old or new? Evidence and implications from some plateaus in northern Norway, *Geomorphology*, 15, 109–121, [https://doi.org/10.1016/0169-555X\(95\)00118-O](https://doi.org/10.1016/0169-555X(95)00118-O), 1996.
- Rinterknecht, V. R., Clark, P. U., Raisbeck, G. M., Yiou, F., Brook, E. J., Marks, L., Zelčs, V., Lunkka, J.-P., Pavlovskaya, I. E., Piotrowski, J. A., and Raukas, A.: The last deglaciation of the southeastern sector of the Scandinavian Ice Sheet, *Science*, 311, 1449–1452, <https://doi.org/10.1126/science.1120702>, 2006.
- Sollid, J. L. and Reite, J. A.: The last glaciation and deglaciation of Central Norway, in: *Glacial deposits of North-West Europe*, edited by: Ehlers, J., Balkema, Rotterdam, 41–59, 1983.
- Steffen, H. and Wu, P.: Glacial isostatic adjustment in Fennoscandia – A review of data and modeling, *J. Geodyn.*, 52, 169–204, <https://doi.org/10.1016/j.jog.2011.03.002>, 2011.
- Stone, J. O., Fifield, L. K., Beer, J., Vonmoos, M., Obrist, C., Grajcar, M., Kubik, P., Muscheler, R., Finkel, R., and Caffee, M.: Co-precipitated silver metal oxide aggregates for accelerator mass spectrometry of Be-10 and Al-26, *Nucl. Instrum. Meth. B*, 223–224, 272–277, <https://doi.org/10.1016/j.nimb.2004.04.055>, 2004.
- Stroeven, A. P., Fabel, D., Hättestrand, C., and Harbor, J.: A relict landscape in the centre of Fennoscandian glaciation: cosmogenic radionuclide evidence of tors preserved through multiple glacial cycles, *Geomorphology*, 44, 145–154, [https://doi.org/10.1016/S0169-555X\(01\)00150-7](https://doi.org/10.1016/S0169-555X(01)00150-7), 2002.
- Stroeven, A. P., Hättestrand, C., Kleman, J., Heyman, J., Fabel, D., Fredin, O., Goodfellow, B. W., Harbor, J. M., Jansen, J. D., Olsen, L., Caffee, M. W., Fink, D., Lundqvist, J., Rosqvist, G. C., Strömberg, B., and Jansson, K. N.: Deglaciation of Fennoscandia, *Quaternary Sci. Rev.*, 147, 91–121, <https://doi.org/10.1016/j.quascirev.2015.09.016>, 2016.
- Svendsen, J. I. and Mangerud, J.: Late Weichselian and Holocene sea-level history for a cross-section of western Norway, *J. Quaternary Sci.*, 2, 113–132, <https://doi.org/10.1002/jqs.3390020205>, 1987.
- Tveten, E., Lutro, O., and Thorsnes, T.: *Geologisk kart over Norge 1 : 250000, Norges Geologiske Undersøkelse, Ålesund*, 1998.
- Winguth, C., Mickelson, D. M., Larsen, E., Darter, J. R., Moeller, C. A., and Stalsburg, K.: Thickness evolution of the Scandina-

vian Ice Sheet during the Late Weichselian in Nordfjord, western Norway: evidence from ice-flow modeling, *Boreas*, 34, 176–185, <https://doi.org/10.1111/j.1502-3885.2005.tb01013.x>, 2005.

Wohlfarth, B.: Ice-free conditions in Sweden during Marine Oxygen Isotope Stage 3?, *Boreas*, 39, 377–398, <https://doi.org/10.1111/j.1502-3885.2009.00137.x>, 2010.